

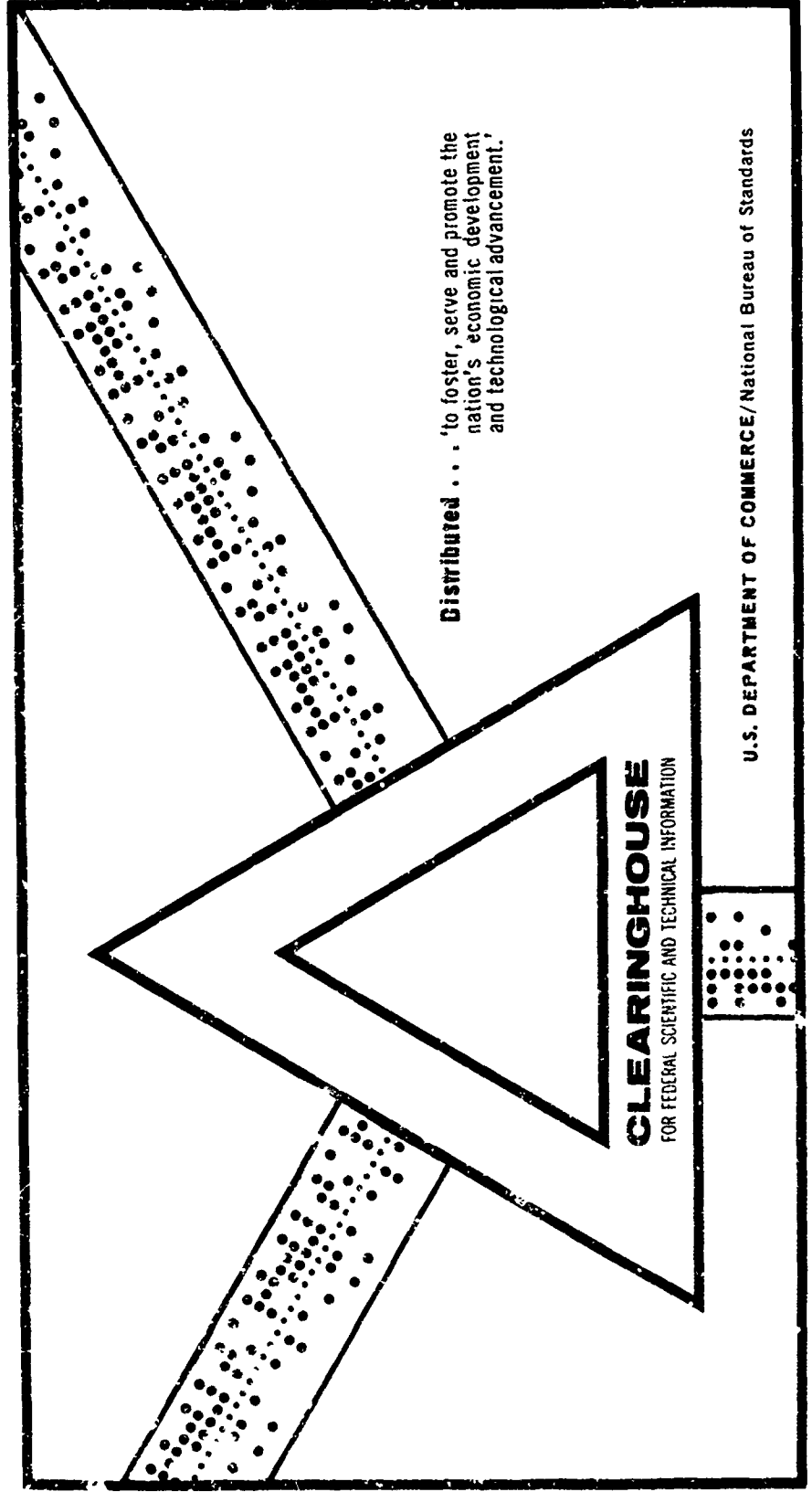
AD 696 163

A TWO-DIMENSIONAL RAY-TRACING METHOD FOR THE CALCULATION  
OF RADOME BORESIGHT ERROR AND ANTENNA PATTERN DISTORTION

N. R. Kilcoyne

Ohio State University  
Columbus, Ohio

2 October 1969



Distributed . . . to foster, serve and promote the  
nation's economic development  
and technological advancement.

**CLEARINGHOUSE**  
FOR FEDERAL SCIENTIFIC AND TECHNICAL INFORMATION

U.S. DEPARTMENT OF COMMERCE/National Bureau of Standards

This document has been approved for public release and sale.



AD696163

A TWO-DIMENSIONAL RAY-TRACING METHOD FOR THE  
CALCULATION OF RADOME BORESIGHT ERROR  
AND ANTENNA PATTERN DISTORTION

N.R. Kilcoyne

The Ohio State University

**ElectroScience Laboratory**

(formerly Antenna Laboratory)

Department of Electrical Engineering  
Columbus, Ohio 43212

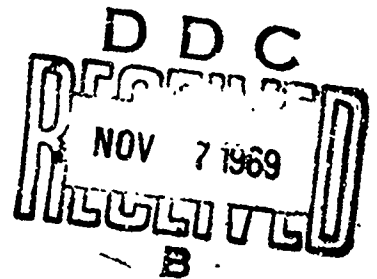
TECHNICAL REPORT 2767-2  
2 October 1969

Contract No. N00019-69-C-0325

RELEASED TO PUBLIC PER  
SEC DEF MEMO TO SEC NAV  
29 May 1969 under 6.1  
category funding program

THIS DOCUMENT HAS BEEN APPROVED  
FOR PUBLIC RELEASE AND SALE;  
ITS DISTRIBUTION IS UNLIMITED

Department of the Navy  
Naval Air Systems Command  
Washington, D.C. 20360



## NOTICES

When Government drawings, specifications, or other data are used for any purpose other than in connection with a definitely related Government procurement operation, the United States Government thereby incurs no responsibility nor any obligation whatsoever, and the fact that the Government may have formulated, furnished, or in any way supplied the said drawings, specifications, or other data, is not to be regarded by implication or otherwise as in any manner licensing the holder or any other person or corporation, or conveying any rights or permission to manufacture, use, or sell any patented invention that may in any way be related thereto.

ADDITION BY		
CPSC	WHITE SECTION	<input type="checkbox"/>
ROC	BLUE SECTION	<input type="checkbox"/>
UNASSIGNED		<input type="checkbox"/>
JUSTIFICATION		
.....		
BY		
DISTRIBUTION/AVAILABILITY CODES		
DISC.	AVAIL.	REG./OR SPECIAL
/		

A TWO-DIMENSIONAL RAY-TRACING METHOD FOR THE  
CALCULATION OF RADOME BORESIGHT ERROR  
AND ANTENNA PATTERN DISTORTION

N.R. Kilcoyne

TECHNICAL REPORT 2767-2  
2 October 1969

Contract No. N00019-69-C-0325

Department of the Navy  
Naval Air Systems Command  
Washington, D.C. 20360

RELEASED TO PUBLIC PER  
SEC DEF MENO TO SEC NAV  
29 May 1969 under 6.1 ✓  
category funding program

THIS DOCUMENT HAS BEEN REPRODUCED  
FOR PRIVATE USE ONLY AND  
ITS DISTRIBUTION IS UNLIMITED

## ABSTRACT

A two-dimensional ray tracing analysis for the calculation of radome boresight error and antenna pattern distortion is presented here. Emphasis has been placed on the development of a method having considerable flexibility, so as to enable application of the method to a wide range of antenna-radome problems, and on relative ease of calculation, so as to minimize calculation time. Several example problems are calculated to demonstrate the usefulness of the approach. Comparisons between calculations and measurements have been included whenever measured data were available. Instructions for use of this completely computerized method are included along with several tables describing variables and the complete computer program with necessary sub-routines. Programs are written in Fortran IV language suitable for use on the OSU version of the IBM system 360/75 (some minor changes may be required for use on other 360/75 installations).

## TABLE OF CONTENTS

	Page
I. INTRODUCTION	1
II. THE BASIC METHOD	1
A. <u>General Considerations</u>	1
B. <u>Ray Tracing</u>	3
C. <u>Pattern Calculation</u>	6
D. <u>Boresight Error</u>	10
III. DISCUSSION OF COMPUTER PROGRAM	12
IV. ANALYSIS AND DESIGN OF ANTENNA-RADOME SYSTEMS	17
A. <u>Convergence Of The Ray-Optics Solution</u>	17
B. <u>Numerical Integration Of The Reconstructed Aperture</u>	19
C. <u>Electrical Design Of A Radome Wall</u>	22
D. <u>Radome Boresight Error Versus System Bandwidth</u>	22
E. <u>Source Taper Effects</u>	23
F. <u>Aperture Blocking</u>	28
G. <u>Electrical Performance Of A Radome In A Hyper-Environment</u>	35
H. <u>Comparison Of Boresight Measurements And Calculations</u>	36
I. <u>Effects Due To The Blunting Of A Radome Nose Section</u>	60
V. CONCLUSIONS	66
ACKNOWLEDGEMENT	66
APPENDIX A	67
APPENDIX B	70

TABLE OF CONTENTS (Cont.)

	Page
APPENDIX C - INSTRUCTIONS FOR USE OF COMPUTER PROGRAM	75
A. <u>Required Input Data</u>	75
B. <u>Description Of A Typical Calculation</u>	78
C. <u>Sample Data Lists</u>	79
1. <u>Boresight error</u>	80
2. <u>Antenna pattern parameters</u>	80
D. <u>Computer Programs</u>	85
 REFERENCES	 113

# A TWO-DIMENSIONAL RAY-TRACING METHOD FOR THE CALCULATION OF RADOME BORESIGHT ERROR AND ANTENNA PATTERN DISTORTION

## I. INTRODUCTION

Streamlined radomes for aircraft and missile guidance systems must be carefully designed for high transmission efficiency and minimum boresight error. Since the usual antenna-radome system is large in terms of wavelengths, exact methods for the calculation of radome errors, such as the integral equation methods of Van Doeren<sup>1</sup> and Hahn,<sup>2</sup> prove to be difficult to apply. Frequently these methods can only be applied to a small portion of the radome such as the vertex region. Therefore approximate methods continue to be useful in radome analysis.

This report presents a two-dimensional approximate method for calculating radome boresight error and antenna pattern distortion. A ray analysis is used to determine the effects of the radome on the antenna. These effects are used to modify the source aperture distribution which is numerically integrated to determine the far-zone field pattern of the antenna-radome system. The Ohio State University-IBM System 360/75 high speed digital computer is used for all calculations. The calculated results agree reasonably well with experimental data and require little computer time. Several calculations of typical radome design problems are discussed.

## II. THE BASIC METHOD

### A. General Considerations

The analysis is based upon a two-dimensional model of the antenna-radome system as shown in Fig. 1. The radome is represented by its cross-section and the source antenna is represented by a one-dimensional aperture having a known amplitude and phase distribution. Rays are traced from the aperture to the radome wall to determine angles of incidence to be used in calculating radome effects. The radome is approximated by a plane multilayer oriented at the calculated angle of incidence at each ray intersection. The plane wave, plane-sheet transmission coefficient and insertion phase delay are calculated for each ray. These values are used to modify the original source distribution function such that a reconstructed aperture distribution is obtained which includes the radome effects. This distribution function is then numerically integrated by high-speed digital computer to determine the approximate far-field pattern of the antenna-radome system which is compared

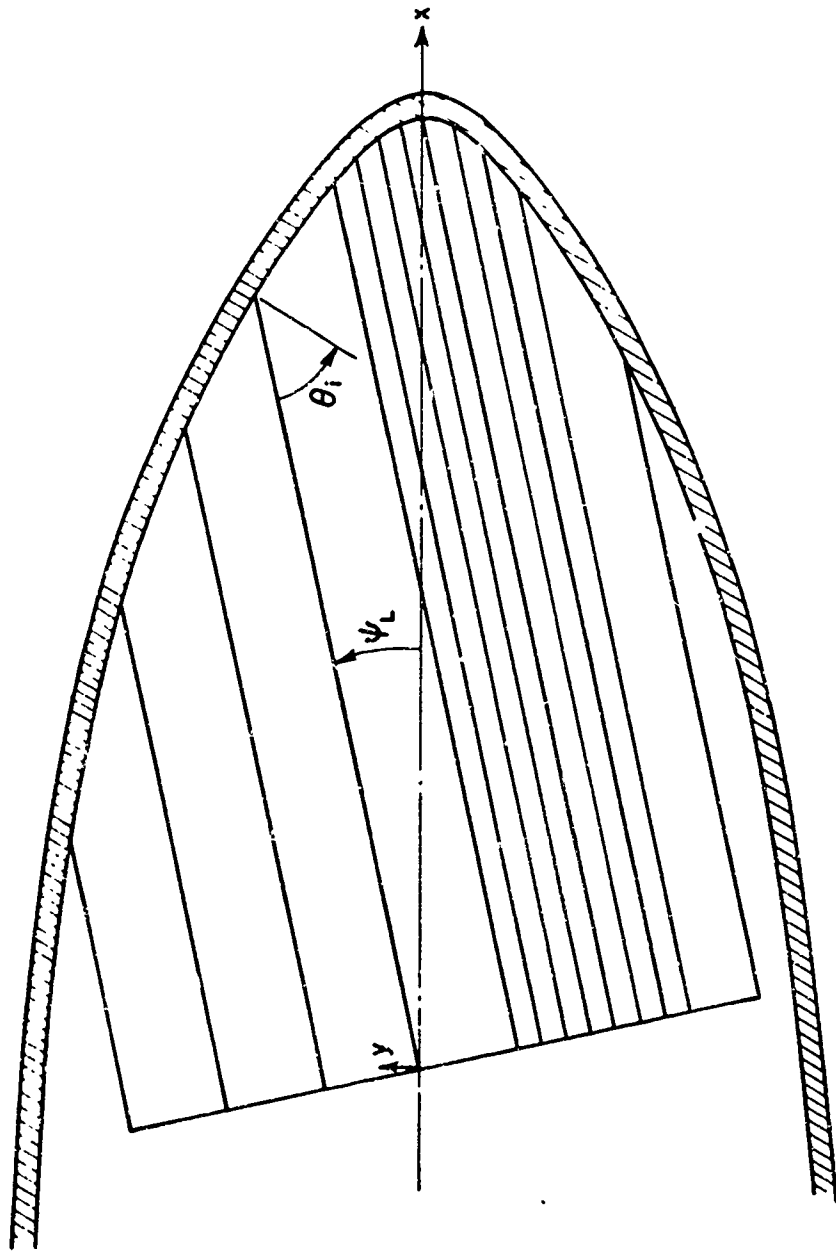


Fig. 1. Two-dimensional model for antenna-radome system.

to the pattern obtained without the radome to determine pattern distortion and boresight error.

### B. Ray Tracing

In the usual antenna-radome system the antenna aperture plane is displaced by some distance  $d_a$  from the gimbaling axes of the antenna. When the antenna is scanned, description of the aperture plane becomes difficult in a fixed coordinate system. For this reason two coordinate systems are used to describe the antenna-radome geometry, as shown in Fig. 2. The radome is described in a fixed  $(x, y)$  frame which has its axes centered on the antenna gimbal axis. The antenna aperture is described in  $(x', y')$  frame which rotates about the antenna gimbal axis with the angle of rotation corresponding to some look angle  $\phi_L$ . Points in the  $(x', y')$  system are related to points in the  $(x, y)$  system by the following transformation:

$$(1) \quad \begin{pmatrix} x \\ y \end{pmatrix} = \begin{pmatrix} \cos \phi_L & -\sin \phi_L \\ \sin \phi_L & \cos \phi_L \end{pmatrix} \begin{pmatrix} x' \\ y' \end{pmatrix}$$

The radome is assumed to be constructed of  $n$  geometry sections which can be described by the following general second-order equation:

$$(2) \quad F(x, y) = a_n x^2 + b_n y^2 + c_n xy + d_n x + e_n y + f_n = 0$$

where  $(x, y)$  are the coordinates of Fig. 2 and  $a_n \dots f_n$  are a set of geometrical constants which define the  $n$ -th radome section. A set of  $m$  equally-spaced rays from the antenna aperture to the radome inner wall are selected to represent the problem. A ray drawn from a point  $(x_a, y_a)$  on the aperture plane to the radome wall is described by the point-slope form as:

$$(3) \quad y - y_a = m_R(x - x_a)$$

where  $m_R$  is the slope of a ray in the  $(x, y)$  frame. The antenna points to be used are determined in the  $(x', y')$  frame by

$$(4) \quad x'_a = d_a$$

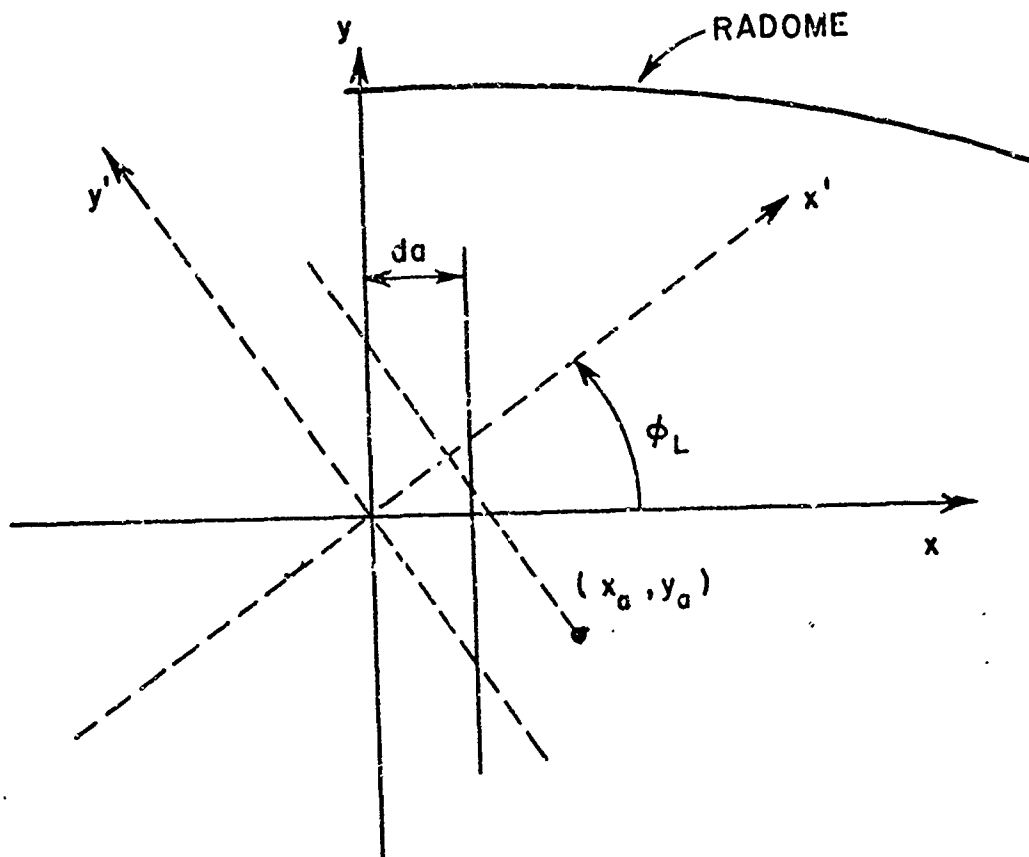


Fig. 2. Coordinate system used to define the antenna-radome geometry.

$$(5) \quad y'_a = \frac{A}{2NR} (2m - 2 - NR)$$

where

A is the total aperture length  
 NR is the number of rays to be used  
 m is the index of a particular ray  
 $d_a$  is the perpendicular distance from the origin to the aperture plane as in Fig. 2.

The set of  $m$  points determined by Eqs. (4) and (5) are transformed by Eq. (1) to the set of  $(x_a, y_a)$  points to be used in Eq. (3). Substituting Eq. (3) into Eq. (2) we get the following quadratic in  $x$ :

$$(6) \quad x_m^2 + \frac{(-2bm_R^2 x_a + 2bm_R y_a - cm_R x_a + cy_a + d + em_R)}{(a + bm_R^2 + cm_R)} x_m + \frac{(-2bm_R y_a x_a + bm_R^2 x_a^2 + by_a^2 - em_R x_a + ey_a + f)}{(a + bm_R^2 + cm_R)} = 0$$

The solution of Eq. (6) gives the  $x$ -coordinate of the point of intersection of the  $m$ -th ray and the radome. Since Eq. (6) is of the form:

$$(7) \quad x_m^2 + 2Bx_m + C = 0$$

the solution of Eq. (6) can be written as

$$(8) \quad x_m = -B \pm \sqrt{B^2 - C}$$

where

$2B$  is the coefficient of the linear term in Eq. (6)  
 $C$  is the constant term in Eq. (6).

From the geometry of the system it is seen that the positive square root is selected in Eq. (8) to give the proper point of intersection. This value of  $x_m$  is substituted into Eq. (3) to obtain the  $y$ -coordinate of the intersection point:

$$(9) \quad y_m = m_R(x_m - x_a) + y_a$$

The derivative of Eq. (2) evaluated at  $(x_m, y_m)$  gives the slope of the tangent to the radome surface at the  $m$ -th intersection point:

$$(10) \quad m_T = -\frac{(2ax_m + Cy_m + d)}{(2by_m + Cx_m + e)}$$

Provided that neither the tangent line to the radome nor the ray is parallel to the y-axis and that the two lines are not perpendicular, the angle of intersection of the two lines is:

$$(11) \quad \theta^m = \text{Tan}^{-1} \frac{m_R - m_T}{1 + m_R m_T}$$

which is the complement of the angle of incidence of the m-th ray and the radome inner wall.

$$(12) \quad \theta_i^m = \frac{\pi}{2} - \theta^m$$

is the angle of incidence. As will be discussed later the average angle of incidence for two adjacent rays will be used in further calculations:

$$(13) \quad \theta_A = (\theta_i^m + \theta_i^{m+1})/2$$

The two exceptions to Eq. (11) mentioned above are treated specifically in the computer program. The constants a through f in Eq. (1) depend upon the specific geometry of the radome. Logic statements in the program assure that the ray intersection is calculated in the proper geometrical section. The angle of incidence calculated in Eq. (13) is stored in an  $m \times n$  array indicating that the m-th ray is used with the n-th set of geometrical and electrical constants. The  $a_n \dots f_n$  constants and the associated n geometry boundaries are usually calculated in the program, however, for specialized cases they may be read in directly.

### C. Pattern Calculation

The basic calculation is that of a section of the far zone field pattern of the antenna radiating in the presence of the radome. The angular range over which the pattern is calculated varies from one degree about the antenna look angle for boresight error calculation and from 10 to 90 degrees about the look angle for pattern distortion calculation. Within the one degree interval used for boresight calculation only a few discrete points are calculated.

The far-zone field pattern for the one-dimensional source representation shown in Fig. 1 is given by:

$$(14) \quad E(\phi) = \int_L F(y) e^{j\phi(y)} e^{jky \sin \phi} dy$$

where:

$F(y)$  is the amplitude distribution function  
 $\phi(y)$  is the phase distribution function  
 $\phi$  is the pattern angle  
 $L$  is the length of the aperture.

In general  $F(y)$  and  $\phi(y)$  are arbitrary functions such that the evaluation of the integral requires numerical methods. These functions are determined by the given source distribution functions and modified later to account for the presence of the radome. Rays are traced from the aperture plane to the radome inner wall where they are modified by the plane wave, plane-sheet transmission coefficient ( $|T|^2$ ) and insertion phase delay (IPD), to a new aperture plane immediately outside the radome. Here a "reconstructed" aperture is defined which determines the far-field of the antenna-radome system according to Eq. (14). A few comments on ray tracing follow.

The usual ray analysis uses a set of  $n$  equally-spaced rays. As this  $n$  is increased the predicted result varies up to some value of  $n$  where further addition of rays no longer changes the answer. This answer is not necessarily the correct answer but merely the best answer that the ray tracing solution can predict. This  $n$  required for a convergent answer using equally spaced rays frequently becomes quite large, typically 500 rays for a  $10\lambda$  aperture and a streamlined radome. Evaluation of Eq. (14) using a large  $n$  consumes an excessive amount of computer time which is undesirable. An alternative to this approach is to use a set of fewer unevenly-spaced weighted rays<sup>3</sup> to analyze the problem such as the set shown in Fig. 1. Since the radome effects,  $|T|^2$  and IPD, are strongly dependent on incidence angle, close spacing of the rays is required only if the radome curvature is changing rapidly. More widely spaced rays can be used in regions where the curvature variation is slight. The most efficient ray analysis uses the fewest number of rays required to obtain the convergent answer. The numerical treatment which will be applied to the reconstructed aperture is equivalent to performing such a weighted ray tracing. This treatment is described below.

The source antenna has associated with it a large number of equally-spaced rays, say 500. A subaperture of the source is defined as that section of the source aperture between two successive rays and has associated with it a ray emanating from its center which intersects the

radome inner wall at angle  $\theta_A$  of Eq. (13). The local amplitude and phase associated with this subaperture is calculated from the known source distribution function. In the case of a circular aperture, as shown in Fig. 3, the equivalent one dimensional source must be tapered by the factor

$$(15) \quad A_0(y) = \cos \left( \sin^{-1} \frac{y}{R} \right)$$

This factor takes into account the effective power radiated from each segment represented by the chord length at the coordinate  $y$ , as in Fig. 3. If the circular aperture itself has an amplitude taper,  $F(r)$ , the equivalent one-dimensional aperture taper required is:

$$(16) \quad A(y) = F(y) A_0(y)$$

where  $A_0(y)$  is found from Eq. (15).

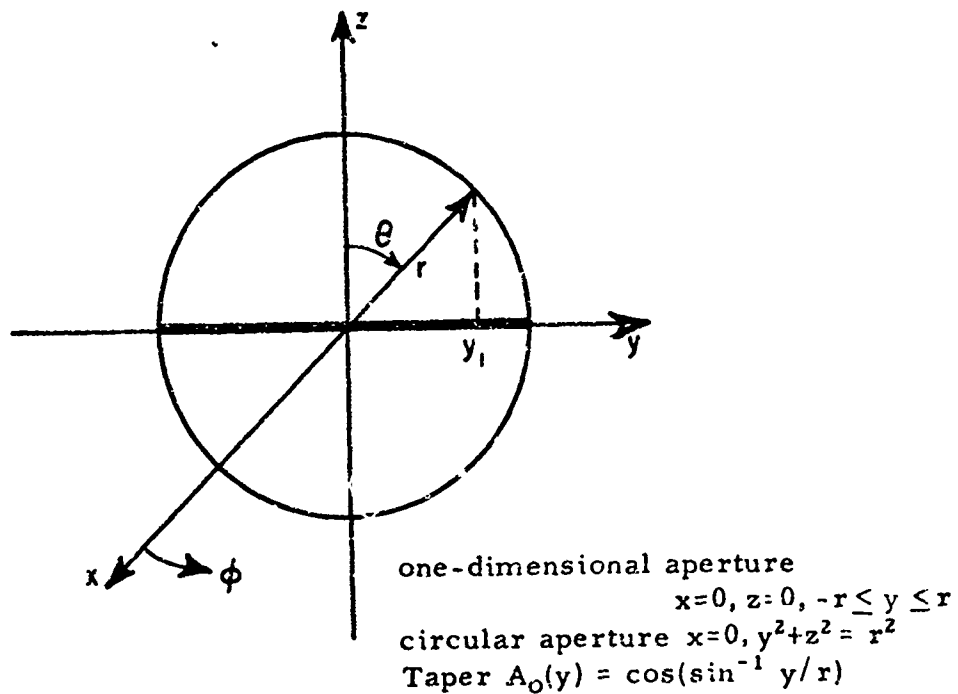


Fig. 3. Amplitude taper of a one-dimensional aperture for equivalence to a two-dimensional circular aperture.

This subaperture, according to conventional ray optics, illuminates only the small subsection of the radome wall lying between its two defining rays which is approximated as a plane sheet oriented at  $\theta_A$ . Plane wave, plane-sheet  $|T|^2$  and IPD are calculated using the method of Richmond<sup>4</sup> for the rays associated with each subaperture. The local subaperture field distribution is modified by the local  $|T|^2$  and IPD. The reconstructed aperture is thus completed specifying the integrand function  $F(y)$  and  $\phi(y)$  of Eq. (14).

The numerical treatment of the aperture integral involves breaking the integral down into several sections, or subapertures, as determined by the rate of change of the integrand, integrating over these subapertures, and summing the integrals. Equation (17) specifies the calculation.

$$(17) \quad E(\phi) = \sum_{n=1}^N \int_{L_n} F_n(y) e^{j\phi_n(y)} e^{jk y \sin \phi} dy$$

where:

- $L_n$  = length of the n-th subaperture
- $\phi_n$  = phase of the n-th subaperture
- $F_n$  = amplitude of the n-th subaperture
- $\phi$  = pattern angle .

The process of determining the aperture subdivision is as follows. Fixed amplitude and phase deviations are specified, usually 0.05 to 0.10 and 2 to 3 degrees respectively. The length, amplitude, and phase of the first subaperture are determined by scanning from the center of the reconstructed aperture, point by point towards the positive endpoint of the aperture, until either of the fixed deviations occurs. At this point the first subaperture boundary is defined and the average value of amplitude and phase are computed for the included points. The first subaperture is then assigned the three constants  $F_1$ ,  $\phi_1$ , and  $L_1$  of Eq. (17). The scan continues across the positive half of the aperture until all points are included, returns to the aperture center and similarly scans the negative portion of the reconstructed aperture. Thus the  $n$  values of  $F_n(y)$ ,  $\phi_n(y)$  and  $L_n$  are determined. Equation (17) is then evaluated as the summation of  $N$  integrals having uniform illuminations. This result is written as:

$$(18) \quad E(\phi) = \sum_{n=1}^N F_n L_n e^{j\phi_n} \frac{\sin\left(\frac{kL_n \sin\phi}{2}\right)}{\frac{kL_n \sin\phi}{2}}$$

where the term  $\phi_n$  contains an additional term which accounts for the n-th subaperture being displaced from the coordinate axis. Eulers equation is used to evaluate Eq. (18) on the computer. The range on  $\phi$  which is calculated is pre-assigned and depends upon the desired end result, i.e., pattern distortion or boresight error. The method of scanning the aperture from the center out to each end is used to preserve the symmetry of the system.

#### D. Boresight Error

The boresight error of an antenna-radome system can be defined as the difference between the actual target direction and the antenna pointing direction. In a well designed system this difference is a few tenths of a degree and is due primarily to phase and amplitude distortions of the antenna pattern caused by the radome. The boresight error is evaluated in this analysis from phase monopulse patterns which are generated by making one-half of the source aperture opposite in sign from the other half. This pattern is characterized by a deep null on the beam axis. The object being tracked or guided by the particular radar system has the characteristic direction of the null which is referred to as the boresight direction. The shift in the location of this null due to the addition of a radome to an antenna system is the radome boresight error. If the antenna is scanning in a particular direction and the boresight error is in the same direction it is defined to be a positive error.

In calculating the boresight error several considerations simplify the task. The null-shift is generally a fraction of a degree, thus making the calculation of only a small portion of the pattern necessary. Also, the pattern over a small interval enclosing the null is monotonically increasing on both sides of the null and approximately symmetrical. The null location is determined by computing one pattern point on each side of the null so as to enclose the null in a bracket. By use of the symmetry and monotone properties of the pattern the relative values of the two points calculated indicate which point is closest to the null. From this information a third point is calculated which halves the size of the bracket containing the null. Examination of the field magnitudes at each end of the new bracket now predicts the calculation of a fourth point which again halves the bracket containing the null. This process can be continued

indefinitely to obtain the null location to any desired accuracy. Starting with a two degree interval the null location will be known to within  $1/2^n$  degrees for  $n$  such calculations. In this analysis an  $n$  of 11 is used which gives an accuracy of 0.0005 degrees in the null location. Figure 4 illustrates a typical calculation.

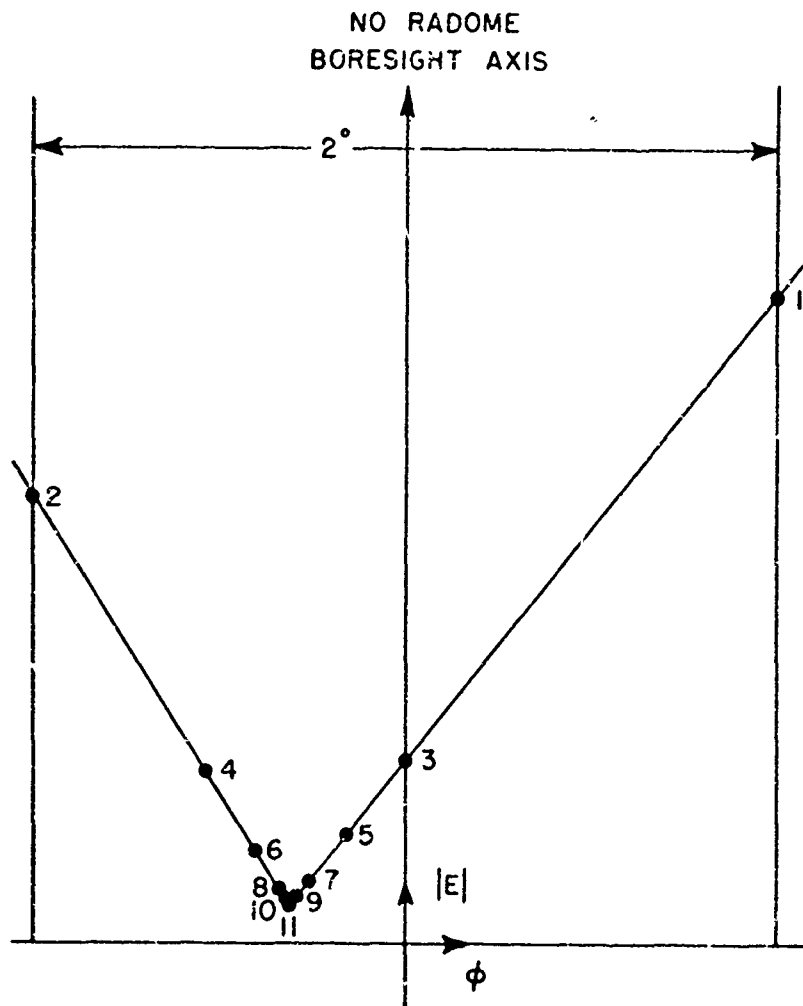


Fig. 4. Far-zone field points calculated to determine the null location for a monopulse difference pattern of an antenna-radome system. The order of the points calculated is indicated by the number.

### III. DISCUSSION OF COMPUTER PROGRAM

The computer program for the discussed calculations is composed of a main deck and several subroutines as illustrated in Fig. 5. The programs are written in Fortran IV language suitable for calculation on the two Ohio State University computers, the IBM 7094 and the IBM System 360/75. A brief description of the function of each routine follows.

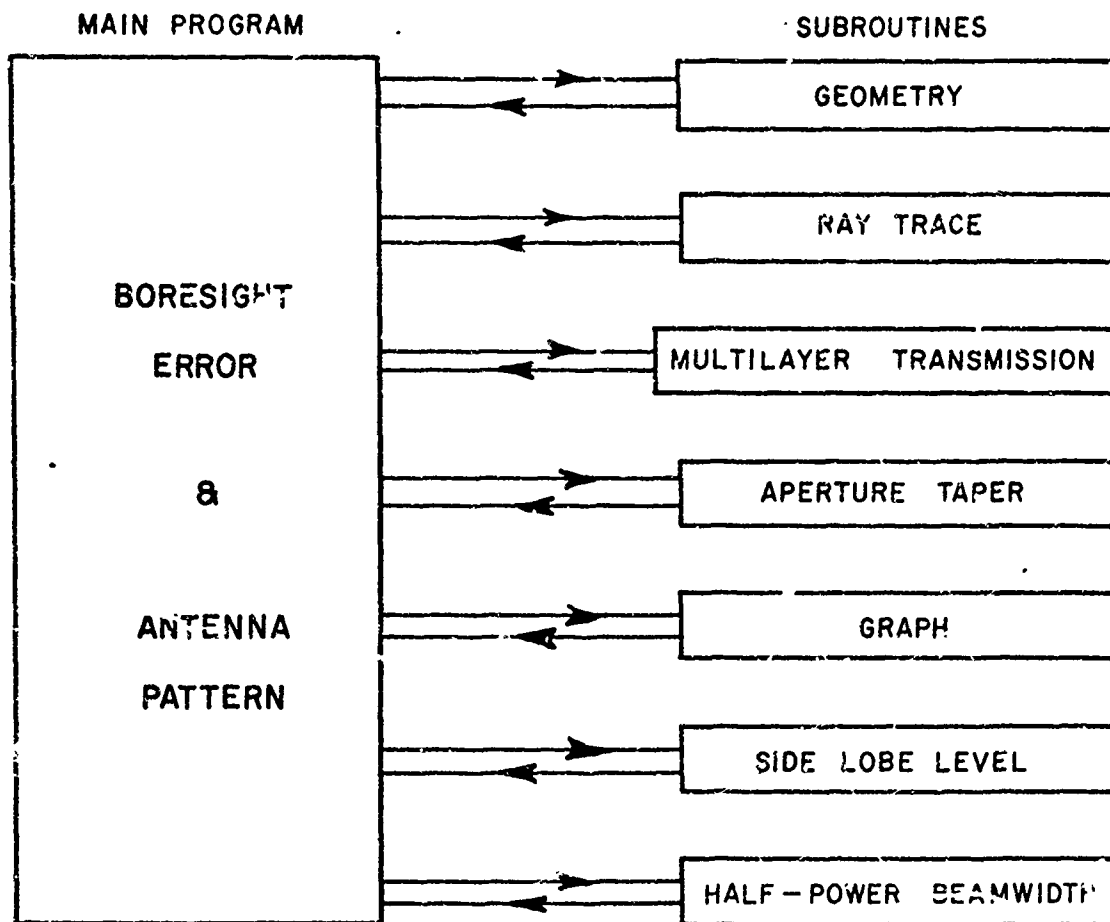


Fig. 5. Organization of computer program.

1. Main Program: Read in all pertinent data; call necessary sub-routines; calculate antenna patterns with and without radome; determines relative power transmission and radome bore-sight error as a function of antenna look angle.
2. Geometry: determines the set a, b, c, d, e, f of geometry coefficients for each of the n radome geometry sections.
3. Ray Trace: determines the boundaries between the n radome geometry sections; determines the  $n \times m$  matrix of incidence angles corresponding to the n geometry sections and the m rays.
4. Multilayer Transmission: determines the transmission coefficient and insertion phase delay for the  $n \times m$  matrix of incidence angles.
5. Aperture Taper: determines the amplitude and phase associated with each ray. Also calculates any aperture blocking or metal nosecap approximations.
6. Graph: calculates and plots the normalized far-zone power pattern in dBs with and without radome.
7. Sidelobe Level: calculates the level of the maximum sidelobe as a percent of main beam intensity and as dBs down from main beam intensity. Also calculates the location of the first sidelobe for the no-radome case and the power level at this location with the radome installed.
8. Half-Power Beamwidth: calculated the half-power beamwidth of the antenna-radome system with and without radome.

Switching from the main program to the desired subroutines is accomplished by means of two input cards named "title" and "source" which contain key words describing the type of calculation desired. For example, if "no" occurs in source (3), indicating that the no-radome case is to be calculated, the multilayer transmission subroutine is not called. Comment cards have been placed at the beginning of the main program which explain all of the options used. Also, most program variables are explained in this extensive set of comment statements.

Figure 6 is a functional flow diagram of the calculation. The significant definitions of terms used in this diagram are listed in Table I

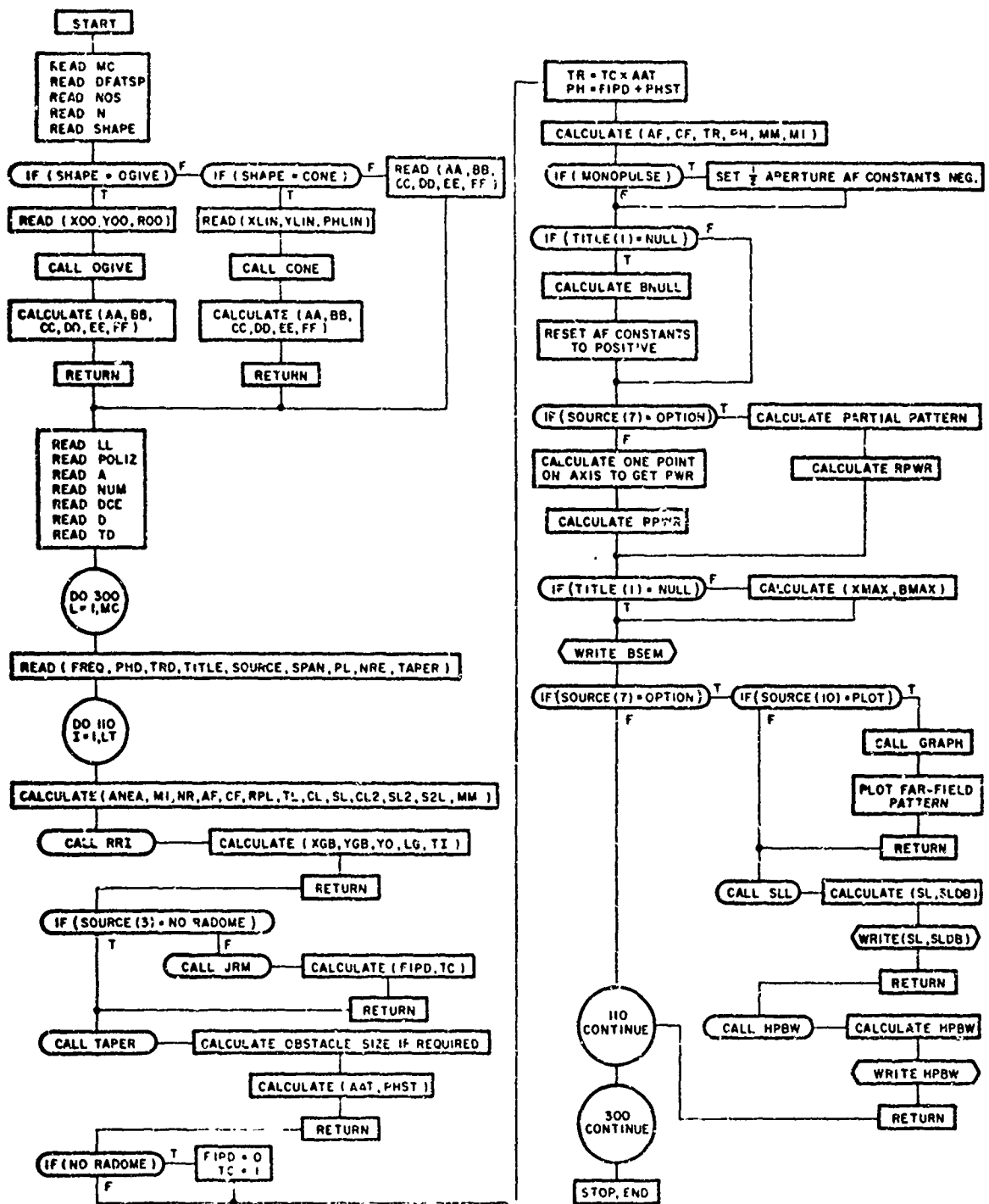


Fig. 6. Functional flow diagram of computer calculation.

TABLE I

MC	= Number of cases to be run
NCS	= Number of geometry sections
N	= Number of layers in each section
SHAPE	= Geometrical shape of each section
(XOO, YOO)	= Coordinates of center of an ogive section
ROO	= Radius of an ogive section
PHLIN	= Included half-angle of a cone section
(XLIN, YLIN)	= Any point on a conical section
AA, ...FF	= Geometry constants of Eq. (1)
LI	= Total number of look angles used
POLIZ	= Polarization
A	= Length of source aperture
NUM	= Number of points calculated in partial pattern
DCE	= Relative dielectric constant of a layer
D	= Thickness of a layer in inches
TD	= Loss tangent of a layer
FREQ	= Frequency in gigahertz
PHD	= Phase allowance used in numerical integration
TRD	= Transmission coefficient allowance
SPAN	= Angular range of pattern calculation
PL	= Look angle in degrees
RPL	= Look angle in radians
TAPER	= Definition of aperture taper used
LT	= Present value of LL
ANEA	= Number of equal length subapertures
MI	= ANEA
NRE	= Number of equal spaced rays
NR	= NRE-1
AF	= Fractional length of a subaperture of source
CF	= Phase-center correction for a subaperture
TL, CL, SL	= Tangent, cosine, sine of look angle
CL2, SL2	= Cosine, sine of twice look angle
S2L	= Sine-squared of look angle
MM	= Number of subaperture immediately below Y-axis (half-aperture subdivision point)
XGB, YGB	= Coordinates of geometry bounds between geometry sections
YO	= Y-coordinate of center of a subaperture
LG	= Number for a specific geometry section
TI	= Angle of incidence
NKRRI	= Ray trace subroutine
NKJRM	= Multilayer transmission subroutine
AAT	= Aperture amplitude taper

TABLE I (Cont.)

PHST	= Aperture phase taper
FIPD	= Insertion phase delay
TC	= Transmission coefficient
TR	= Transmission factor for a subaperture
PH	= Phase factor for a subaperture
RPWR	= Relative power normalized to no radome case
XMAX	= Pattern maximum
BMAX	= Angle at which XMAX occurs
BNULL	= Angle at which pattern null occurs
BSEM	= Boresight error in milliradians
SLL	= Sidelobe level in percent
SLDB	= Sidelobe level in dB
HPBW	= Half-power beamwidth in degrees

To indicate the execution time for various program calculations the following table is presented. 500 rays are used with a 4 section radome in all cases. IBM System 360/75.

TABLE II

<u>Calculation</u>	<u>Execution Time for 500 Rays</u>
Ray Trace	0.350 seconds
Multilayer	0.625 "
Taper	0.083 "
Average Aperture Distribution	0.025 "
Null	0.050 "
100 Point Partial Pattern	2.400 "
Plot 100 Pt Pattern	0.250 "
Combined Sidelobe and Half-Power Beamwidth	0.017 "

It is seen above that calculations which constitute one look angle can often be executed in less than one minute.

#### IV. ANALYSIS AND DESIGN OF ANTENNA-RADOME SYSTEMS

In this section several problems in antenna-radome system design will be investigated in order to demonstrate the use of the method as well as to point out its applicability to a wide range of problems. It should be emphasized at this time that all calculations are based on the two-dimensional model of the antenna-radome system and that the accuracy of the calculations is unknown. Verification of results is possible either by comparison with measurements or by comparison with results obtained using a more rigorous theory. As was stated earlier rigorous theories presently available are not easily applied if they can be applied at all. Therefore, whenever possible, results will be compared to measured data.

Two specific modern radome configurations will be used in most of the calculations to follow. The first radome is characterized as a half-wave-wall design having an ogival body with a hemispheric nose cap. The aft portion of the radome is conically faired to the associated missile body. Construction is entirely of pyroceram ( $\epsilon_r = 5.5$ ). The radome wall thickness is approximately one-half wavelength. The fineness ratio, which is defined as the ratio of the axial length to the base diameter of a radome, is 2.0. The second radome is derived from the first by removing the hemispheric nose cap and extending the ogive body to form a closed radome. All parameters remain the same with the exception of the Fineness Ratio which becomes 2.25. The choice of these two shapes will allow an evaluation of the effects of blunting the nose of a radome, which is frequently necessary because of aerodynamic heating at the radome tip. Some other radome configurations are analyzed which will be specifically described when considered. Some special design situations require modification of the basic method; these will be pointed out when necessary.

##### A. Convergence Of The Ray- Optics Solution

As was pointed out in Section II-C a ray tracing calculation has the property of converging to a fixed answer as the number of rays used is increased. This section presents calculations on two radome geometries to illustrate this convergence and to examine the number of rays required to obtain the convergent solution. Figure 7 shows the calculated boresight error versus the number of equally spaced rays used in the calculation for the pyroceram radome having an ogival body and a hemispheric nose cap. Two representative look angles are used to

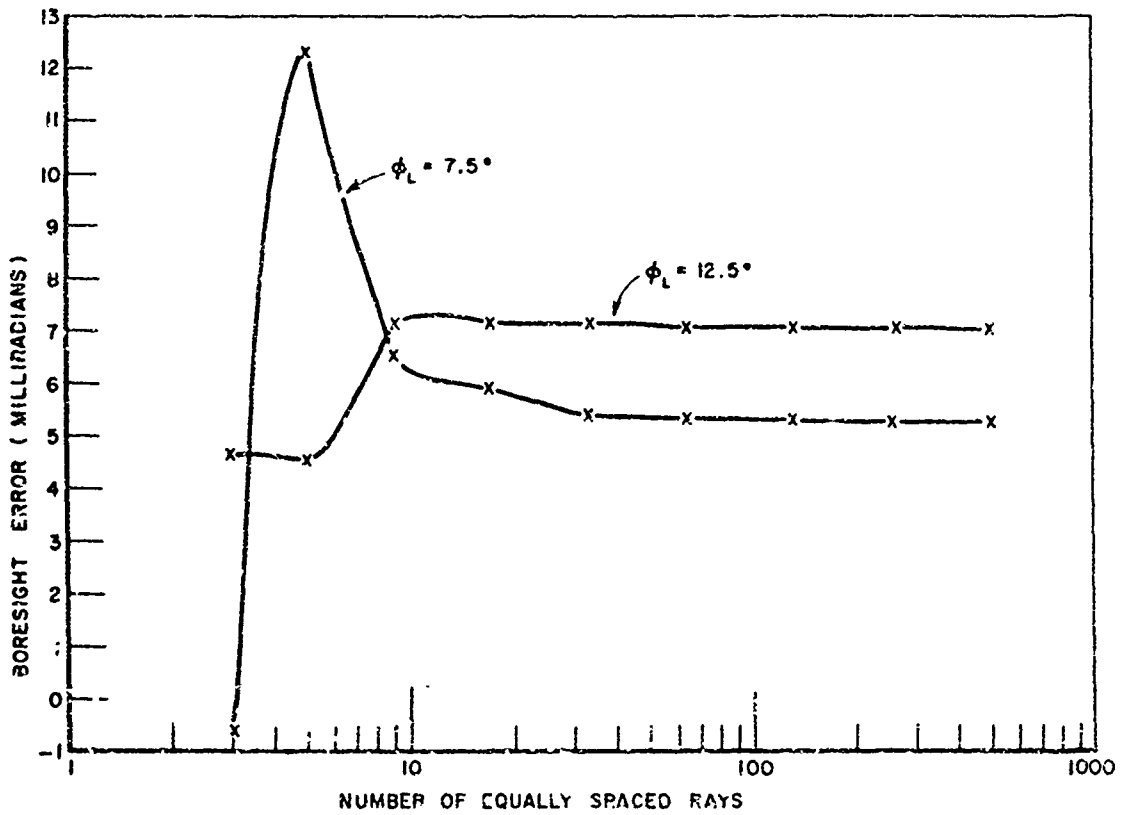


Fig. 7. Calculated boresight error vs. number of equally spaced rays at two representative look angle. Center design frequency and perpendicular polarization for the pyroceram ogive radome with hemispheric nose cap.

illustrate the convergence; complete tabulated data for this calculation at ten look angles are included as Appendix A. Figure 8 shows the same calculation for the radome with the nose cap removed and the ogive extended to complete the radome. Figure 9 shows the percent difference from the final answer for the 7.5° look angle case. It is seen that to obtain the convergent solution (0% error) a large number of equally-spaced rays is required. The presence of the nose cap is seen to have little effect on the convergence of the solution if more than 10 rays are used.

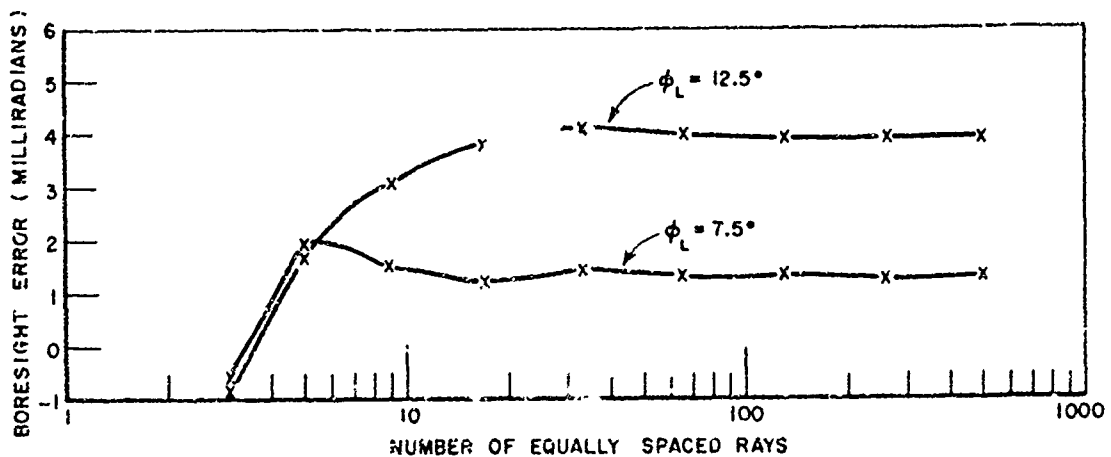


Fig. 8. Calculated boresight error vs. number of equally spaced rays at two representative look angles. Center design frequency and perpendicular polarization for the pyroceram ogive radome without hemispheric nose cap.

#### B. Numerical Integration Of The Reconstructed Aperture

This section demonstrates the convergence obtained using the numerical integration technique of weighted subapertures explained in Section II-C. 501 equally-spaced rays are used to represent the ten wavelength aperture used with the radomes of Figs. 7 through 9 in all of the following calculations. Boresight error (BSE), relative on-axis power (RPWR), and the number of weighted subapertures obtained (N) are calculated for various combinations of phase allowance (PHD) and amplitude allowance (TRD) in approximating the field over each subaperture by uniform amplitude and phase. Table III shows some representative calculated results with BSE and PHD in degrees. Appendix B gives the complete data for this calculation at ten look angles. The values obtained for 0 amplitude and  $0^\circ$  phase allowances are the same results obtained in Section A of this Chapter, i.e., the convergent answer from a large number of equally spaced rays. The number of aperture points indicated in the table are the number of subsections of the aperture which result for a given phase and amplitude allowance combination and indicate the relative time consumption for a computer pattern calculation. The table shows that the convergent answer is obtained using almost any of the given allowances - for the complete ogive radome the answer is obtained using as few as 7 subsections of the original 500 point aperture

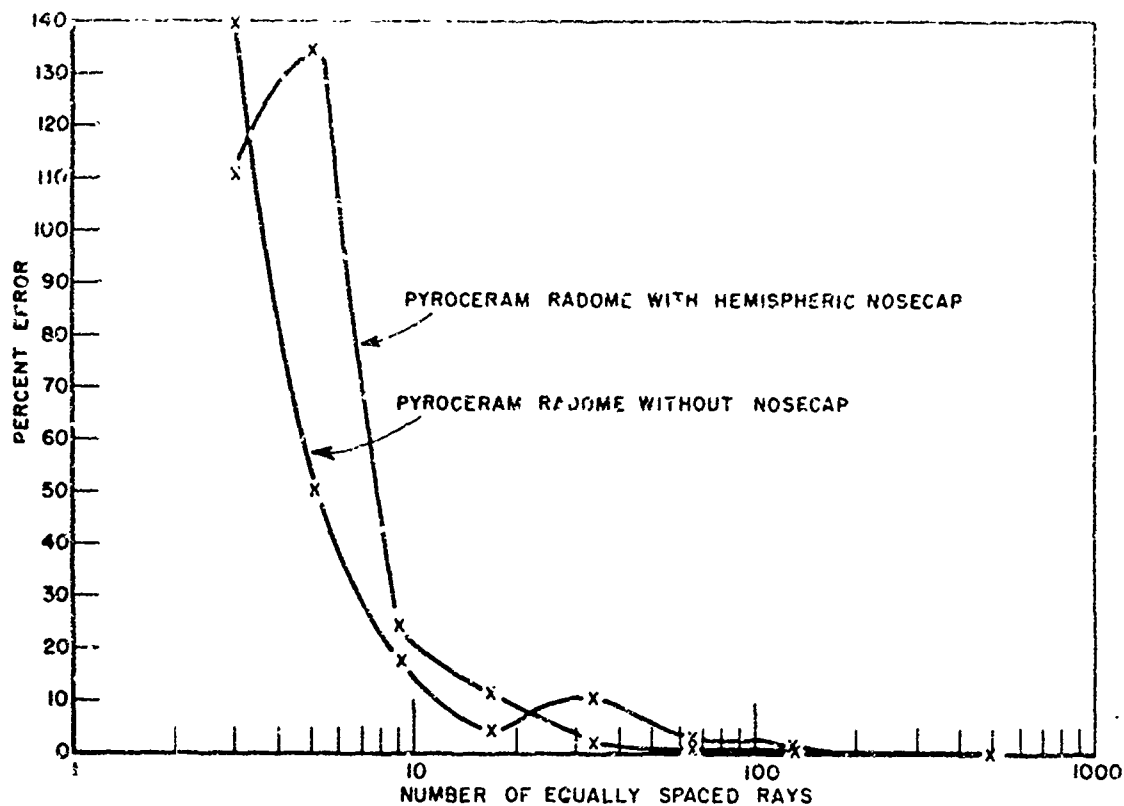


Fig. 9. Percent difference from convergent ray-tracing solution vs. number of rays. Perpendicular polarization at center design frequency. Look angle  $7.5^\circ$ .

approximation. With the large phase and amplitude allowances,  $30^\circ$  and  $0.2$  respectively, the error is still less than 2%. In calculations to follow an amplitude allowance of  $0.1$  and a phase allowance of  $3.0$  degrees are generally used. 501 equally spaced rays are used throughout since this number assures that the convergent solution can be obtained. The combined time consumption for tracing 501 rays and computing the associated values of  $|T|^2$  and IPD is only on the order of 1 second. As was pointed out earlier the significant computer time usage occurs in calculating pattern points. This is because each pattern point requires summing contributions from each aperture point used. For example using 500 equally spaced rays, 10 look angles, and calculating 100 points in the far-field pattern the total number of calculations is 500,000. If only 10 aperture points are used the number of calculations is reduced to 10,000 which is quite significant.

TABLE III  
 Boresight Error Obtained Using Various Amplitudes and Phase Allowances in Averaging  
 the Reconstructed Aperture Distribution Functions at 1.5° Look Angle. Pyroceram  
 Ogive With and Without Hemispheric Cap. Perpendicular Polarization

Phase Allowance	Amplitude Allowance	Boresight Error		Relative Power		No. of Aperture Points	
		Ogive	Ogive-Hemi	Ogive	Ogive-Hemi	Ogive	Ogive-Hemi
0	0.0	1.30	5.29	0.987	0.952	500	500
1.0	0.05	1.30	5.29	0.987	0.952	18	41
1.0	0.1	1.30	5.29	0.987	0.952	18	41
2.0	0.05	1.30	5.29	0.987	0.952	10	24
2.0	0.1	1.30	5.29	0.987	0.952	10	24
3.0	0.05	1.30	5.29	0.987	0.952	7	19
3.0	0.1	1.30	5.29	0.987	0.952	7	19
5.0	0.05	1.30	5.29	0.988	0.953	4	11
5.0	0.1	1.30	5.29	0.988	0.953	4	11
10.0	0.05	1.30	5.29	0.989	0.954	3	7
10.0	0.1	1.30	5.29	0.989	0.954	3	7
30.0	0.2	1.32	5.38	0.993	0.969	2	3

### C. Electrical Design Of A Radome Wall

The high speed attained using the two-dimensional analysis results in relatively low cost calculations. This allows the method to be used to advantage as a design tool. The approach is to select an approximate design in terms of the complex dielectric constants, wall thicknesses, number of layers, and geometrical shape. A specific parameter, for example wall thickness, is varied in small steps above and below the design specification. Calculations of desired electrical parameters, such as boresight error, transmission, sidelobe level, etc. are made at each incremental variation. Data are then compared to determine an optimum design. One such example follows.

Figure 10 shows the calculated boresight error for the pyroceram radome as a function of its wall thickness. The current design thickness is specified as 0 percent. From the curves it can be seen that for any look angle the boresight error approaches a low value in the range of -3 to -5 percent. Further, in this range the actual value of error for a given look angle remains relatively constant. This indicates that the radome would operate well in this region and show practically no change in error due to small frequency drifts, dimensional tolerances, or thermal gradients.

If we examine the curves near 0 percent or higher we find that the radome will be sensitive to the above three mentioned considerations and operate with significantly higher boresight error as well. Thus it appears that a 4 percent reduction in wall thickness would reduce the maximum boresight error by 50 percent. The on-axis transmission efficiency of the radome is calculated simultaneously with the boresight error in order that the effects of a design change on transmission can be observed. Figure 11 shows that decreasing the wall thickness by 4 percent causes a 14 percent net loss in transmitter power. This is probably not excessive in view of the improvement in boresight performance.

### D. Radome Boresight Error Versus System Bandwidth

If the calculated curves of Fig. 10 are correct, precise agreement between calculated and measured data in the region of design thickness (0%) is unexpected. A small dimensional error could easily cause a 15-20 percent change in boresight error. Figure 12 shows a comparison between calculated and measured data for the pyroceram radome. Agreement is only fair in this case. The frequencies in Fig. 12 correspond to the upper and lower frequencies of a 1.5 percent bandwidth design.

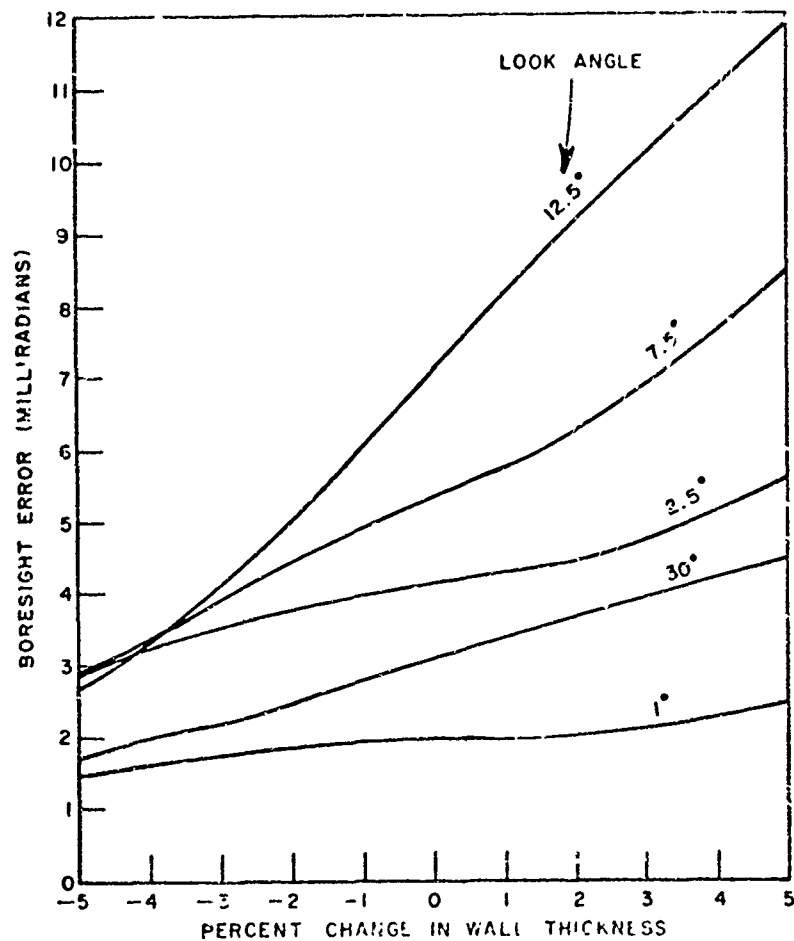


Fig. 10. Calculated boresight error for pyroceram ogive radome with hemispheric nose cap as a function of its wall thickness. Perpendicular polarization at design frequency.

#### E. Source Taper Effects

Many radar designs utilize carefully controlled amplitude tapers in order to achieve an antenna pattern having very low sidelobes. Phased array techniques available today emphasize this method. A study to determine the pattern distortion in terms of change in sidelobe level and half-power beamwidth due to the addition of a radome to such an antenna system was carried out. In addition, the effects of the use of an amplitude taper on the system boresight error characteristics were calculated. Two antenna-radome systems were analyzed, the pyroceram ogive radome with the hemispheric nose cap (blunted nose case) and the complete ogive

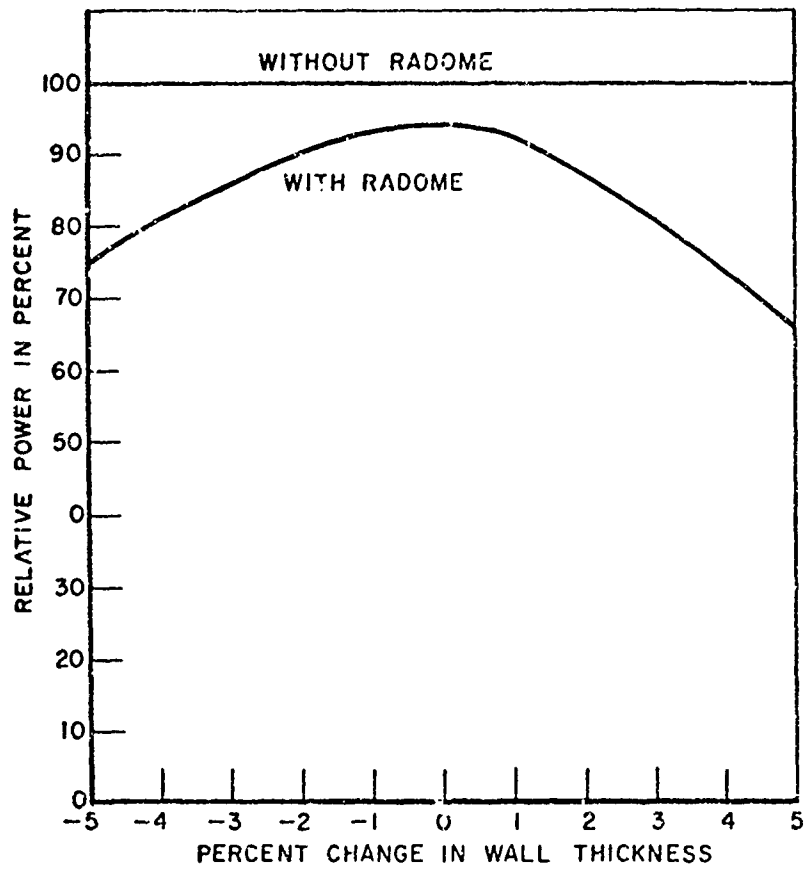


Fig. 11. On-axis transmission efficiency for pyroceram ogive radome with hemispheric nose cap as a function of its wall thickness. Perpendicular polarization at design frequency.

radome (pointed nose case). An identical antenna having a variable amplitude taper was analyzed for the two radomes. Particular emphasis was placed on the "cosine-squared on a pedestal" distribution since it provides a convenient method for varying the antenna pattern over a broad range of sidelobe levels. Also, this distribution is commonly used to achieve low-sidelobe pencil beam antennas.

Figure 13 shows the sidelobe level obtained using the two antenna-radome systems. The blunted nose radome is seen to degrade the antenna performance severely while the pointed nose radome produces inconsequential pattern distortion. All calculations were made at look angle  $0^\circ$  in order to emphasize the difference between the two systems. These calculations are corroborated to some extent by measurements performed

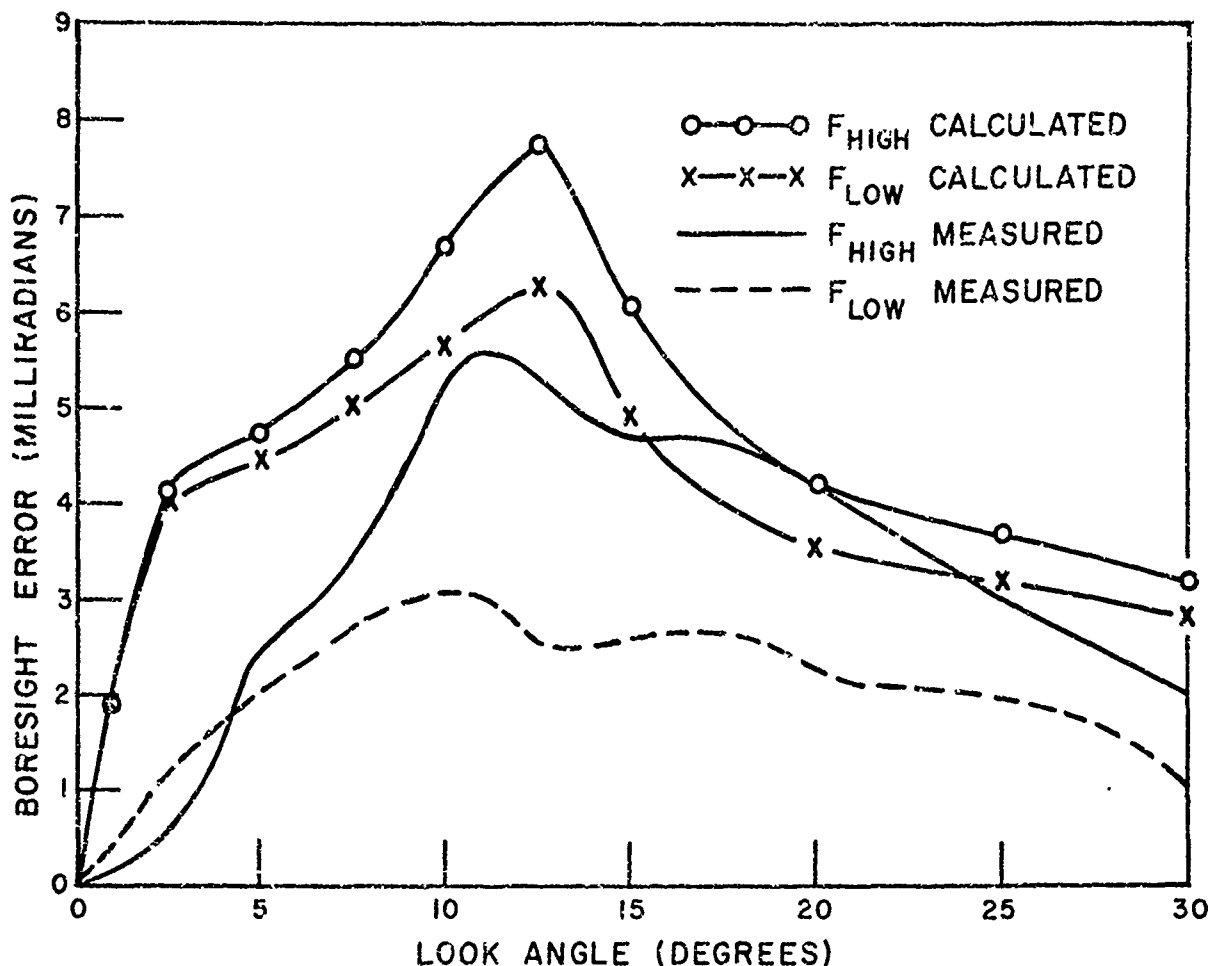


Fig. 12. Calculated and measured boresight error for pyroceram ogive radome with hemispheric nose cap.  $F_{HIGH}$  and  $F_{LOW}$  denote the two extremes of a 1.5% bandwidth design. Perpendicular polarization.

on a similar antenna-radome system by Styron and Hoots<sup>5</sup> of the Brunswick Corporation. They measured pattern distortion due to a blunted nose conical radome in terms of sidelobe degradation for three aperture tapers. They found that a basic 30 dB sidelobe antenna was reduced to an approximately 21 dB system and that the radome controlled the sidelobe level rather than the aperture taper. No similar set of measurements are available for the pointed nose radome, however, Styron and Hoots stated that the pattern degradation was most severe at offsets where the center antenna ray impinged near the radome nose and that for offsets further from the nose the degradation was minimal. This tends to verify the calculations for the pointed nose case.

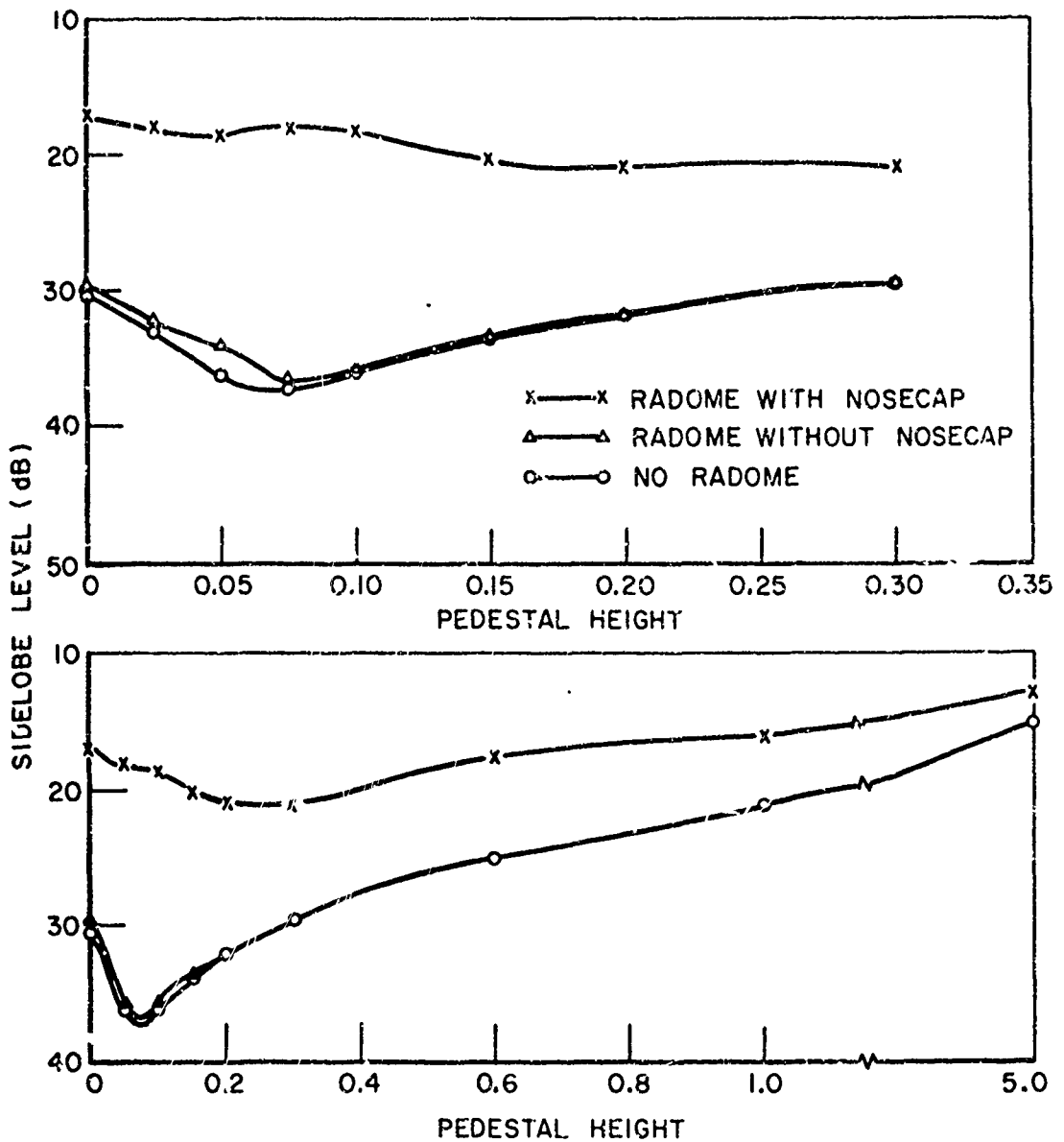


Fig. 13. Calculated sidelobe level for the pyroceram ogive radome with and without hemispheric nose cap. Look angle  $0^\circ$ , perpendicular polarization, design frequency. Aperture amplitude taper is cosine-squared on a variable pedestal.

Figure 14 shows that the half-power beamwidth is relatively unaffected by the presence of the blunt nose radome. Similar results were obtained for the pointed nose case.

Figures 15 and 16 show the effects of several amplitude tapers on the boresight error performance of the two antenna-radome systems. The blunted-nose radome is seen to have considerably poorer boresight performance when an amplitude taper is used. This may be attributed to the much smaller radius of curvature in the vertex region which causes considerable phase distortion in the aperture distribution. Also, since this ray-tracing analysis uses a collimated beam projecting from the source through the radome, it is likely that the resulting higher concentrations of energy near the vertex region tend to over-emphasize the effects of the vertex region. Thus the effects of the blunted nose on the

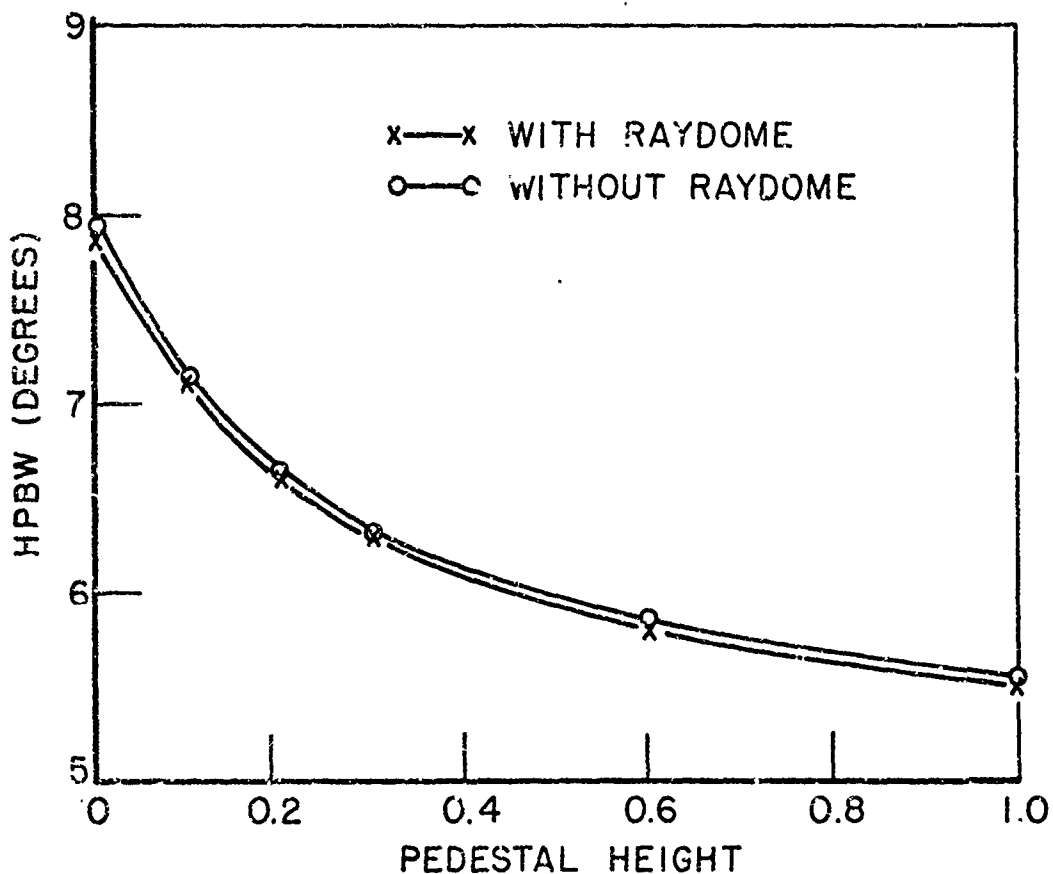


Fig. 14. Effect of an aperture amplitude taper on antenna-radome system bandwidth. Blunt nose pyroceram ogive radome, design frequency, perpendicular polarization.

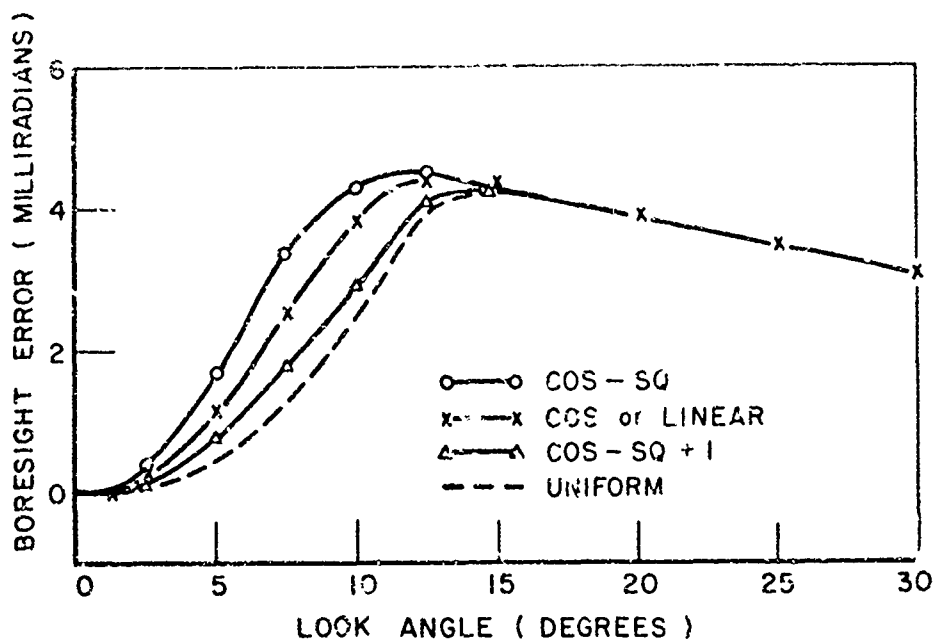


Fig. 15. Effects of several aperture amplitude tapers on system boresight error. Pointed nose pyroceram ogive radome, perpendicular polarization at design frequency.

radome are somewhat exaggerated. From the error curves it is seen that in both cases the more nearly uniform aperture distributions produce the lowest boresight error. The best boresight performance is obtained with the uniform distribution, however, the cosine-squared on a pedestal, or something similar, can be used for sidelobe control without seriously affecting the boresight performance. Measurements by Styron and Hoots<sup>5</sup> support the above calculations for the blunted nose radome case.

#### F. Aperture Blocking

In the two dimensional ray-tracing approximation a metallic portion of a radome, such as a protective rain-erosion cap, is treated as an aperture block. This requires specific changes in the computer program for two reasons. First, the perfectly collimated beam assumed in the ray tracing approach predicts that the effects of an obstacle in front of an antenna are independent of the distance between the obstacle and the antenna. The second problem is that the portion of the source aperture

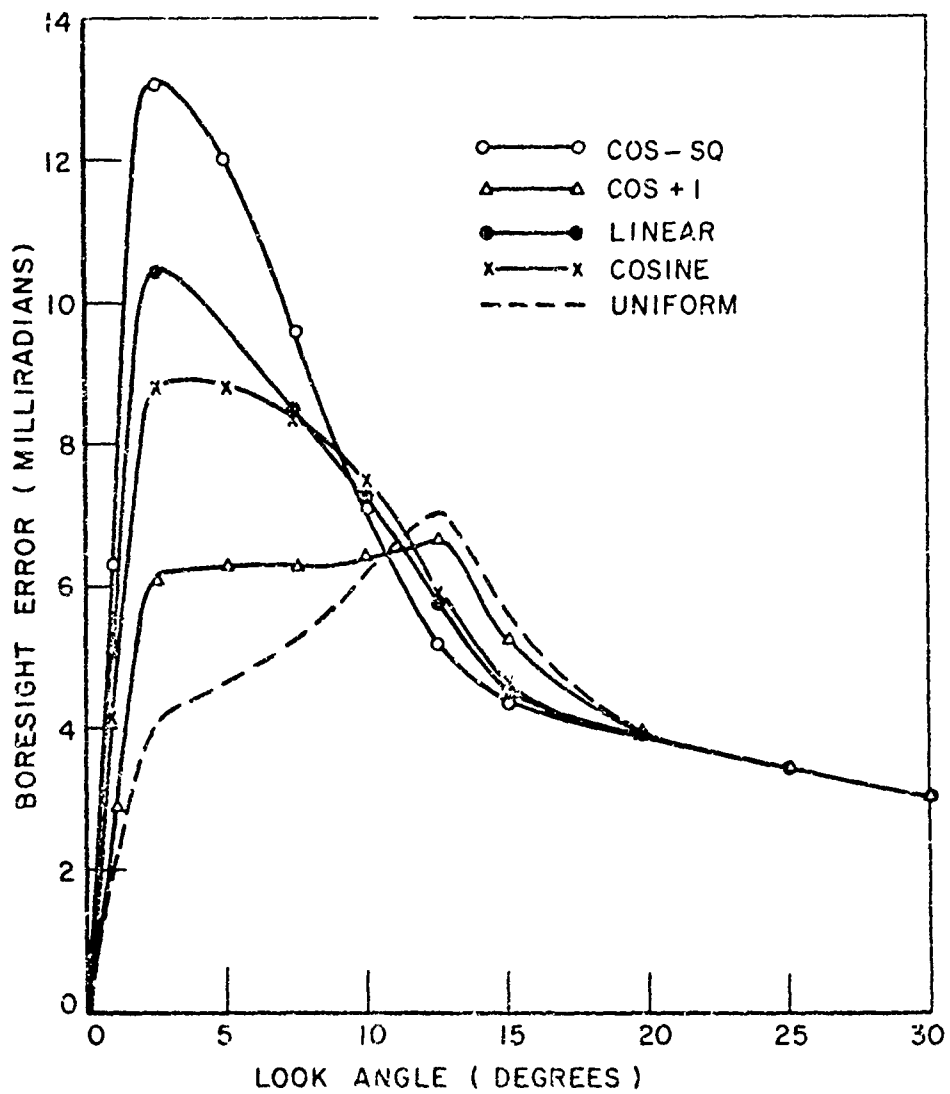


Fig. 16. Effects of several aperture amplitude tapers on system boresight error. Pointed nose pyroceram ogive radome, perpendicular polarization at design frequency.

blocked in the two-dimensional model is much larger than the actual area blockage in the three-dimensional problem. A study was made to determine a suitable two-dimensional representation of the three-dimensional block. Details of the specific treatment for aperture blocks are given below.

Figure 17 shows an aperture block of radius  $h$  located at a distance  $l$  from an antenna aperture of radius  $R$ . The source aperture is projected to the plane of the block using a divergence angle  $\theta_1$  equal to the half-power beamwidth to determine a projected aperture radius  $R'$ :

$$(19) \quad R' = R + l \sin \theta_1 \quad .$$

The ratio of the block area to the projected source area is calculated as:

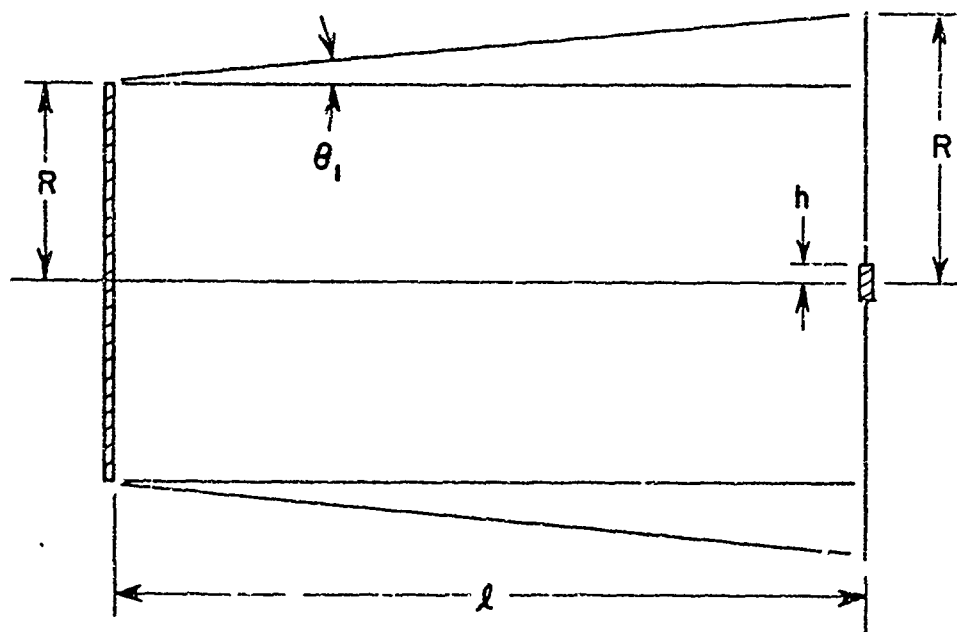


Fig. 17. Geometry for aperture blocking calculation.

$$(20) \quad \text{Ratio} = \frac{h^2}{(R + \ell \sin \theta_1)^2}$$

Equation (20) gives that fraction of the source area to be blocked out for any value of  $\ell$ . In the one-dimensional aperture approximation for a planar source the block is inserted at  $\ell = 0$  even though the block is located at  $\ell$ ; hence  $h$  must be reduced to account for the distance  $\ell$ . The effective blocked area at the source is:

$$(21) \quad A_{\text{BLOCKED}} = A_{\text{SOURCE}} * \text{RATIO}$$

which gives:

$$(22) \quad h' = \left( \frac{A_{\text{BLOCKED}}}{\pi} \right)^{\frac{1}{2}}$$

as the reduced length of the block. This is the approximate method used to account for the antenna-obstacle separation.

A second approximation is required because the one-dimensional block does not represent the two-dimensional block in the other dimension. Figure 18 shows that the blockage in the two-dimensional case represented by the one-dimensional block is a strip across the entire aperture. The approximation used here is to reduce the block length such that the resulting strip area is equal to the actual area of the block. In this way, even though the shapes of the aperture blocks differ, the source area blocked out is the same. With reference to Fig. 19, the strip area is:

$$(23) \quad A_{\text{STRIP}} = R^2 (\pi - \theta + \sin \theta)$$

where  $\theta$  in radians is given by:

$$(24) \quad \theta = 2 \cos^{-1}(y/R)$$

Using Eq. (21) we set  $A_{\text{STRIP}} = A_{\text{BLOCKED}}$ :

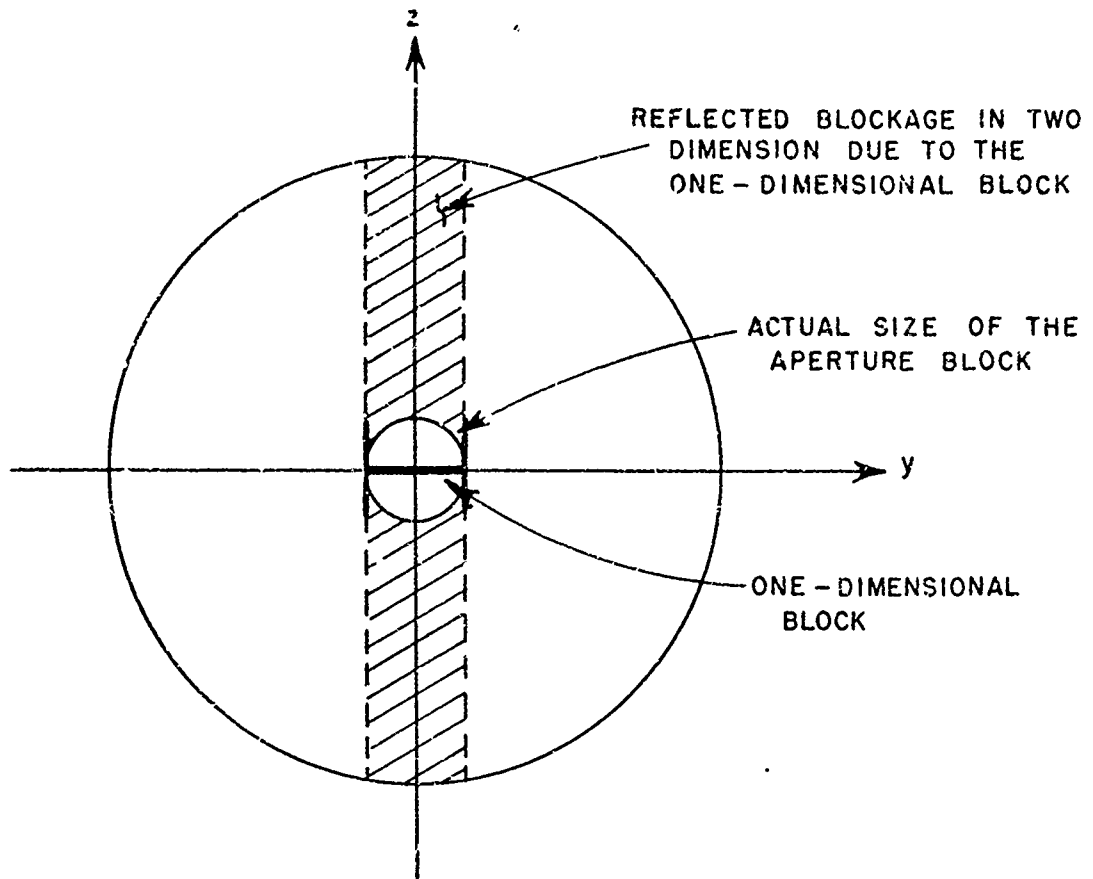


Fig. 18. Effective aperture blockage in two dimensions by a one-dimensional aperture block.

$$(25) \quad \pi R^2 \times \text{RATIO} = R^2(\pi - \theta - \sin \theta)$$

Removing the  $R^2$  terms and rewriting Eq. (25) in homogeneous form:

$$(26) \quad \theta - \sin \theta - \pi(1 - \text{RATIO}) = 0$$

This equation can be solved to any degree of accuracy using Newton's method

$$(27) \quad a_2 = a_1 - \frac{f(a_1)}{f'(a_1)}$$

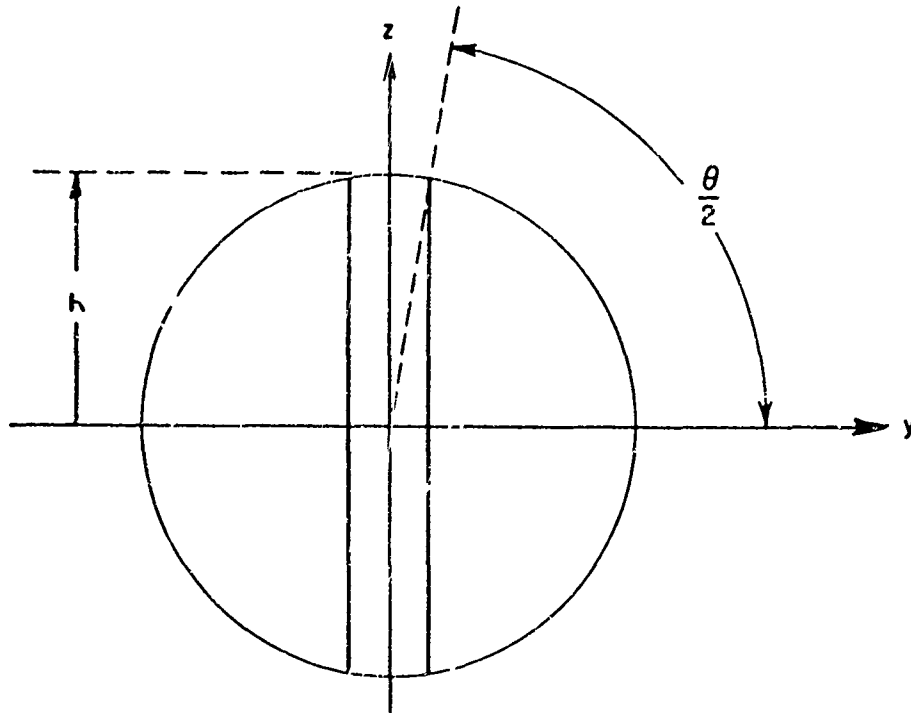


Fig. 19. Geometry used in calculating the area of a circular strip.

where  $a_1$  is an approximate solution of Eq. (26) which is  $f$  in Eq. (27). The value  $a_2$  is a better approximate solution than  $a_1$ . By iterating Eq. (27) we can obtain any desired accuracy in the approximation. Since most blocks are small a value of  $170^\circ$  is used for  $a_1$  in the program. In the problem being considered Eq. (27) takes the form

$$(28) \quad \theta_2 = \theta_1 - \frac{\theta_1 - \sin \theta_1 - \pi(1 - \text{RATIO})}{1 - \cos \theta_1}$$

The resulting block width in the one-dimensional aperture approximation using this approximation is:

$$(29) \quad h'' = 2 R \cos(\theta/2)$$

where  $\theta$  is the angle associated with the strip as shown in Fig. 19.

In order to determine the accuracy obtained using the above two-dimensional aperture blocking approximations some sample calculations were made and compared to the calculated and measured aperture blocking results of Collier.<sup>6</sup> In his report Collier used a  $16.4\lambda$  parabolic dish having a  $2.2\lambda$  diameter feed located  $2.2\lambda$  in front of the aperture plane. He considered obstacles ranging in size from  $3.4\lambda$  to  $9.7\lambda$  which could be positioned from  $20\lambda$  to  $100\lambda$  from the aperture plane. The frequency was 32.7 GHz. The medium sized obstacle of  $4.7\lambda$  was chosen for comparison here. Collier used a severe radial taper, as shown in Fig. 20, to represent the antenna aperture distribution. The central amplitude of zero was used to account for the aperture blocking due to the feed. The measured pattern reported showed an approximately  $5^\circ$  beamwidth and 16.5 dB sidelobes. This taper was represented here by a piecewise linear approximation with the exception that the curve was extended to 10 at the origin and the feed treated as a separate aperture block. The calculated pattern using

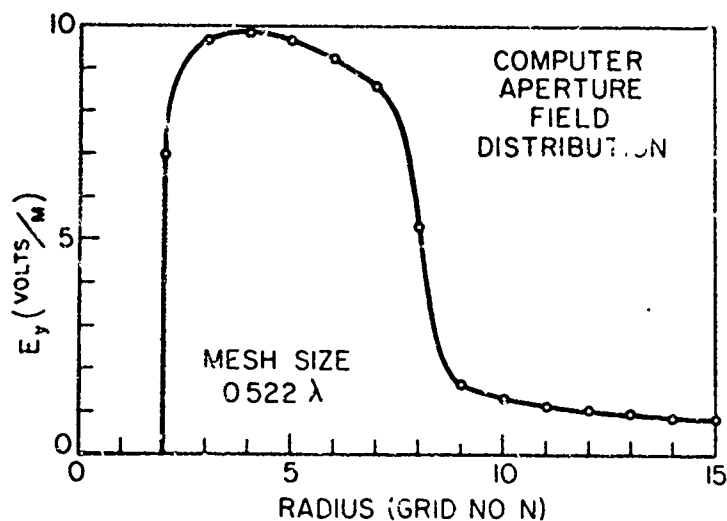


Fig. 20. Aperture amplitude taper used in Collier aperture blocking calculation.

the two-dimensional approximations showed a beamwidth of  $5.29^\circ$  and a sidelobe level of 16.32 dB which is in excellent agreement with Collier's measurements. Figure 21 shows the calculated sidelobe level for the antenna in the presence of the obstacle as a function of aperture-obstacle separation. The modified two-dimensional model generally shows very good agreement with measurements and with the three-dimensional calculations.

### C. Electrical Performance Of A Radome In A Hyper-Environment

Due to the high speed of modern aircraft and missiles, radomes are often subjected to severe environments. Nonuniform temperature distributions exist about the radome wall which result in variations in the temperature dependent quantities of dielectric constant, loss tangent, and wall thickness. The variations in these quantities alter the

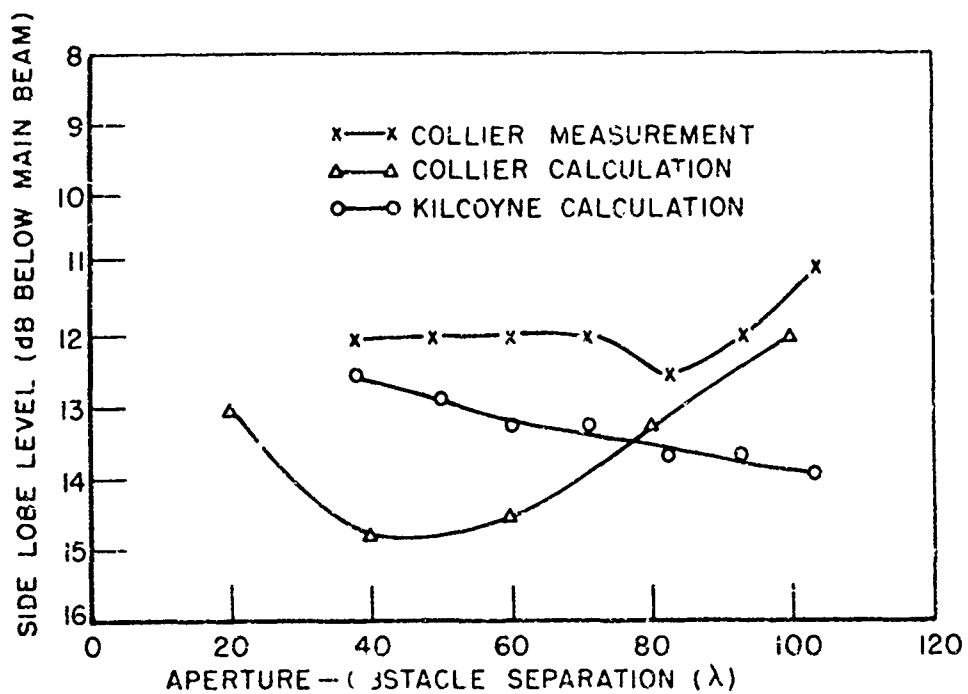


Fig. 21. Comparison of calculated sidelobe level by two-dimensional approximate method with three-dimensional calculations and measurements.

boresight error performance of the antenna-radome system. Figure 22 shows a representative temperature profile which a radome may encounter. The boresight error characteristics of the pyroceram radome having a hemispheric nose cap were calculated for this temperature profile as an example. To approximate the effects of the temperature profile, the radome is subdivided into several sections, each of which has a fixed set of dielectric constant, loss tangent, and wall thickness parameters. The subdivision is determined by observing the rate of change of these parameters with temperature and the rate of change of temperature along the radome wall. References 7 and 8 were used for this purpose. Figure 23 shows the calculated boresight error in the presence of the temperature profile of Fig. 22. Figure 24 shows a similar set of curves with the original wall thickness reduced by 1.5%. These results indicate that the boresight error performance of the radome may actually improve in a severe thermal environment. The effect of the temperature profile in this case is seen to be similar to the design technique of constructing a tapered radome wall to improve radome performance.

As shown in Fig. 22 there is a temperature gradient from the outside to the inside of the radome wall. In the above example the temperature was assumed to vary linearly with distance through the wall. In case there is a nonlinear variation in temperature or parameter constants as a function of temperature through the wall, a further approximation consisting of subdividing each section into several layers having variable parameters can be used. Thus the final subdivision of the radome in this case would be one of several geometry sections having differing numbers of layers.

#### H. Comparison Of Boresight Measurements And Calculations

Boresight calculations using the ray tracing method described in this report are compared in this section with measured data supplied by The U.S. Naval Air Development Center at Johnsville, Pa. and with calculations and measurements taken from the literature. Exact radome geometry was not always known in the following cases, hence some comparisons were made on the best estimate basis.

##### Case 1

The previously described half-wave wall conically-faired ogive radome with a hemispheric nose cap is examined here. A constant wall thickness of pyroceram ( $\epsilon = 5.5$ ) was used throughout. Calculations and

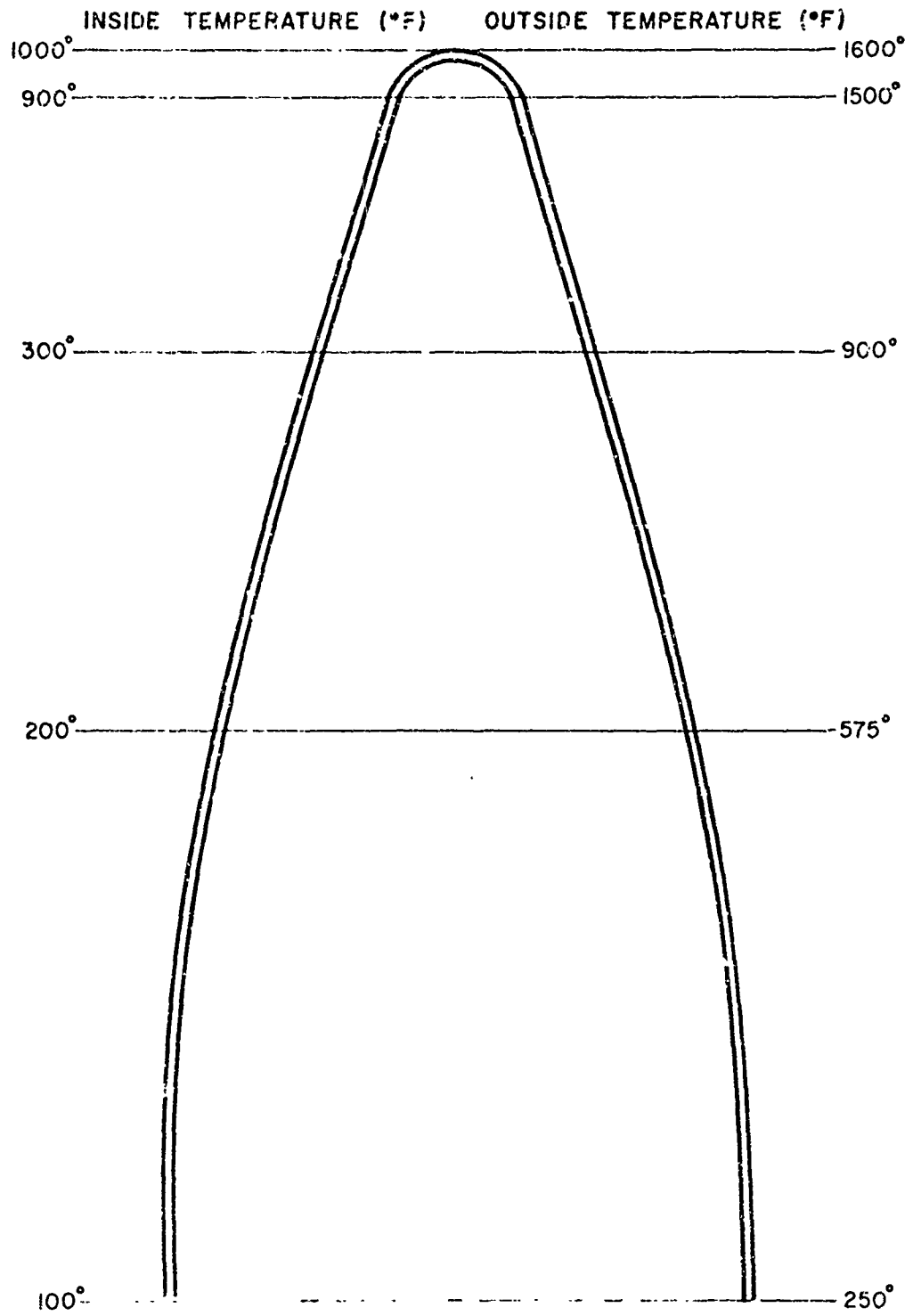


Fig. 22. Temperature profile used to simulate the case of a radome operating in a hyper-environment.

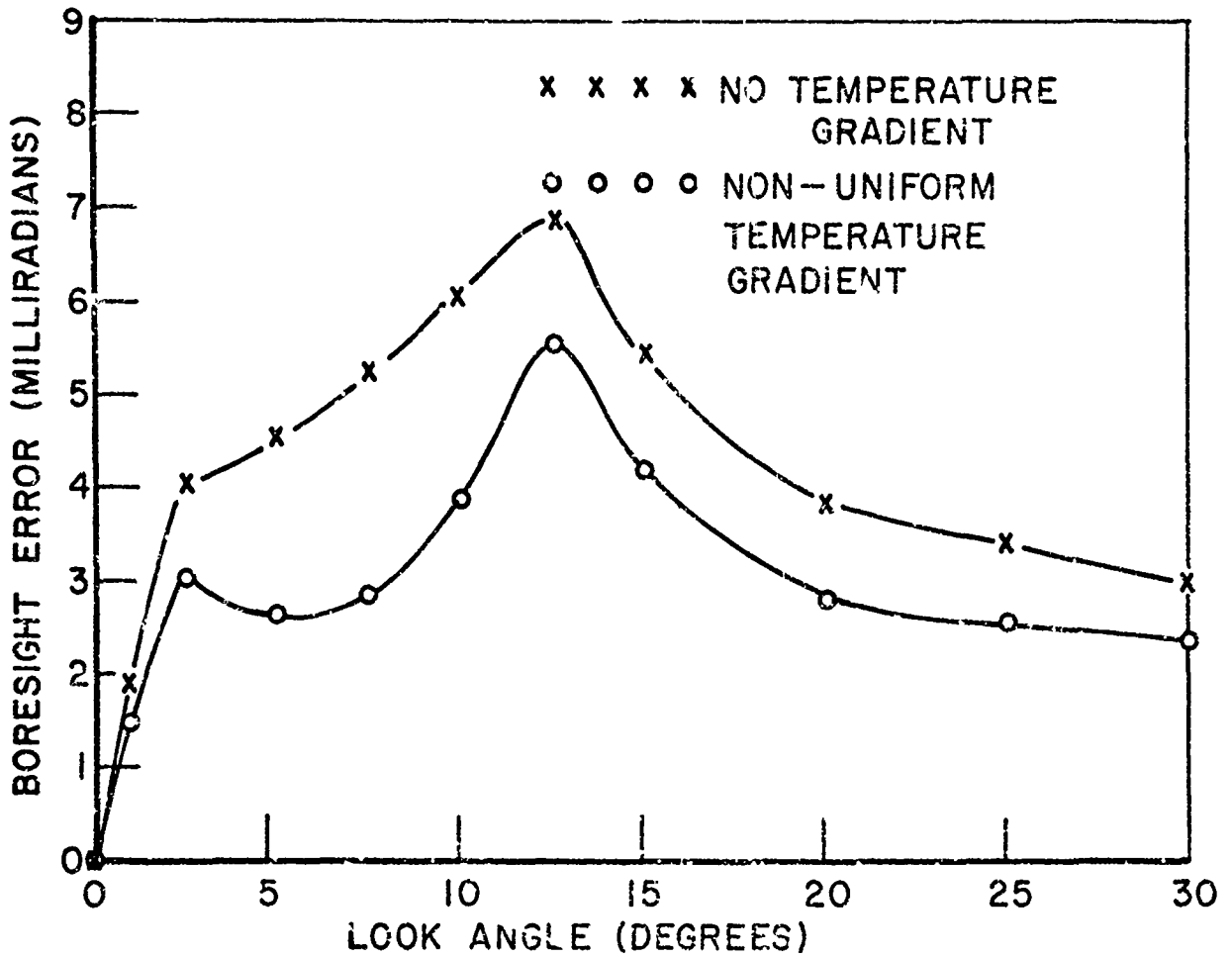


Fig. 23. Calculated boresight error for blunt-nosed pyroceram ogive radome in the presence of the temperature profile of Fig. 22. Perpendicular polarization at design frequency.

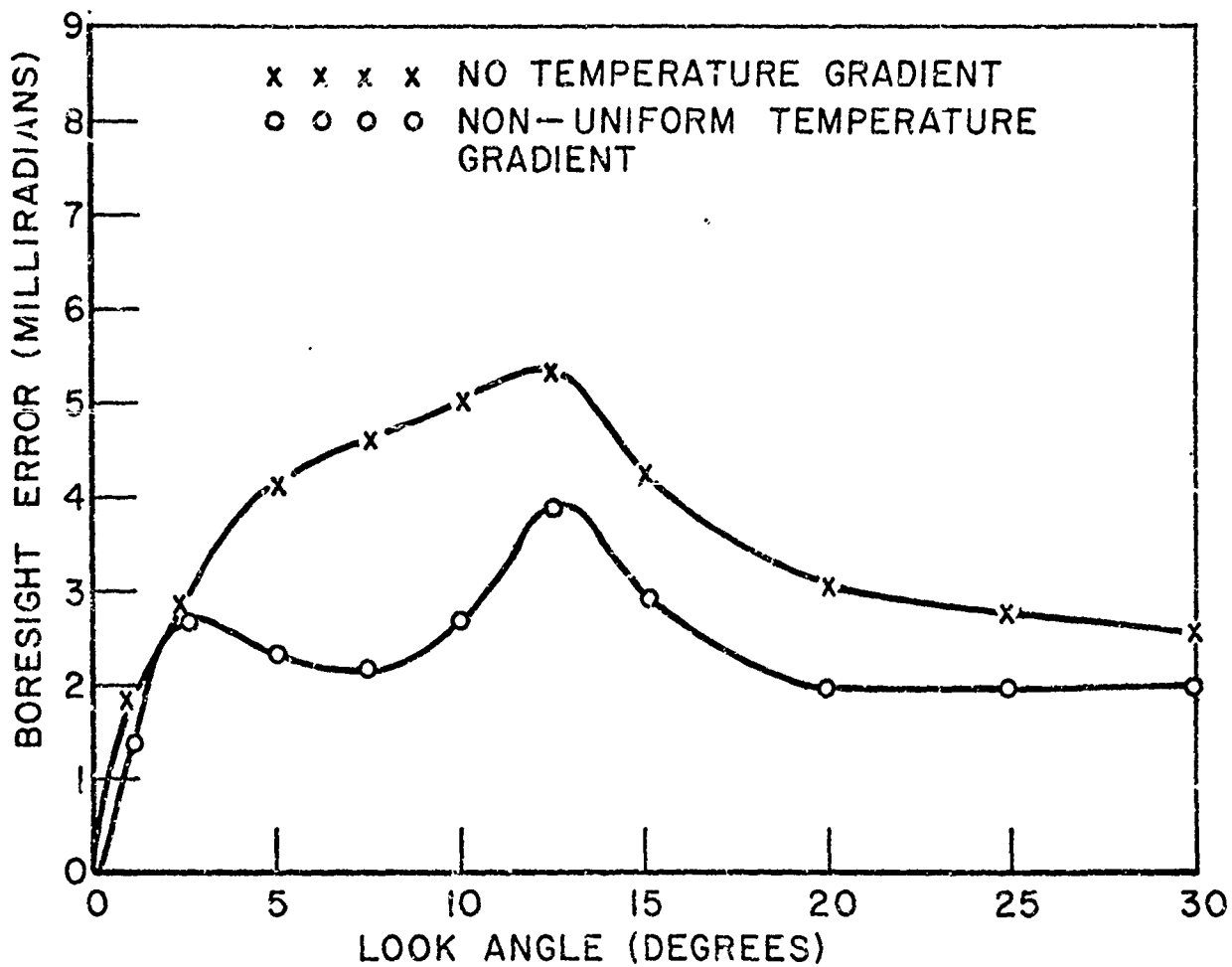


Fig. 24. Calculated boresight error. Same case as Fig. 23 with radome wall thickness reduced by 1.5%.

measurements at the high, low, and center frequencies of a 1.5% bandwidth design were made for both perpendicular and parallel polarizations. Two sets of measurements were furnished by the USNADC;<sup>9,10</sup> both of which are included in the comparisons to give an indication of experimental deviations. This deviation is generally a result of a lack of symmetry in the radome. Figures 25 and 26 show the comparisons between calculations and measurements for perpendicular and parallel polarization at the low frequency end of the band. Agreement between calculation and measurement is reasonably good for the perpendicular polarization case, however, the agreement is poor for parallel polarization. Figures 27 and 28 give the same comparisons for the design frequency. Perpendicular polarization shows very good agreement in this case while agreement remains poor for parallel polarization. Figures 29 and 30 show the comparison for the high end of the frequency band. Agreement is also very good for the case of perpendicular polarization and poor for parallel polarization.

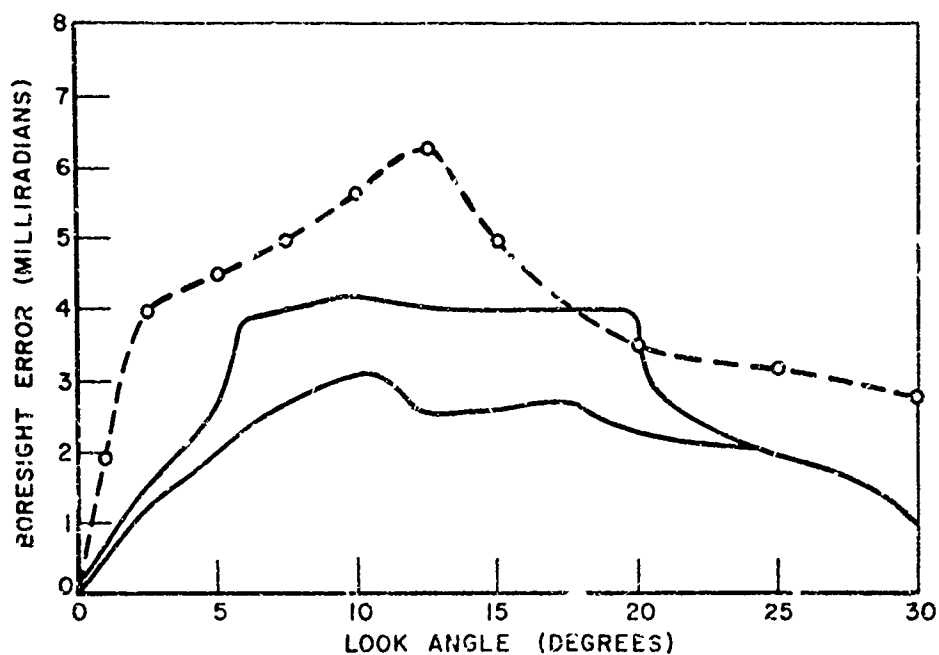


Fig. 25. Calculated and measured boresight error for a blunted-nose pyroceram ogive radome at the lower limit of a 1.5% bandwidth design. Perpendicular polarization.

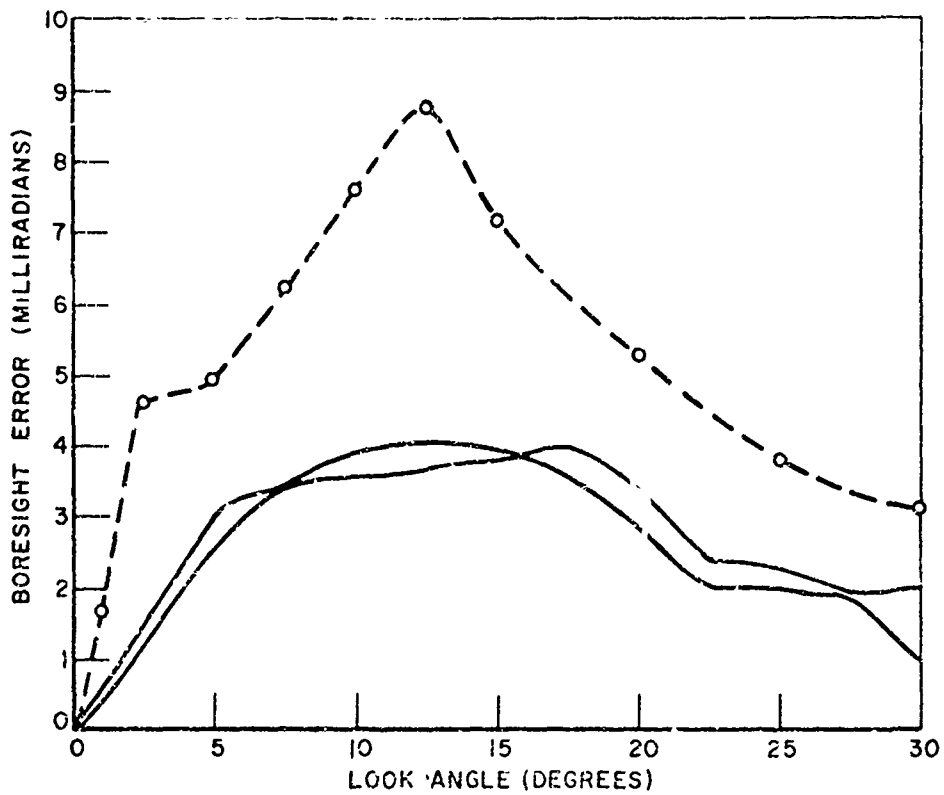


Fig. 26. Calculated and measured boresight error for a blunted-nose pyroceram ogive radome at the lower limit of a 1.5% bandwidth design. Parallel polarization.

Case 2

This comparison uses the same radome geometry as in Case 1 except that the construction is of polyimide ( $\epsilon = 4.2$ ). Measurements and calculations at the design frequency for perpendicular and parallel polarizations are shown in Fig. 31. Agreement is good for both polarizations in this example. Measurements were furnished by USNADC.<sup>10</sup>

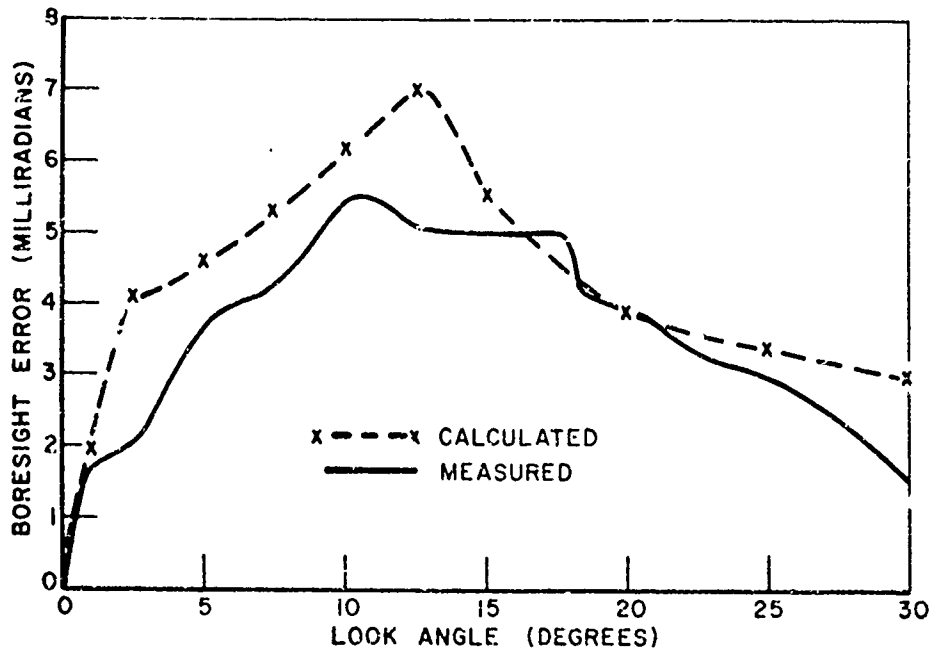


Fig. 27. Calculated and measured boresight error for a blunted-nose pyroceram ogive radome at the design frequency. Perpendicular polarization.

### Case 3

This comparison uses a radome having basically the same construction as in Case 1, i.e., conical fairing, ogive body, and hemispheric nosecap. The main body of the radome was constructed of polyimide ( $\epsilon = 4.2$ ). A rain erosion cap of alumina ( $\epsilon = 8.9$ ) was sprayed on the tip end of the radome extending back six inches. Exact dimensional data was unavailable for this case, therefore, estimates were made as to the probable design. Calculations of boresight error (BSE) and transmission efficiency ( $|T|^2$ ) were made at the probable design thickness and at  $\pm 2.5\%$  and  $\pm 5\%$  increments about this design thickness. In the region of the alumina nosecap the main body of the radome was assumed to be of thinner wall to adjust for the increased dielectric constant of the cap material. The source of measured data was a report by The Brunswick Corporation.<sup>11</sup> Reference 11 also stated that the radome had been "corrected" - which amounts to adding patches of dielectric material to the radome inner wall to locally alter the phase shift value through the wall. Thus the geometry is relatively uncertain. High and low frequency

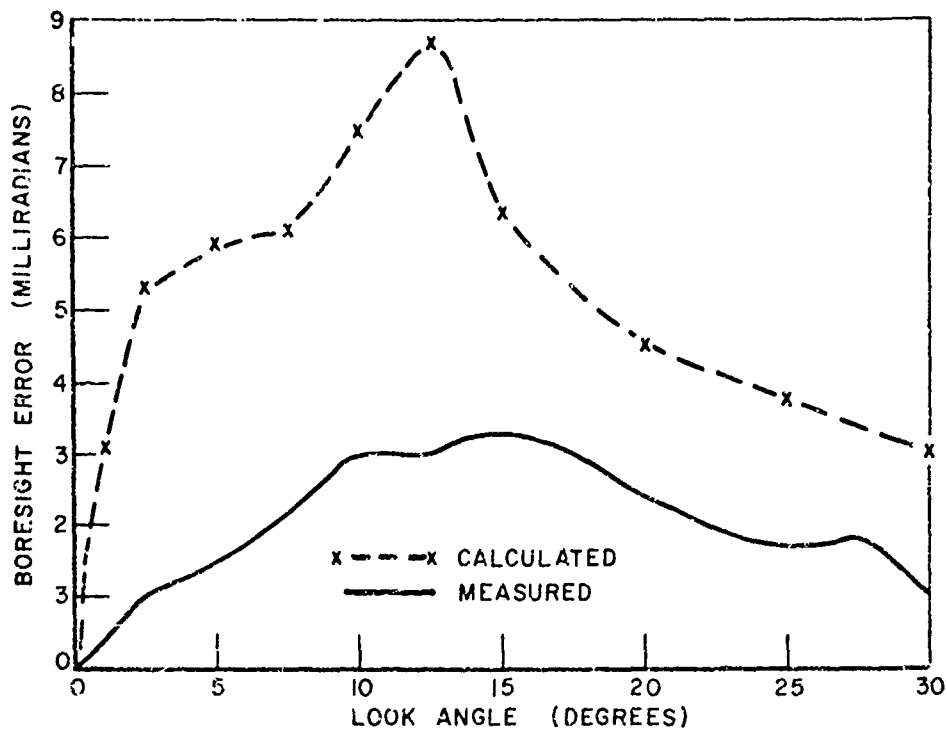


Fig. 28. Calculated and measured boresight error for a blunted-nose pyroceram ogive radome at the design frequency. Parallel polarization.

calculations were made at perpendicular polarization since these corresponded to the reported measurements. Figures 32 and 33 show the high and low frequency boresight error calculations for the estimated geometrical construction compared to the measurements reported in Ref. 11. Measurements were made at several roll angles resulting in the spread of value shown by the shaded portions in Figs. 32 and 33. Agreement was not expected to be good in this case, however, considering the assumptions required, agreement is satisfactory. The general shape of the curves, i.e., the initial negative error at small look angles and the shift to positive error at larger look angles is predicted. The amplitude of the negative swing is considerably larger than the measurement, however, the positive error amplitude is in good agreement with the measurements. This could be explained by the "correction" performed

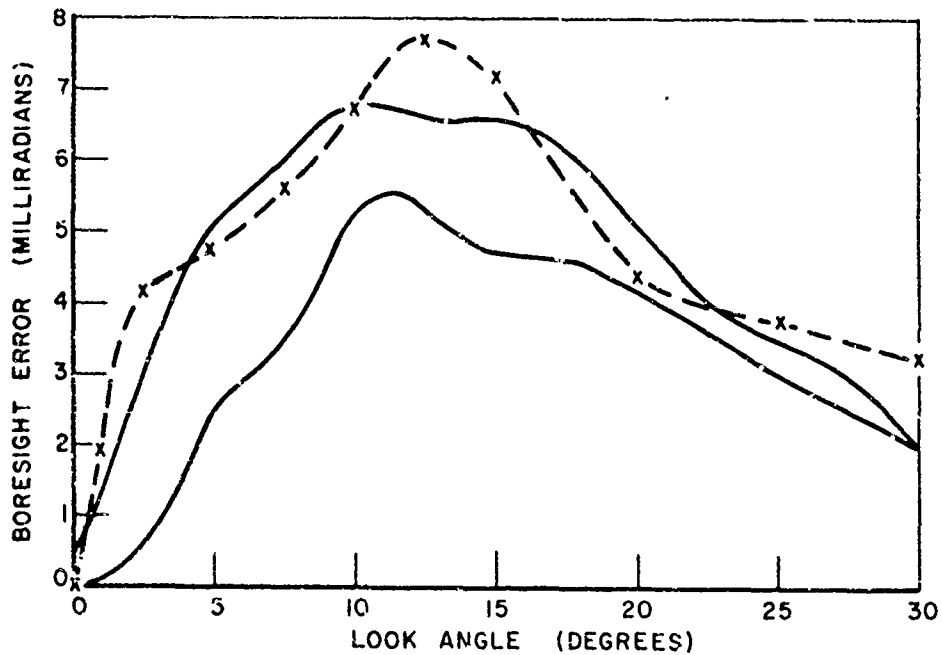


Fig. 29. Calculated and measured boresight error for a blunted-nose pyroceram ogive radome at the upper limit of a 1.5% bandwidth design. Perpendicular polarization.

on the radome as mentioned above. Using the main body (aft of the nose cap) wall dimensions corresponding to Figs. 32 and 33 as a base the radome error was then calculated at  $\pm 2.5\%$  and  $\pm 5\%$  of this value with the nose dimensions held constant. In all cases the rain erosion cap was taken to be 0.030 inches thick. Figures 34 and 35 show these calculations compared to the measurements. Excellent agreement between calculations and measurements is obtained for the  $+2.5\%$  case indicating that this wall thickness is probably closer to the actual value than the original assumed value. Another view of this same data is shown in Fig. 37 which indicates that  $+2.5\%$  is about optimum for a boresight error design point. The computer program simultaneously calculates transmission efficiency with boresight error. Figure 37 shows the

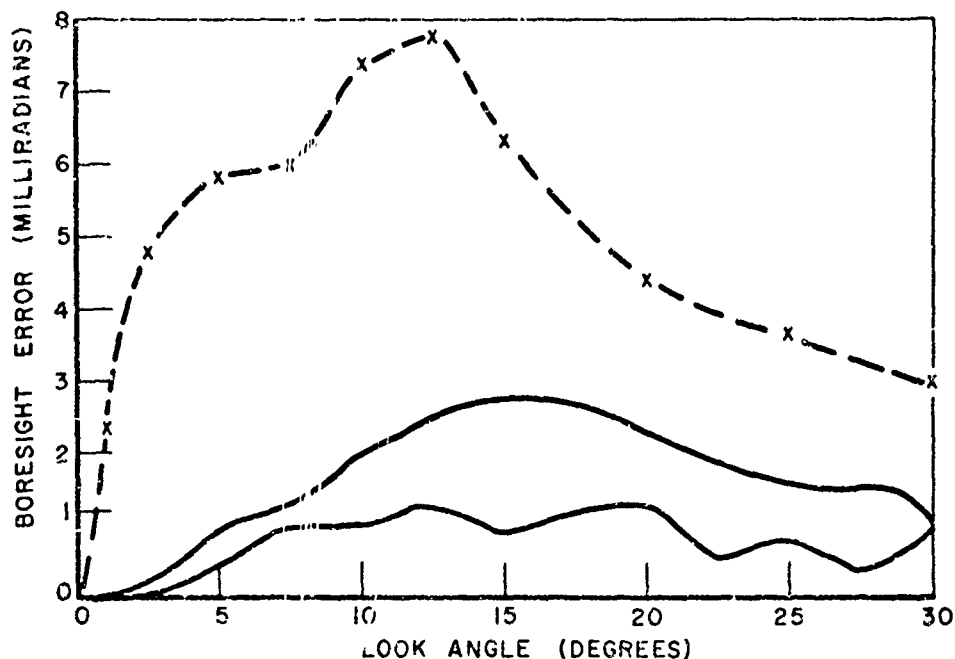


Fig. 30. Calculated and measured boresight error for a blunted-nose pyroceram radome at the upper limit of a 1.5% bandwidth design. Parallel polarization.

$|T|^2$  curves which correspond to Figs. 33 through 36. Since radomes of this type are frequently designed for maximum transmission, the indication is that the design wall thickness was + 2.5% or more above the assumed value.

#### Case 4

Several radome body geometries previously analyzed by General Dynamics are examined. Calculations of boresight error are made and compared to similar calculations by G.P. Tricoles of General Dynamics Corporation, San Diego, California.<sup>12</sup> Since Tricoles uses a different ray-tracing calculation these comparisons are presented merely to show similarities and disagreements between the calculated results. Table IV indicates the geometrical differences among the

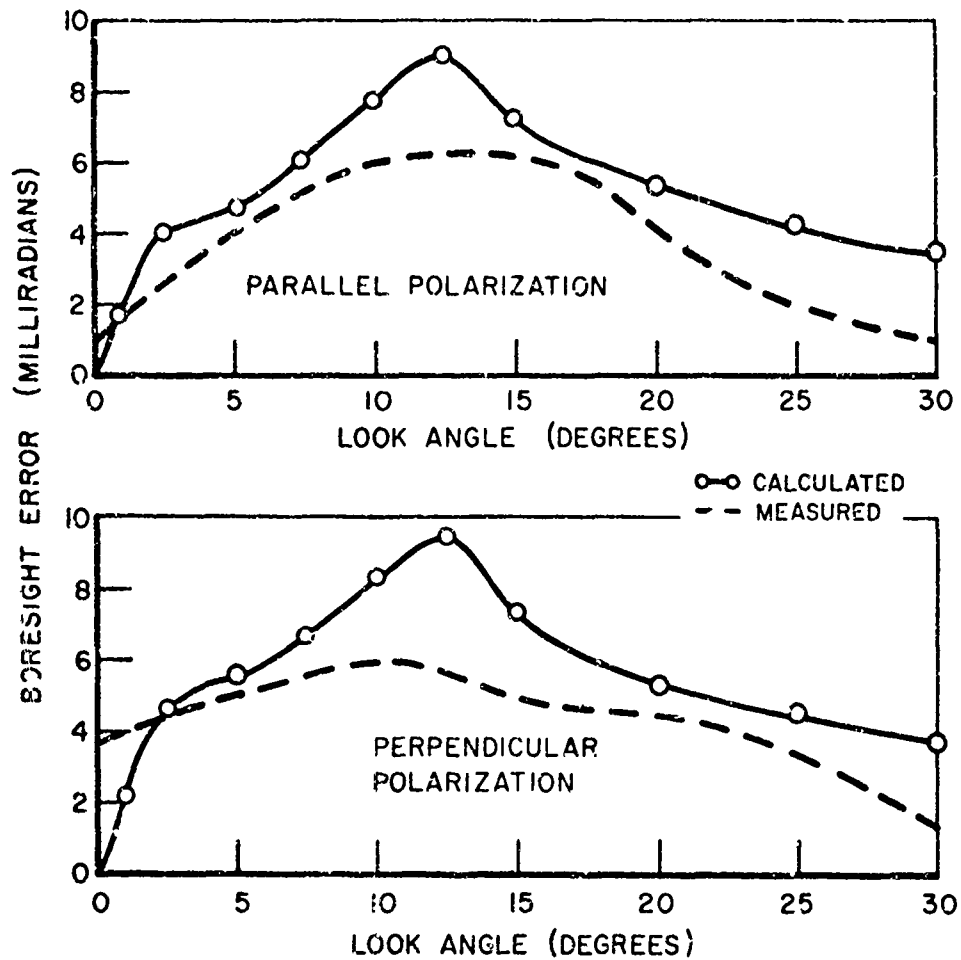


Fig. 31. Calculated and measured boresight error for a blunt-nose polyimide radome at the design frequency.

various radome configurations. Table V follows the radome curves to indicate the general agreement between the two calculations. The comparisons are given for the several configurations at the high and low ends of a 1.5% bandwidth for perpendicular and parallel polarizations in Figs. 38 through 51.

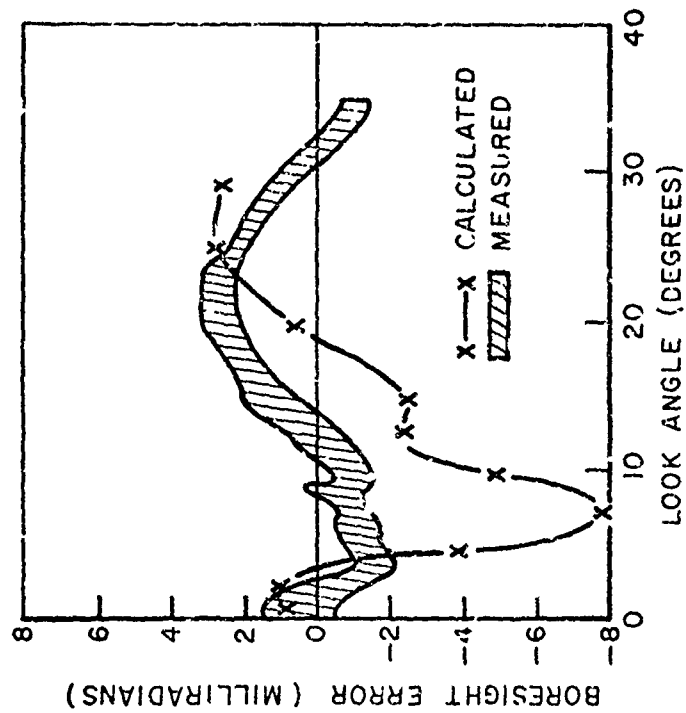


Fig. 33. Comparison between measurements and calculations for the "estimated" geometrical construction of radome of perpendicular polarization, low frequency of a 1.5% bandwidth.

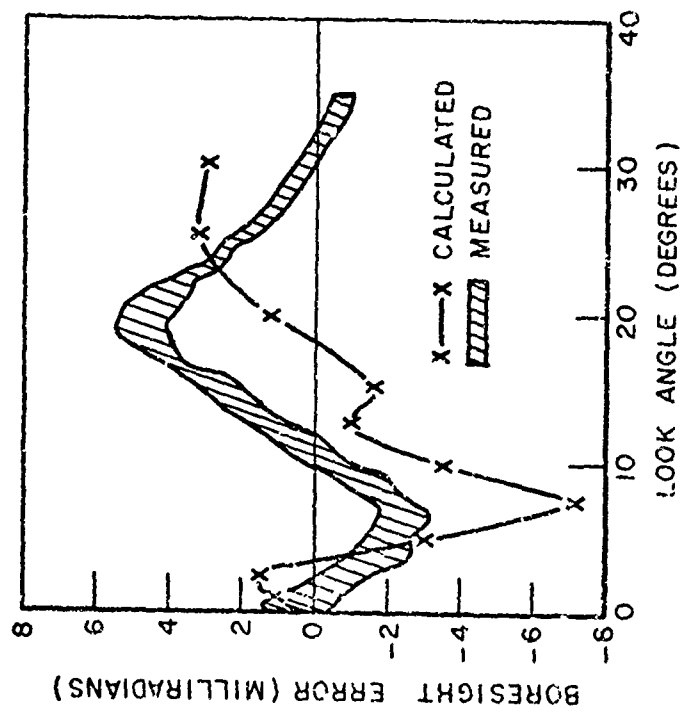


Fig. 32. Comparison between measurements and calculations for the "estimated" geometrical construction of a polyimide radome having an alumina nosecap. Perpendicular polarization. High frequency of 1.5% bandwidth design. Main radome body thickness assumed to be 0.340 inches.

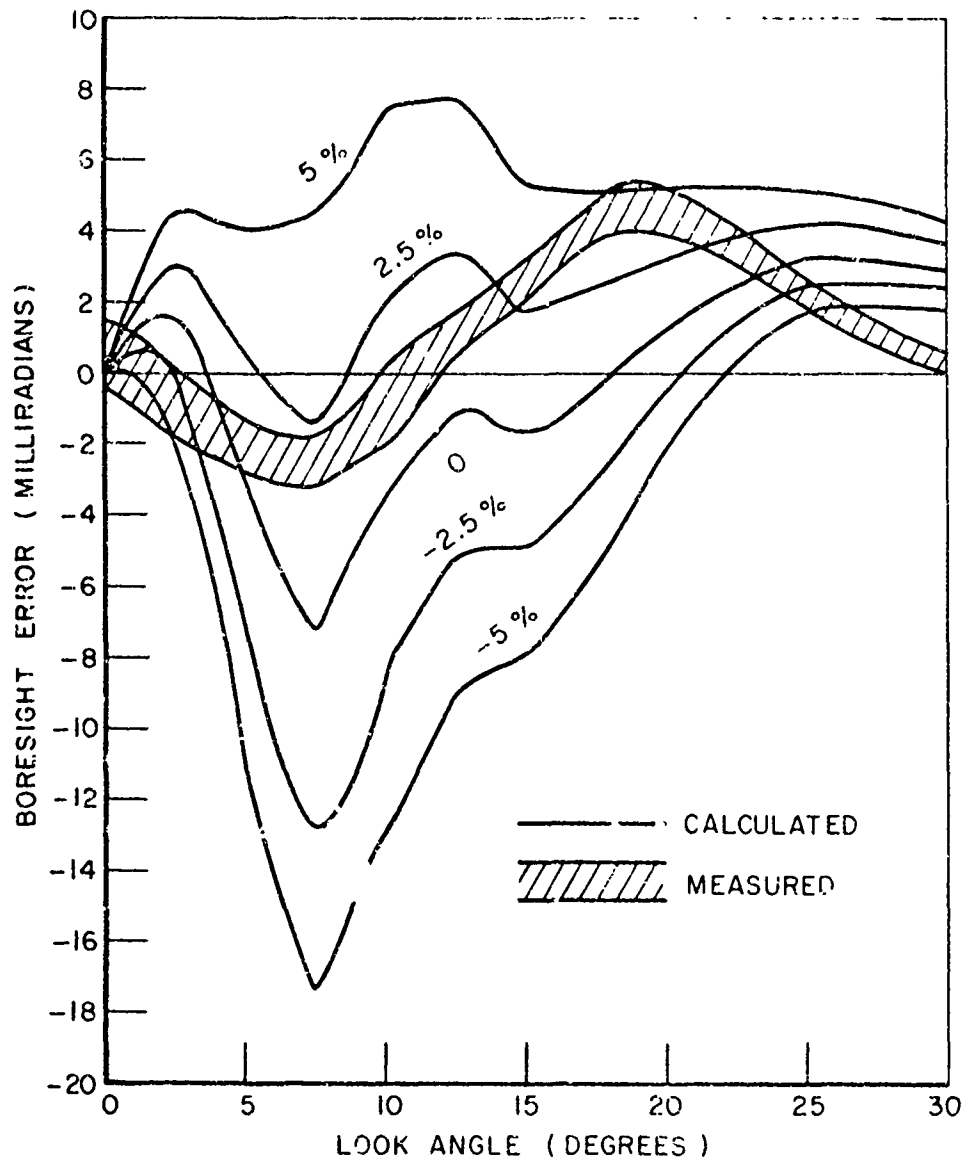


Fig. 34. Comparison between measurements and calculations at  $\pm 2.5\%$  and  $\pm 5\%$  of the probable design thickness of the main body or the radome of Fig. 32. Perpendicular polarization, high frequency.

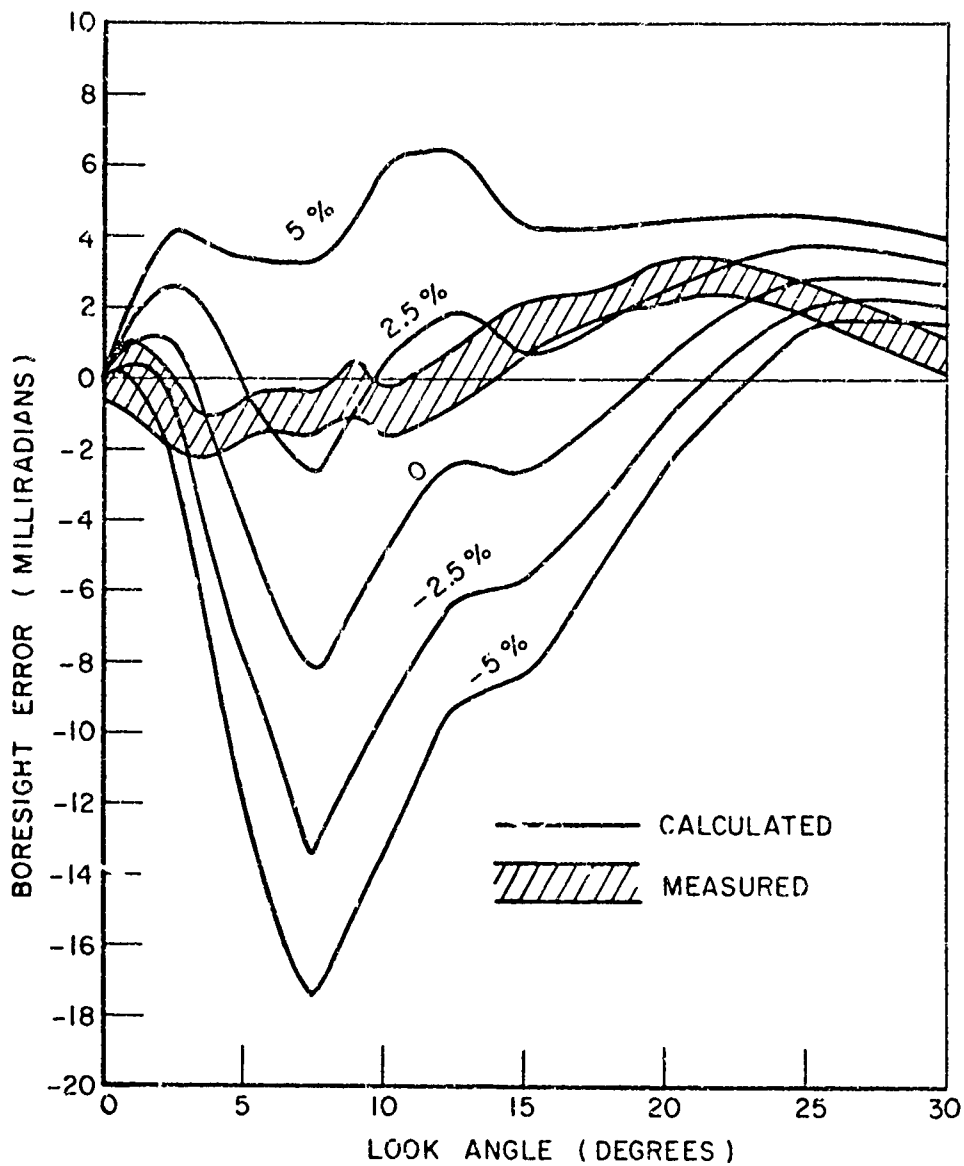


Fig. 35. Comparison between measurements and calculations at  $\pm 2.5\%$  and  $\pm 5\%$  of the probable design thickness of the main radome body for the radome of Fig. 32. Perpendicular polarization at the low frequency.

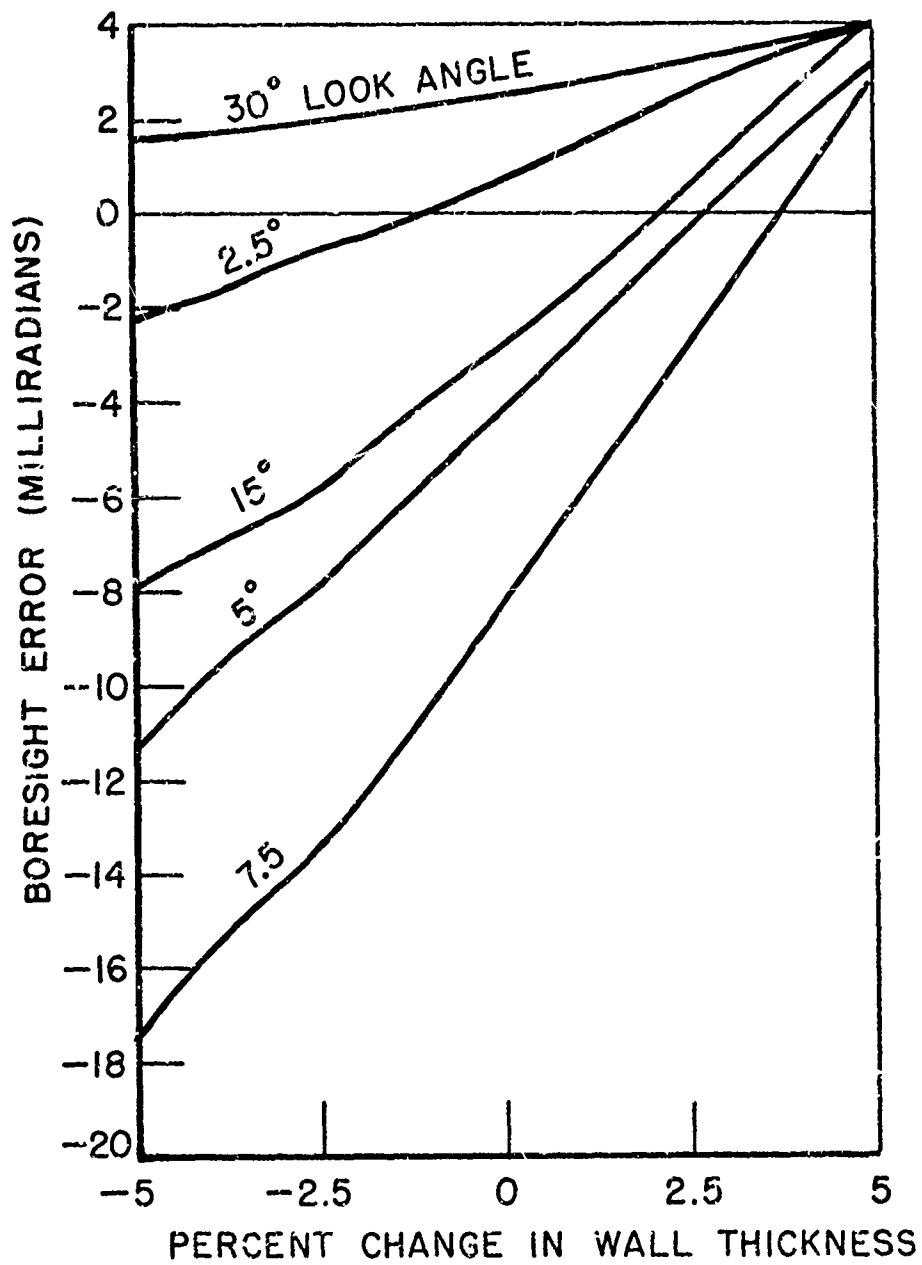


Fig. 36. Calculated transmission efficiency vs wall thickness vs look angle for the radome of Fig. 32. Perpendicular polarization at the high frequency.

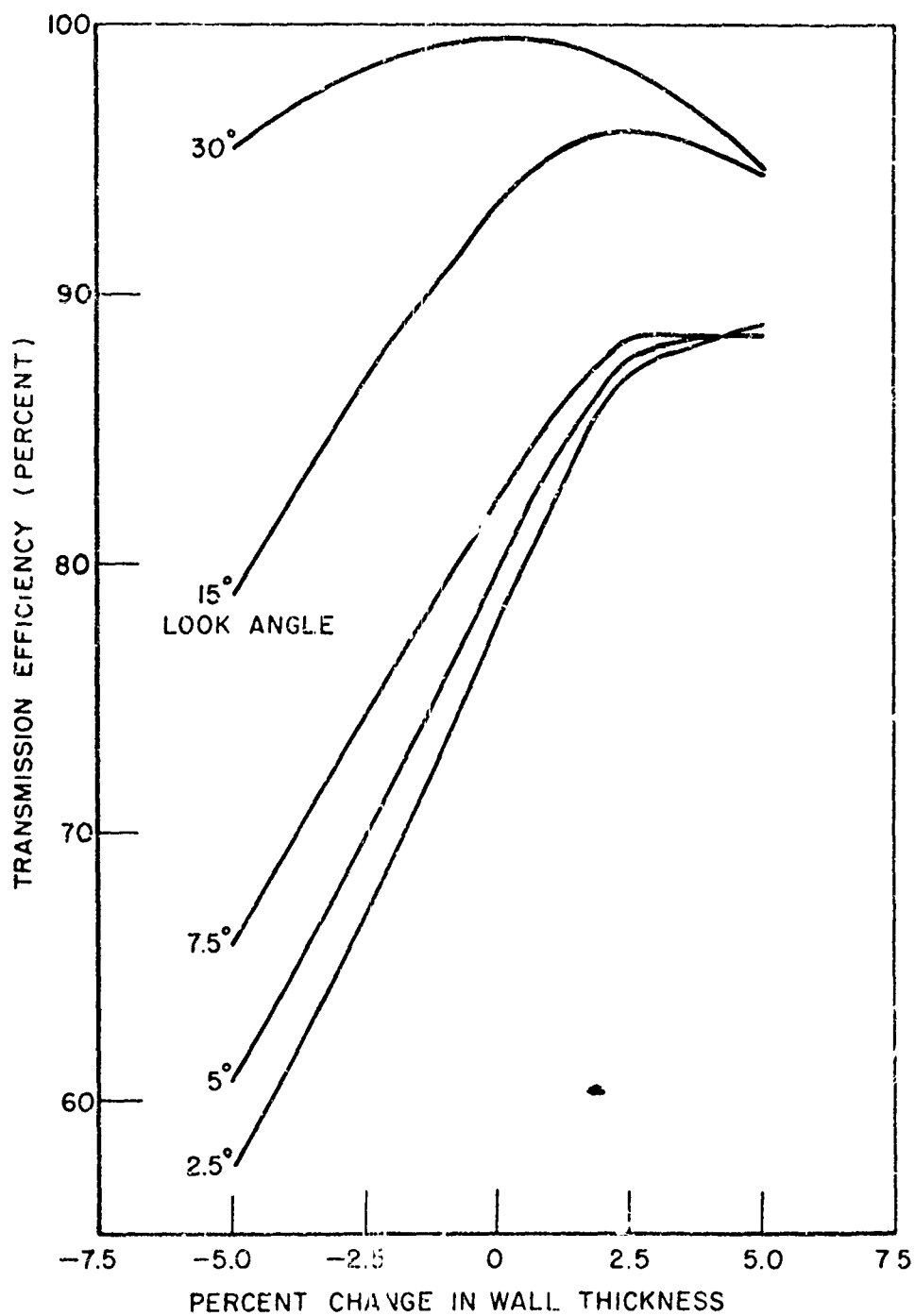
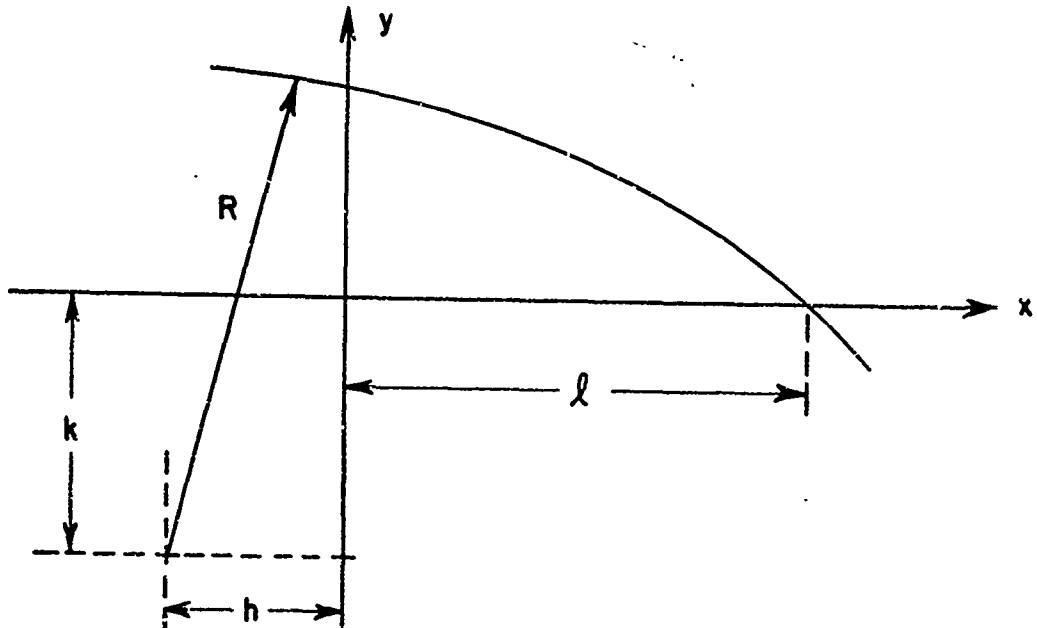


Fig. 37. Calculated transmission efficiency vs wall thickness vs look angle for the radome of Fig. 32. Perpendicular polarization at the high frequency.

TABLE IV  
 Description of Seven Example Radomes, All Dimensions  
 are in Inches. Sketch Pertains to Secant Ogives Only.



No.	Fine-ness Ratio	Shape	$\epsilon_r$	Geometrical Constants			
				R	h	l	k
1	2.0	Tangent Ogive	5.5				
2	2.11	Tangent Ogive	5.5				
3	2.0	Tangent Ogive	6.4				
4	2.0	Tangent Ogive	9.7				
5	2.0	Secant Ogive	5.5	127.5	-15.692	30.0	-119.031
6	2.5	Secant Ogive	5.5	195.0	-19.35	37.5	-186.529
7	2.5	Secant Ogive	5.5	195.0	-19.35	37.3	-186.529

x ——— KILCOYNE CALCULATION FH  
 o ——— KILCOYNE CALCULATION FL  
 x - - - - TRICOLES CALCULATION FH  
 o - - - - TRICOLES CALCULATION FL

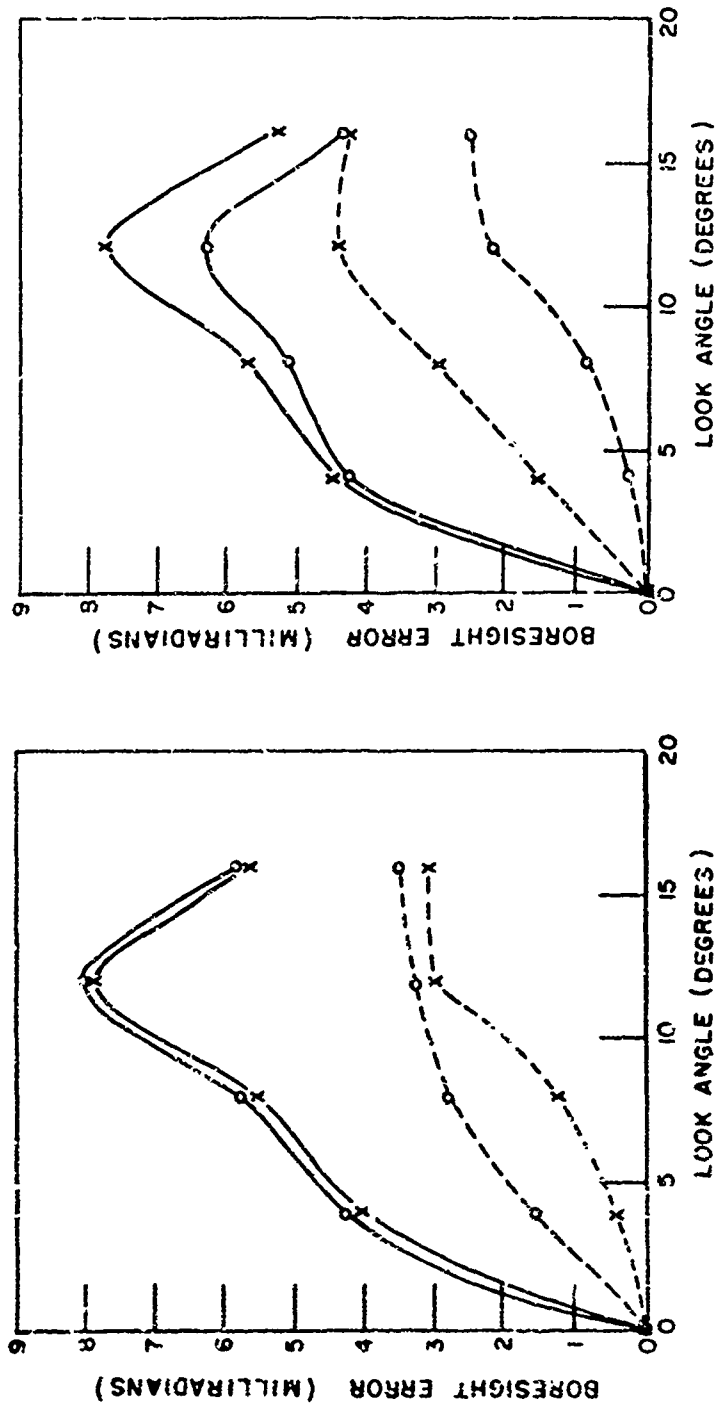


Fig. 38. Comparison between Tricoles and Kilcoyne calculations. Radome 1 in Table IV. Parallel polarization. FL and FH denote the low and high frequencies of a 1.5% bandwidth.

Fig. 39. Comparison between Tricoles and Kilcoyne calculations. Radome 1 in Table IV. Perpendicular polarization.

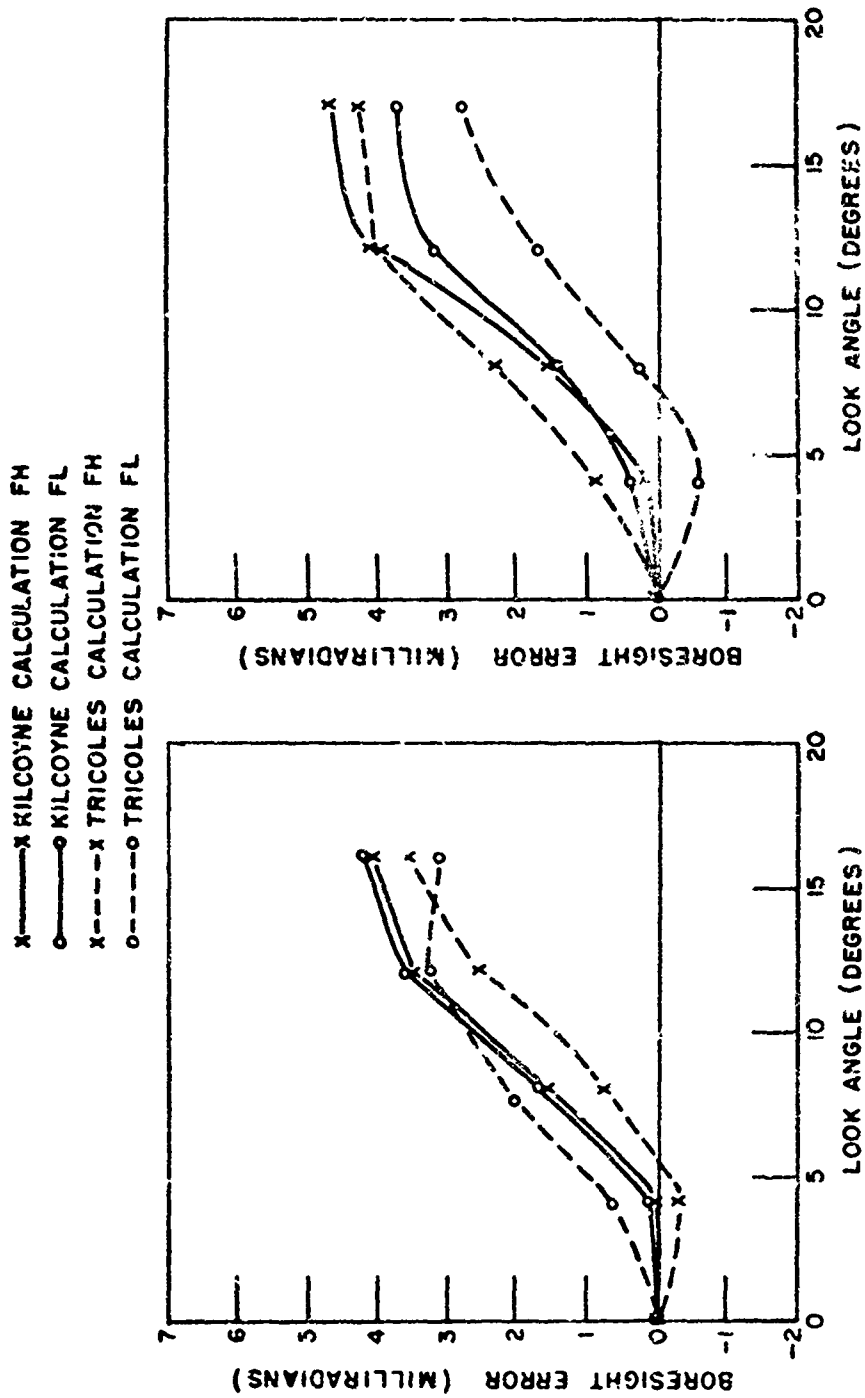


Fig. 40. Comparison between Tricoles and Kilcoyne calculations. Radome 2 in Table IV. Parallel polarization.

Fig. 41. Comparison between Tricoles and Kilcoyne calculations. Radome 2 in Table IV. Perpendicular polarization.

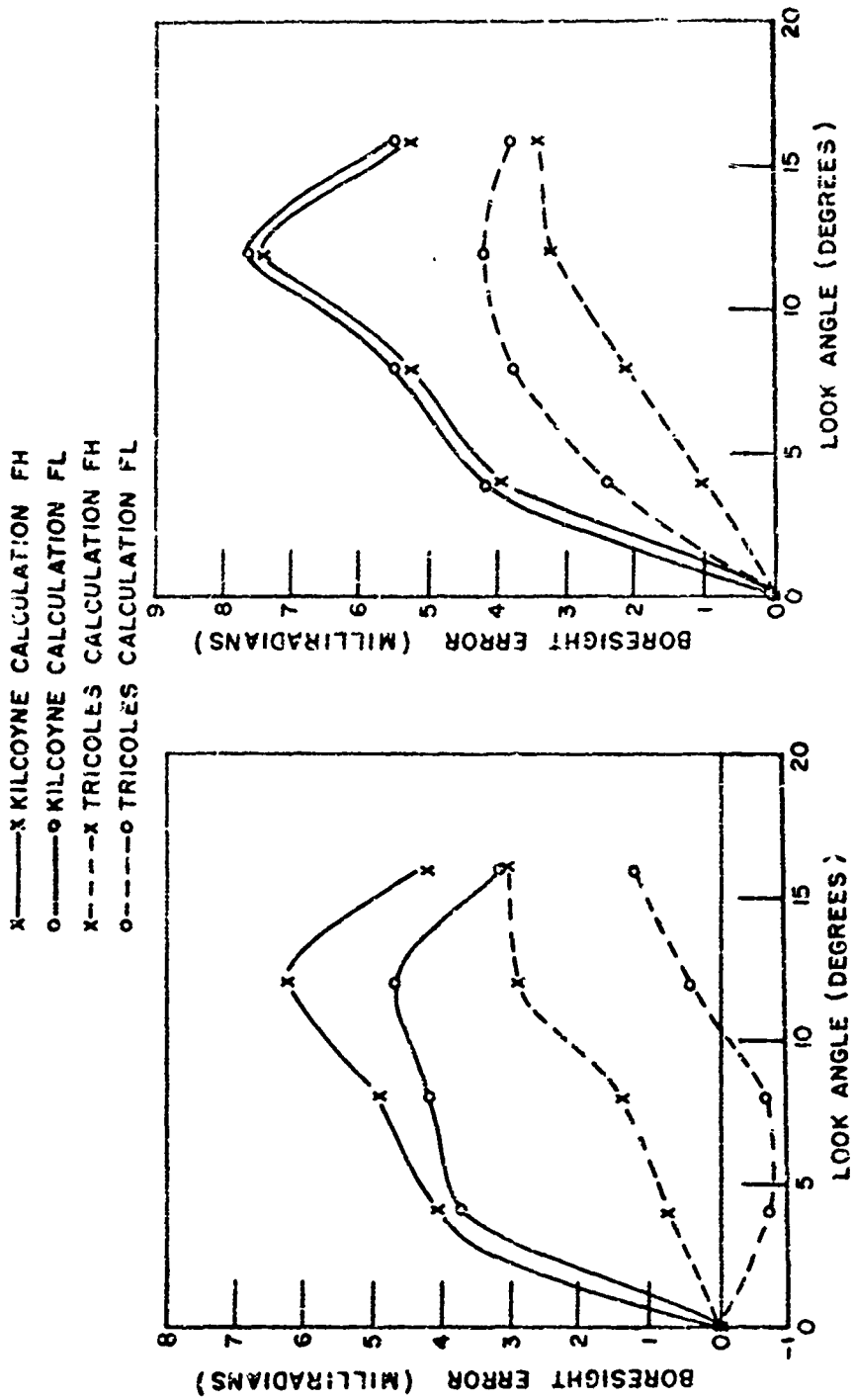


Fig. 43. Comparison between Tricoles and Kilcoyne calculations. Radome 3 in Table IV. Perpendicular polarization.

Fig. 42. Comparison between Tricoles and Kilcoyne calculations. Radome 3 in Table IV. Parallel polarization.

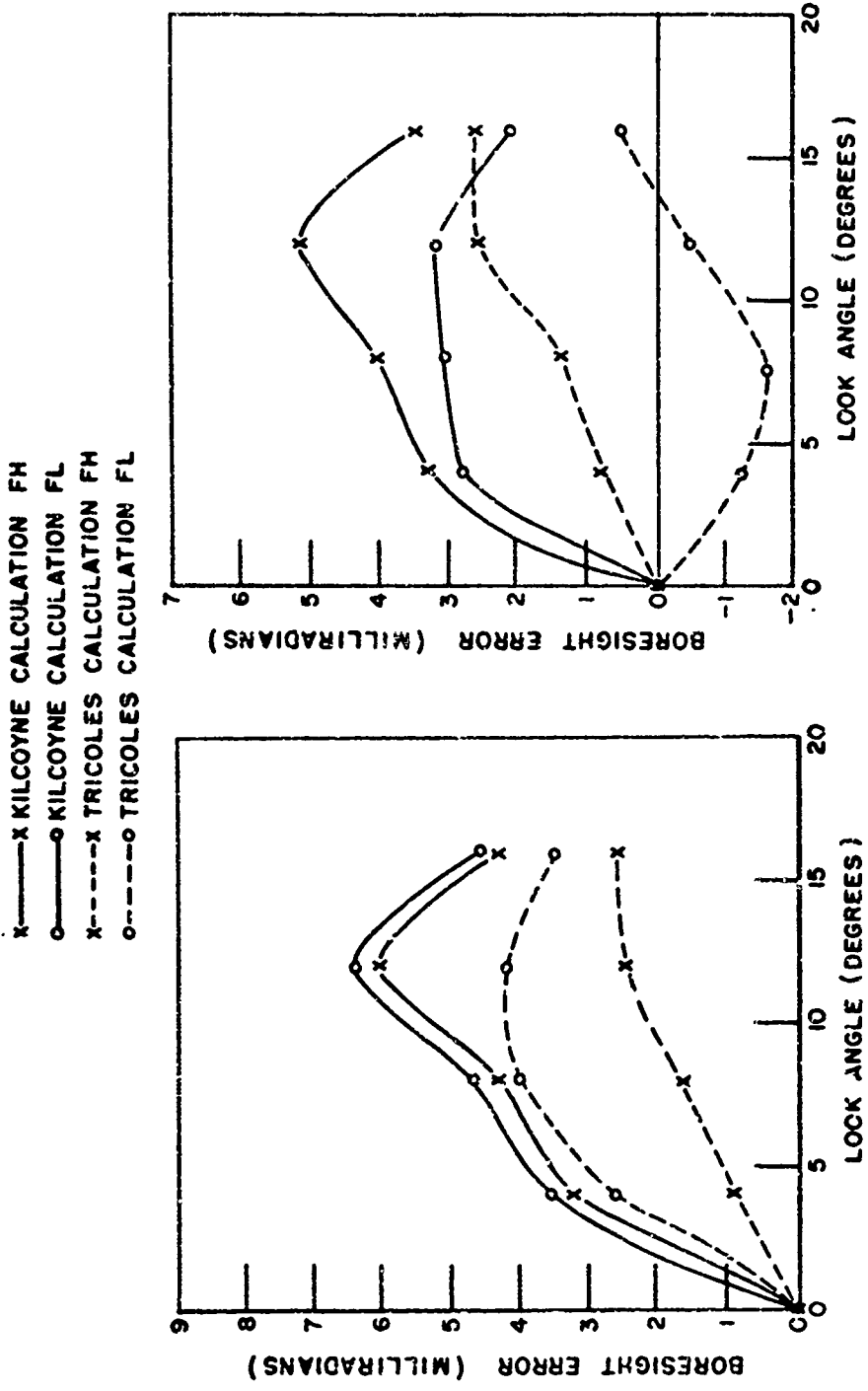


Fig. 44. Comparison between Tricoles and Kilcoyne calculations. Radome 4 in Table IV. Parallel polarization.

Fig. 45. Comparison between Tricoles and Kilcoyne calculations. Radome 4 in Table IV. Perpendicular polarization.

x-----x KILCOYNE CALCULATION FH  
 o-----o KILCOYNE CALCULATION FL  
 x-----x TRICOLES CALCULATION FH  
 o-----o TRICOLES CALCULATION FL

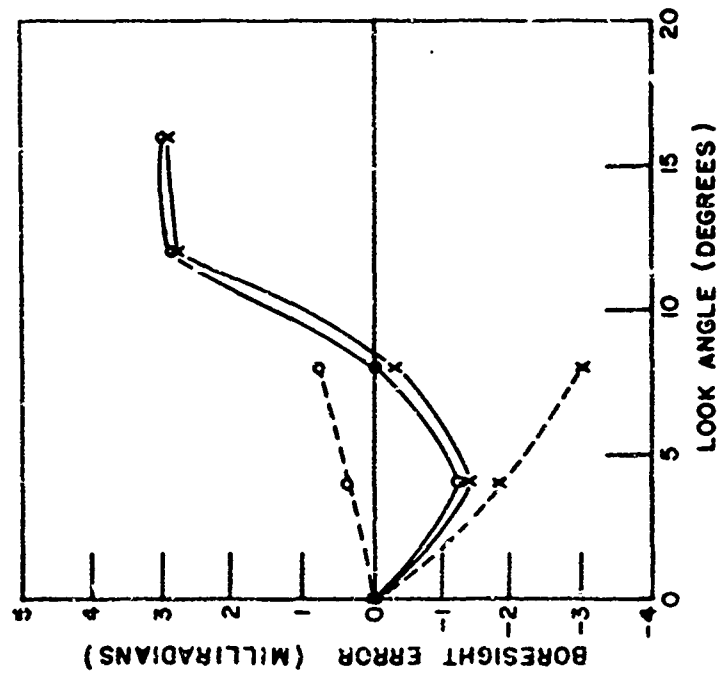
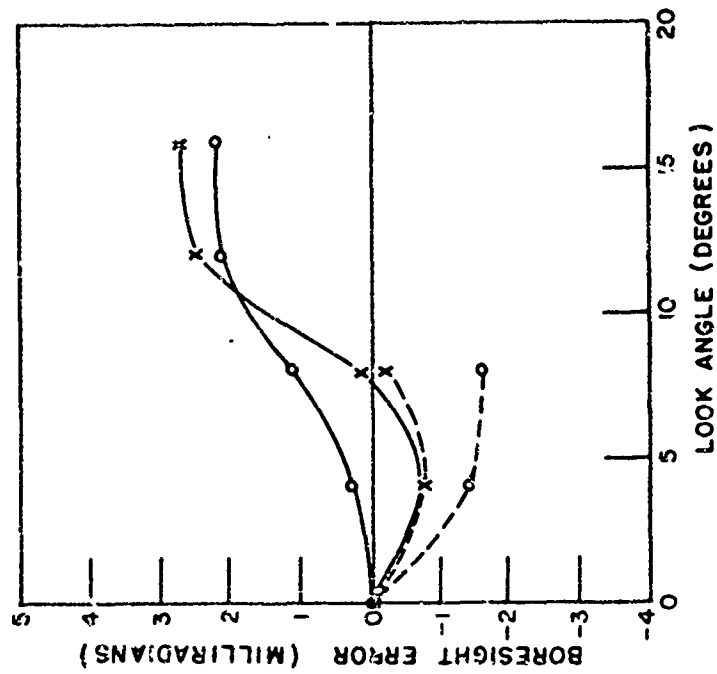


Fig. 47. Comparison between Tricoles and Kilcoyne calculations. Radome 5 in Table IV. Perpendicular polarization.

Fig. 46. Comparison between Tricoles and Kilcoyne calculations. Radome 5 in Table IV. Parallel polarization.

x-----x KILCOYNE CALCULATION FH  
 o-----o KILCOYNE CALCULATION FL  
 x-----x TRICOLES CALCULATION FH  
 o-----o TRICOLES CALCULATION FL

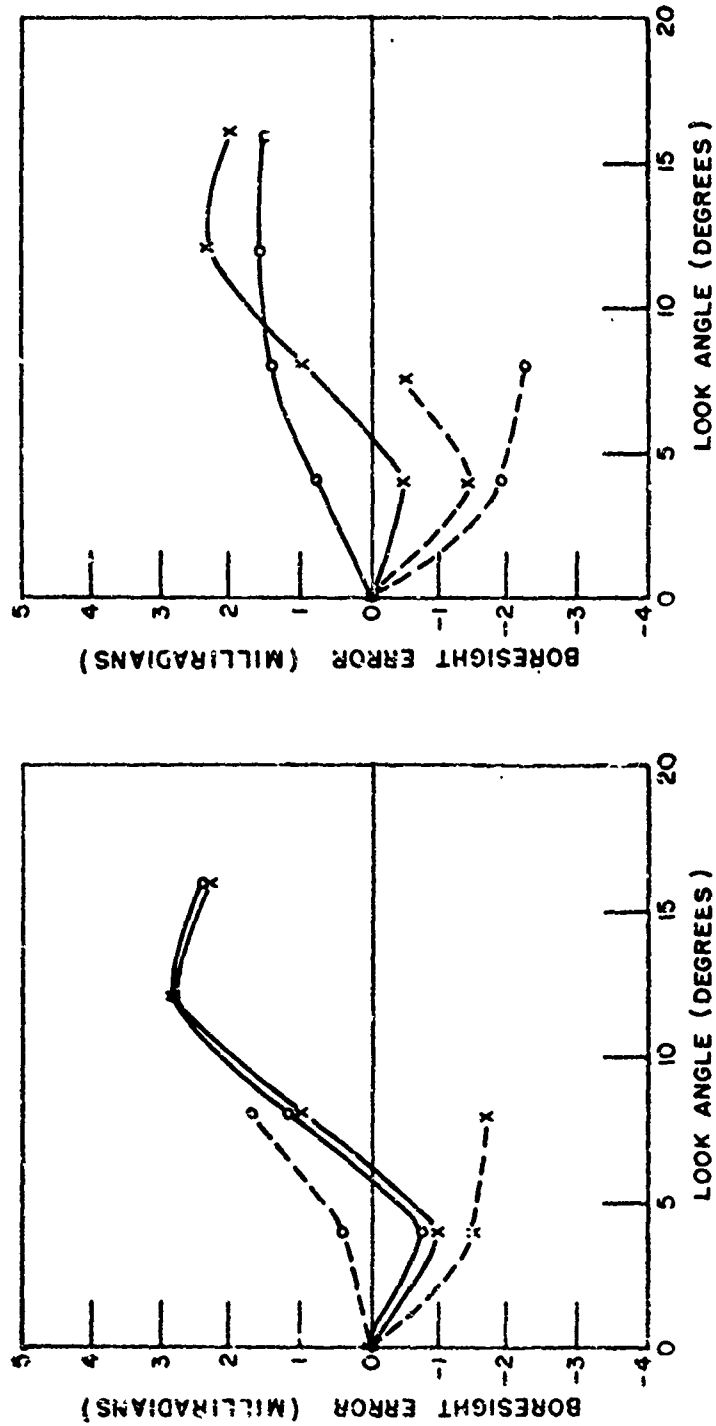


Fig. 48. Comparison between Tricoles and Kilcoyne calculations. Radome 6 in Table IV. Parallel polarization.

Fig. 49. Comparison between Tricoles and Kilcoyne calculations. Radome 6 in Table IV. Perpendicular polarization.

x-----x KILCOYNE CALCULATION FH  
 o-----o KILCOYNE CALCULATION FL  
 x-----x TRICOLES CALCULATION FH  
 o-----o TRICOLES CALCULATION FL

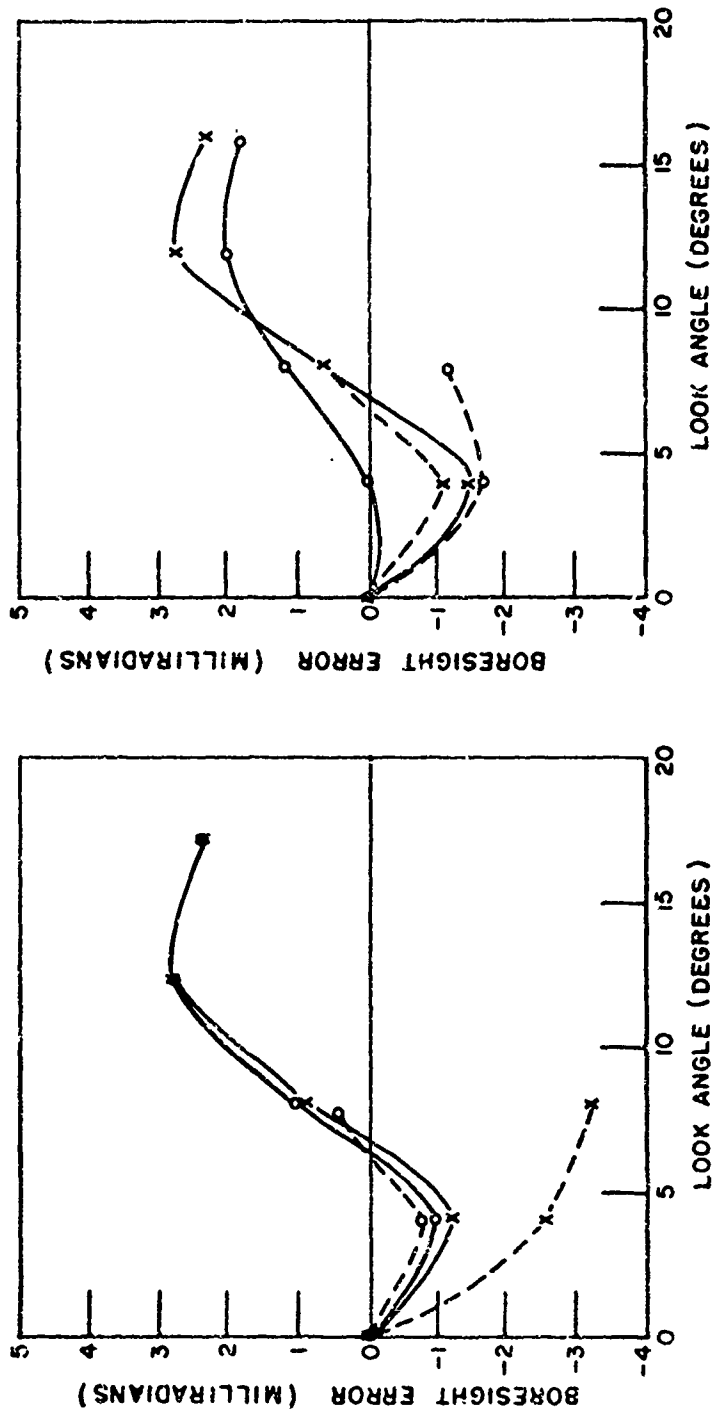


Fig. 50. Comparison between Tricoles and Kilcoyne calculations. Radome 7 in Table IV. Parallel polarization.

Fig. 51. Comparison between Tricoles and Kilcoyne calculations. Radome 7 in Table IV. Perpendicular polarization.

TABLE V  
Relative Agreement Between Tricoles and Kilcoyne Calculations  
FH = 1.015 FL

FR	Radome		Perpendicular		Parallel	
	Shape	$\epsilon$	FL	FH	FL	FH
2.0	Tan-Ogive	5.5	Poor	Fair	Poor	Poor
2.11	Tan-Ogive	5.5	Good	Excellent	Excellent	Excellent
2.0	Tan-Ogive	6.4	Poor	Poor	Fair	Poor
2.0	Tan-Ogive	9.7	Poor	Fair	Good	Poor
2.0	Sec-Ogive	5.5	Poor	Excellent	Poor	Poor
2.5	Sec-Ogive	5.5	Poor	Fair	Good	Poor
2.5	Sec-Ogive	5.5	Poor	Excellent	Excellent	Poor
Weighted Average			Poor	Good	Good	Poor

I. Effects Due to the Blunting of a Radome Nose Section

The high speed of a modern aircraft or missile frequently results in the generation of temperatures at the leading edge (tip) that are above the maximum safe operating temperatures of even the best ceramic radome materials. When it is necessary to locate a radome at the tip section, special design precautions are required which generally take the form of either blunting the radome tip, which increases the tip area, or placing a protective metal cap at the tip of a pointed system. This section is included to summarize the electrical effects due to the blunting of the radome tip which have been indicated in previous sections and to illustrate the far-zone power pattern plot which the computer program generates. Calculations of boresight error, transmission efficiency, and antenna pattern distortion are presented for an identical antenna system operating with a pointed radome and with a blunted version of the same radome. All calculations are for perpendicular polarization at the center design frequency. The two radomes used in this example are the pyroceram ogive radomes described earlier with and without the hemispheric nose cap.

Figure 52 shows the effects of blunting the radome tip on the boresight error characteristics of the antenna-radome system. Figure 53 shows the relative on-axis transmitted power calculated from the sum pattern of the monopulse antenna for the two systems. The "no-radome"

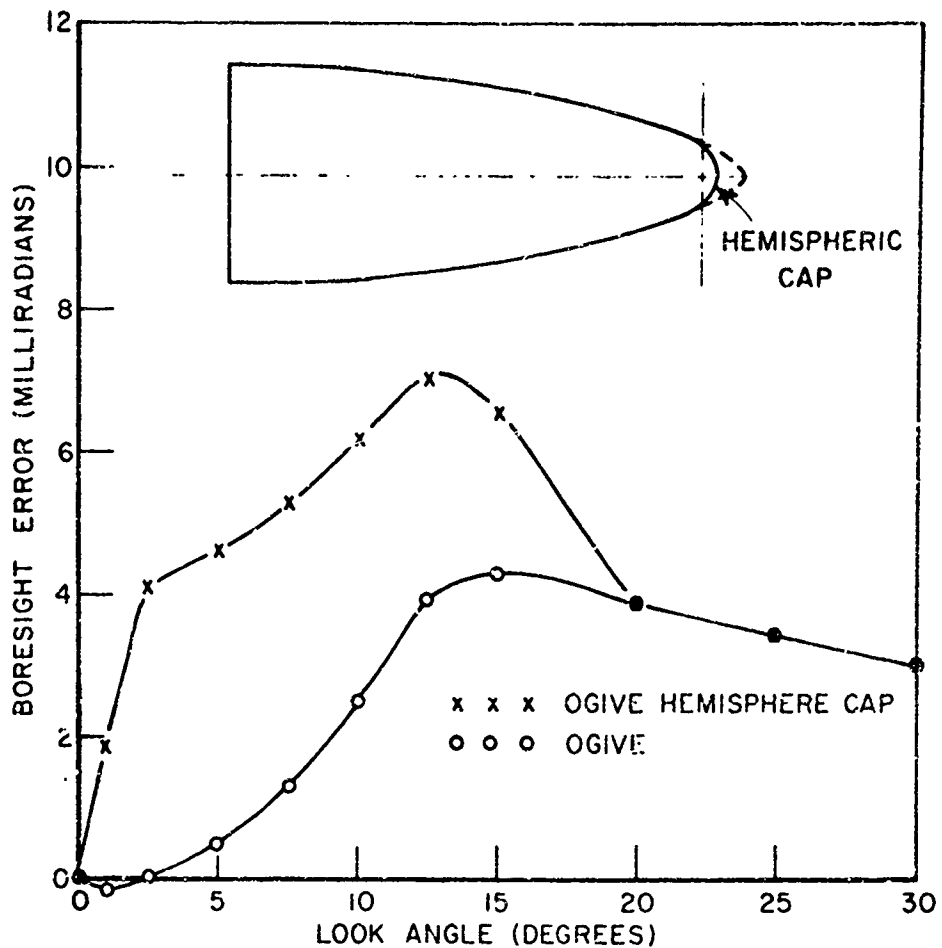


Fig. 52. Calculated effects on radome boresight error due to the blunting of the tip of a pyroceram ogive radome. Perpendicular polarization at the design frequency.

case is represented by the 100% relative power level at all look angles. From these figures it can be seen that the ray tracing theory predicts the pointed-nose case to give considerably better boresight error performance as well as having about 5% greater on-axis power transmission.

Figures 54, 55, and 56 show the normalized far-zone power patterns for the antenna without radome, with pointed radome, and with the blunted radome respectively for look angle 0°.

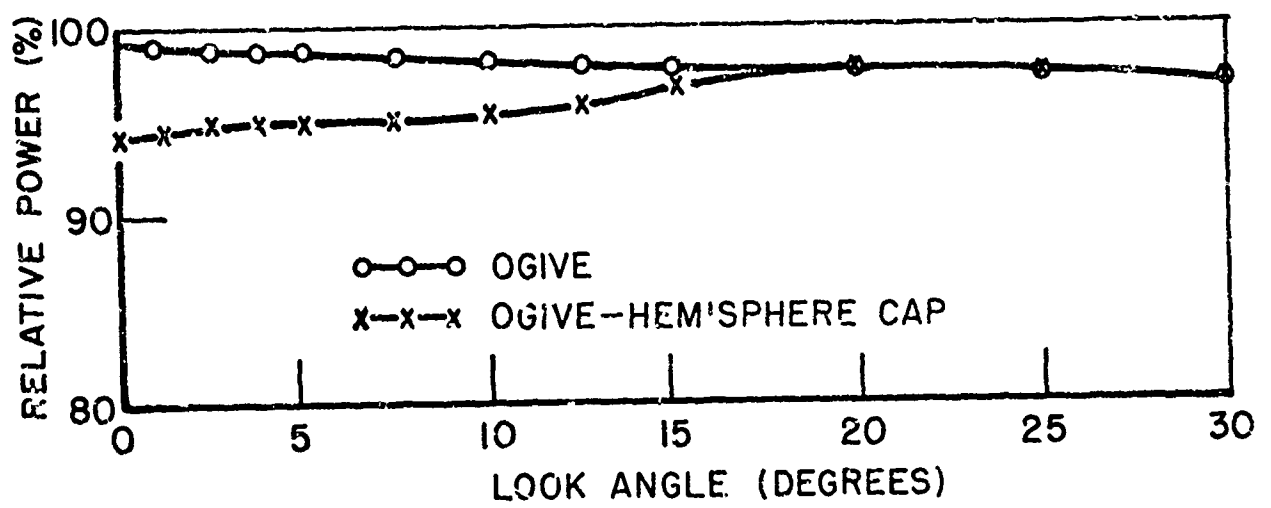


Fig. 53. Calculated transmission efficiency for the case of the radome of Fig. 52.

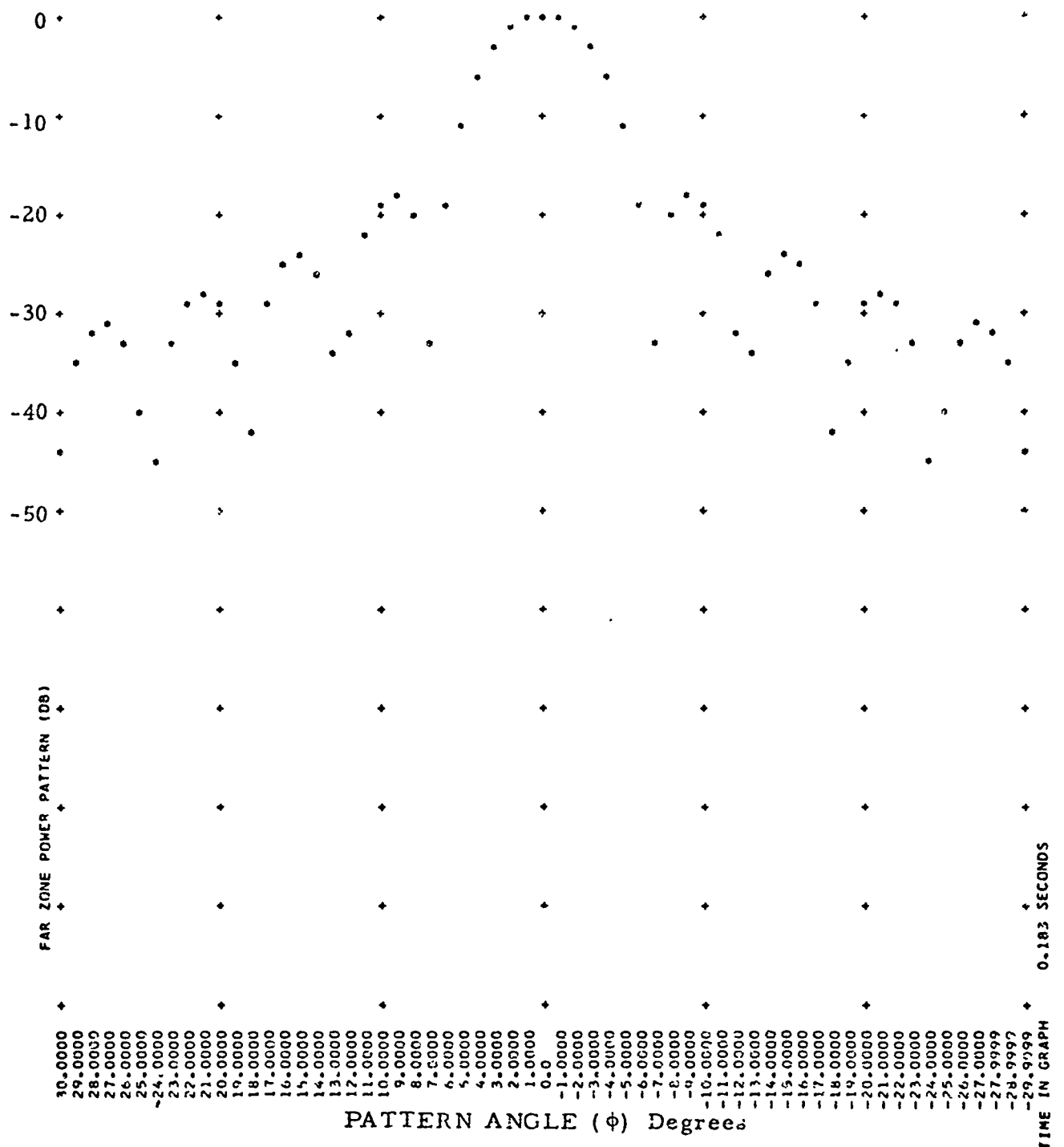


Fig. 54. Computer generated far-zone power pattern for the antenna without radome.

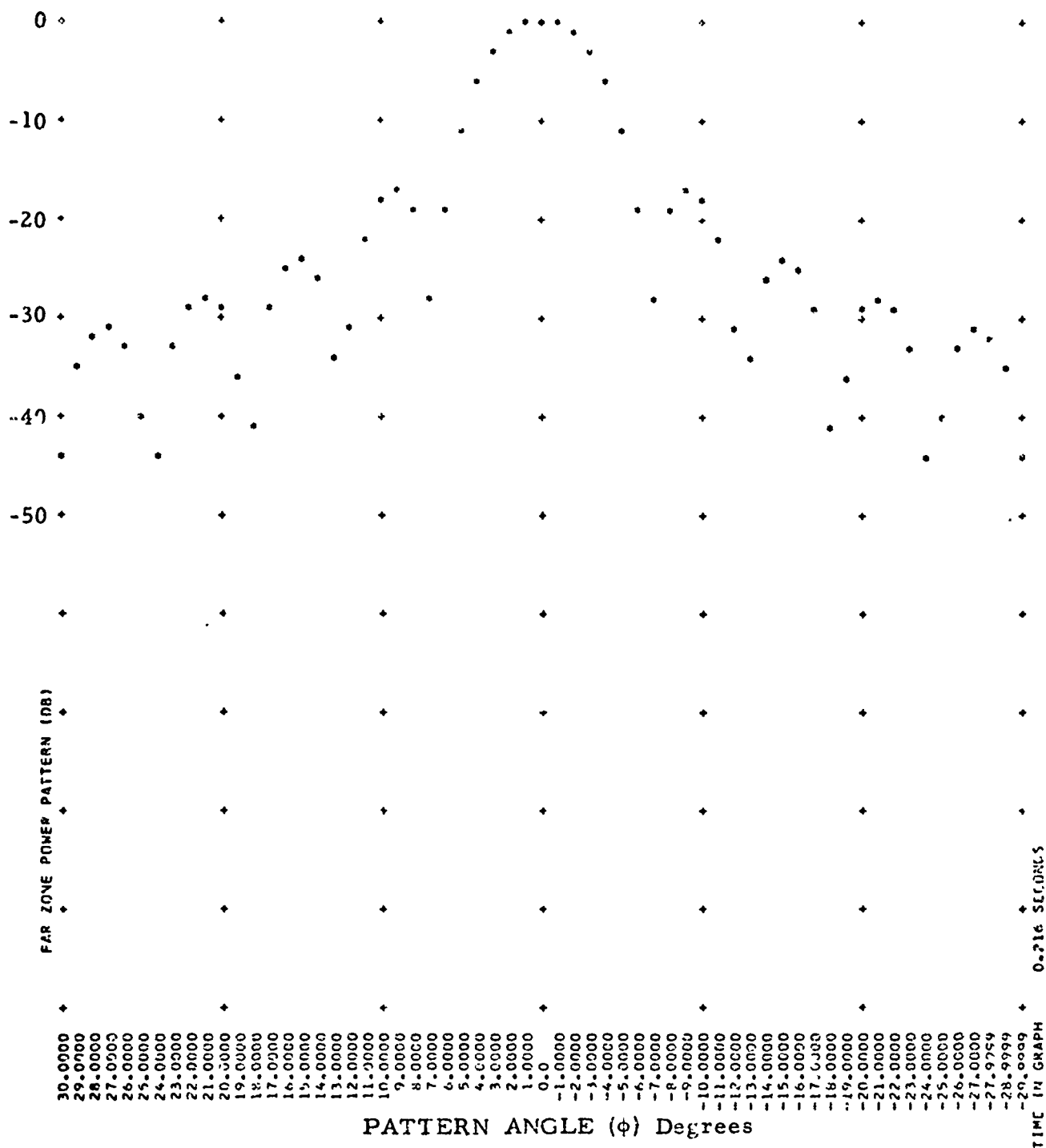


Fig. 55. Computer generated far-zone power pattern for the antenna in the presence of a pointed-nose ogive radome. Perpendicular polarization at the design frequency.

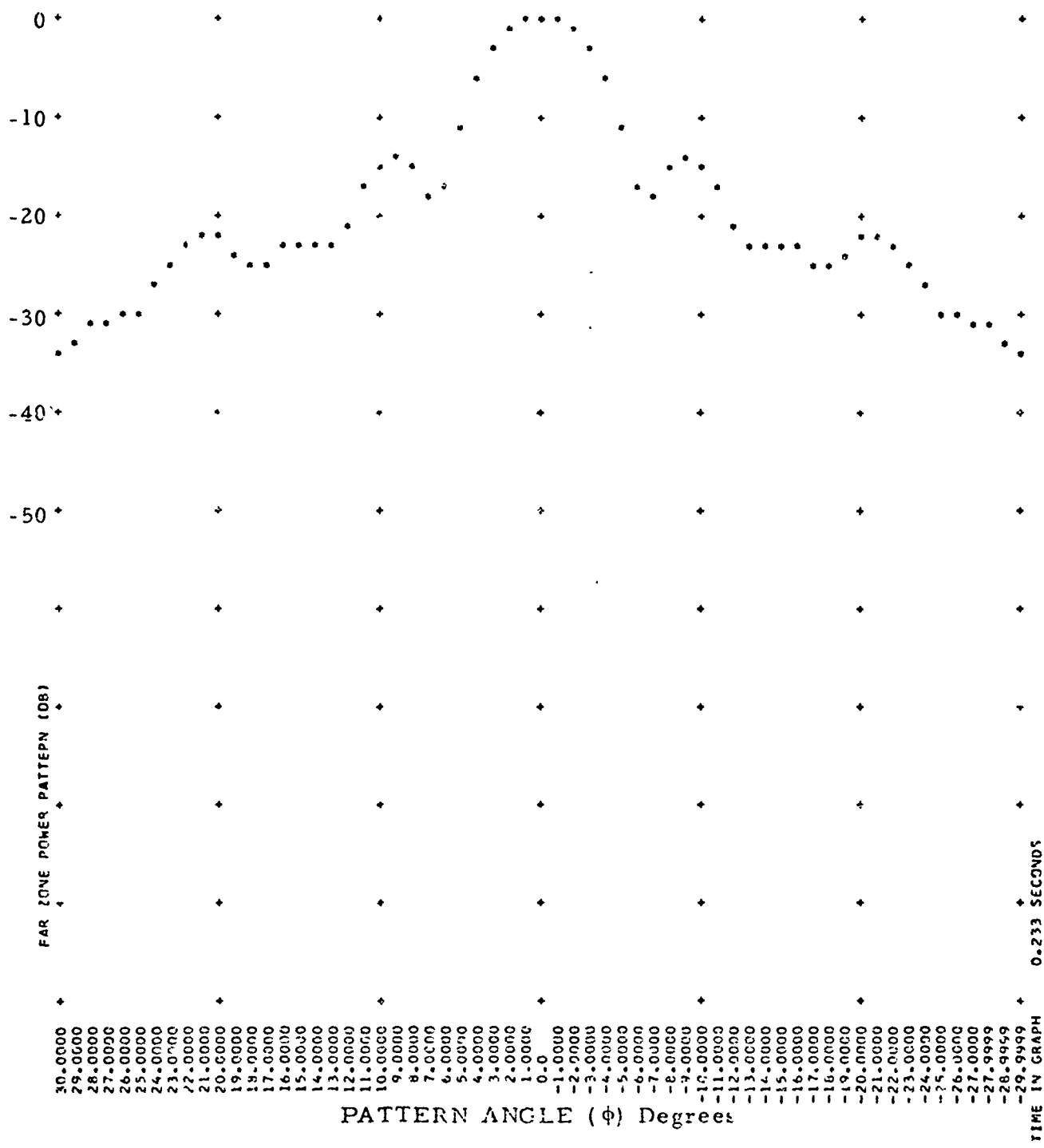


Fig. 56. Computer generated far-zone power pattern for the blunted-nose version of the radome of Fig. 55.

## V. CONCLUSIONS

A completely computerized two-dimensional ray tracing analyses of radome boresight error and antenna pattern distortion has been developed. Application of this method to several complicated antenna-radome problems has been demonstrated which shows the usefulness of the method both for the design and the analysis of antenna-radome systems. Several example cases were calculated and compared with experimental data and with other calculations. Agreement between measurements and calculations was in general reasonably good. The method was modified to include the analysis of aperture blocking effects in order to form a basis for the calculation of radome systems involving metallic nosecaps. Calculations and measurements of this case will be included in a future report.

The computer program written for the calculation of this two-dimensional method is relatively long and involved; however, it has been written in such a way as to make its use by others relatively simple and convenient.

The method can be applied to a wide range of antenna-radome problems. Calculation of results is extremely fast, thus making the method an economical approach to radome design and modification.

## ACKNOWLEDGEMENT

Measured data and some calculations used in comparisons in this report were furnished by The U.S. Naval Air Development Center, Johnsville, Warminster, Pennsylvania. The author gratefully acknowledges Mr. Walter C. Beamer of USNADC.

## APPENDIX A

This appendix contains calculated boresight error (BSE) and relative power transmission (RPWR) for several equally-spaced ray selections at ten look angles to further demonstrate the convergence of the ray tracing solution which was explained in Chapter IV-A. Tables VI and VII show the BSE and RPWR as a function of the number of equally-spaced rays (NRE) used for the pyroceram ogive radome with and without the hemispheric nose cap. Perpendicular polarization was used throughout. BSE is in milliradians and RPWR has a value of 1.0 for the no-radome case. Look angle ( $\phi_L$ ) is in degrees.

TABLE VI  
Pyroceram Ogive With Hemispheric Nosecap

NRE	$\phi_L = 1.0$		$\phi_L = 2.5$		$\phi_L = 5.0$		$\phi_L = 7.5$		$\phi_L = 10.0$	
	BSE	RPWR	BSE	RPWR	BSE	RPWR	BSE	RPWR	BSE	RPWR
3	-0.111	0.975	-0.281	0.998	-0.435	1.00	-0.588	1.0	-0.690	1.0
5	-0.060	0.942	-0.162	0.985	3.55	0.988	12.37	0.935	2.85	0.989
9	+0.690	0.955	3.98	0.957	5.77	0.957	6.55	0.949	6.71	0.969
17	2.02	0.952	3.81	0.951	5.05	0.951	5.89	0.951	6.13	0.959
33	2.00	0.949	4.01	0.949	4.76	0.950	5.41	0.953	6.20	0.956
65	1.95	0.949	4.08	0.949	4.64	0.950	5.33	0.952	6.21	0.955
129	1.92	0.949	4.08	0.949	4.63	0.950	5.29	0.952	6.21	0.955
257	1.92	0.949	4.08	0.949	4.61	0.950	5.29	0.952	6.21	0.955
501	1.93	0.949	4.08	0.949	4.61	0.950	5.29	0.952	6.21	0.955

NRE	$\phi_L = 12.5$		$\phi_L = 15.0$		$\phi_L = 20.0$		$\phi_L = 25.0$		$\phi_L = 30.0$	
	BSE	RPWR								
3	4.66	0.985	12.54	0.932	4.0	0.981	3.54	0.977	3.09	0.971
5	4.53	0.984	8.17	0.951	3.93	0.980	3.49	0.976	3.06	0.971
9	7.17	0.963	6.16	0.965	3.91	0.979	3.47	0.975	3.06	0.971
17	7.18	0.959	5.79	0.968	3.89	0.979	3.47	0.975	3.06	0.971
33	7.13	0.958	5.56	0.970	3.89	0.979	3.47	0.975	3.06	0.970
65	7.06	0.958	5.55	0.970	3.89	0.979	3.47	0.975	3.06	0.970
129	7.06	0.958	5.51	0.970	3.89	0.979	3.47	0.975	3.06	0.970
257	7.06	0.958	5.51	0.970	3.89	0.979	3.47	0.975	3.06	0.970
501	7.06	0.958	5.51	0.970	3.89	0.979	3.47	0.975	3.06	0.970

TABLE VII  
Pyroceram Ogive Without Nosecap

NRE	$\phi_L = 1.0$		$\phi_L = 2.5$		$\phi_L = 5.0$		$\phi_L = 7.5$		$\phi_L = 10.0$	
	BSE	RPWR	BSE	RPWR	BSE	RPWR	BSE	RPWR	BSE	RPWR
3	-0.093	0.999	-0.230	0.999	-0.430	1.000	-0.568	1.000	-0.690	1.000
5	-0.060	0.994	-0.162	0.994	-0.330	0.994	1.95	0.992	1.87	0.992
9	-0.060	0.992	-0.145	0.993	+0.366	0.994	1.53	0.989	3.23	0.987
17	0.0	0.992	+0.026	0.992	+0.724	0.989	1.24	0.988	2.87	0.986
33	-0.3	0.992	+0.111	0.991	+0.605	0.990	1.44	0.987	2.65	0.985
65	-0.3	0.992	+0.077	0.991	+0.537	0.990	1.36	0.987	2.53	0.985
129	-0.3	0.992	+0.060	0.991	+0.503	0.990	1.32	0.987	2.48	0.985
257	-0.3	0.992	+0.060	0.991	+0.486	0.990	1.29	0.987	2.45	0.985
501	-0.3	0.992	+0.060	0.991	+0.486	0.990	1.30	0.987	2.45	0.985

NRE	$\phi_L = 12.5$		$\phi_L = 15.0$		$\phi_L = 20.0$		$\phi_L = 25.0$		$\phi_L = 30.0$	
	BSE	RPWR								
3	-0.780	0.999	4.49	0.984	4.00	0.981	3.54	0.977	3.09	0.971
5	1.78	0.991	4.35	0.982	3.93	0.979	3.49	0.976	3.06	0.971
9	3.13	0.987	4.32	0.982	3.91	0.979	3.47	0.975	3.06	0.971
17	3.81	0.985	4.30	0.982	3.89	0.979	3.47	0.975	3.06	0.971
33	4.15	0.984	4.30	0.982	3.89	0.979	3.47	0.975	3.06	0.970
65	4.01	0.983	4.30	0.982	3.89	0.979	3.47	0.975	3.06	0.970
129	3.96	0.983	4.30	0.982	3.89	0.979	3.47	0.975	3.06	0.970
257	3.91	0.983	4.30	0.982	3.89	0.979	3.47	0.975	3.06	0.970
501	3.93	0.983	4.30	0.982	3.89	0.979	3.47	0.975	3.06	0.970

## APPENDIX B

This appendix contains calculated boresight error and on-axis power transmission for several choices of phase allowance (PHD) and amplitude allowance (TRD) parameters in the numerical integration technique explained in Chapter IV-B. The radomes used are the same as those of Appendix A. Look angle ( $\phi_L$ ) is in degrees, boresight error (BSE) is in milliradians, PHD is in degrees, TRD and relative on-axis power (RPWR) are normalized fractions. The number of subapertures (N) used refers to the number of subsections of the 500 point reconstructed aperture remaining after averaging the aperture distribution functions. Tables VIII, IX, X, and XI show the calculated BSE, RPWR, and N for 12 choices of PHD and TRD for the blunted (with hemispheric nose cap) and pointed (without nose cap) radomes respectively.

TABLE VIII  
Ogive Radome With Hemispheric Nosecap

PHD	TRD	$\phi_L = 1.0$			$\phi_L = 5.0$			$\phi_L = 7.5$		
		BSE	RPWR	N	BSE	RPWR	N	BSE	RPWR	N
		0.0	1.93	0.040	500	4.61	0.950	500	5.29	0.952
1.0	1.92	0.949	42	4.61	0.950	41	5.29	0.952	41	
1.0	1.92	0.949	42	4.61	0.950	41	5.29	0.952	41	
2.0	1.92	0.949	24	4.61	0.950	25	5.29	0.952	24	
2.0	1.92	0.949	24	4.61	0.950	25	5.29	0.952	24	
3.0	1.93	0.949	18	4.61	0.950	19	5.29	0.952	19	
3.0	1.93	0.949	18	4.61	0.950	19	5.29	0.952	19	
5.0	1.93	0.949	12	4.61	0.951	12	5.29	0.953	11	
5.0	1.93	0.949	12	4.61	0.951	12	5.29	0.953	11	
10.0	1.93	0.950	8	4.63	0.952	7	5.29	0.954	7	
10.0	1.93	0.950	8	4.63	0.952	7	5.29	0.954	7	
30.0	1.92	0.960	4	4.73	0.965	3	5.38	0.969	3	

TABLE IX  
Ogive Radome With Hemispheric Nosecap

PHD	TDR	$\phi L = 12.5$			$\phi L = 20.0$			$\phi L = 30.0$		
		BSE	RPWR	N	BSE	RPWR	N	BSE	RPWR	N
0.0	0.0	7.06	0.958	500	3.89	0.979	500	3.06	0.970	500
1.0	0.05	7.06	0.958	36	3.89	0.979	15	3.06	0.970	12
1.0	0.10	7.06	0.958	36	3.89	0.979	15	3.06	0.970	12
2.0	0.05	7.06	0.958	20	3.89	0.979	9	3.06	0.971	7
2.0	0.10	7.06	0.958	40	3.89	0.979	9	3.06	0.971	7
3.0	0.05	7.06	0.958	16	3.89	0.979	6	3.06	0.971	5
3.0	0.10	7.06	0.958	16	3.89	0.979	6	3.06	0.971	5
5.0	0.05	7.06	0.959	10	3.89	0.980	4	3.06	0.971	3
5.0	0.10	7.06	0.959	10	3.89	0.980	4	3.06	0.971	3
10.0	0.05	7.06	0.961	4	3.89	0.981	2	3.06	0.971	2
10.0	0.10	7.06	0.961	4	3.89	0.981	2	3.06	0.971	2
30.0	0.20	7.10	0.971	2	3.89	0.981	2	3.06	0.971	2

TABLE X  
Ogive Radome Without Nosecap

PHD	TRD	$\phi_L = 1.0$			$\phi_L = 5.0$			$\phi_L = 7.5$		
		BSE	RPWR	N	BSE	RPWR	N	BSE	RPWR	N
0.0	0.0	-0.03	0.992	500	0.486	0.990	500	1.30	0.987	500
1.0	0.05	-0.03	0.992	19	0.486	0.990	18	1.30	0.987	18
1.0	0.10	-0.03	0.992	19	0.486	0.990	18	1.30	0.987	18
2.0	0.05	-0.03	0.992	10	0.486	0.990	9	1.30	0.987	10
2.0	0.10	-0.03	0.992	10	0.486	0.990	9	1.30	0.987	10
3.0	0.05	-0.03	0.992	6	0.486	0.990	8	1.30	0.987	8
3.0	0.10	-0.03	0.992	6	0.486	0.990	8	1.30	0.987	8
5.0	0.05	-0.03	0.993	4	0.486	0.990	4	1.30	0.988	5
5.0	0.10	-0.03	0.993	4	0.486	0.990	4	1.30	0.988	5
10.0	0.05	-0.03	0.994	2	0.486	0.991	3	1.30	0.989	3
10.0	0.10	-0.03	0.994	2	0.486	0.991	3	1.30	0.989	3
30.0	0.20	-0.03	0.994	2	0.503	0.994	2	1.32	0.993	2

TABLE XI  
Ogive Radome Without Nosecap

PHD	TRD	$\phi_L = 12.5$			$\phi_L = 20.0$			$\phi_L = 30.0$		
		BSE	RPWR	N	BSE	RPWR	N	ESE	RPWR	N
0.0	0.0	3.93	0.983	500	3.89	0.979	500	3.06	0.970	500
1.0	0.05	3.93	0.983	18	3.89	0.979	15	3.06	0.970	12
1.0	0.10	3.93	0.983	18	3.89	0.979	15	3.06	0.970	12
2.0	0.05	3.93	0.983	10	3.89	0.979	9	3.06	0.971	7
2.0	0.10	3.93	0.983	10	3.89	0.979	9	3.06	0.971	7
3.0	0.05	3.93	0.983	8	3.89	0.979	6	3.06	0.971	5
3.0	0.10	3.93	0.983	8	3.89	0.979	6	3.06	0.971	5
5.0	0.05	3.93	0.983	5	3.89	0.980	4	3.06	0.971	3
5.0	0.10	3.93	0.983	5	3.89	0.980	4	3.06	0.971	3
10.0	0.05	3.93	0.985	3	3.89	0.981	2	3.06	0.971	2
10.0	0.10	3.93	0.985	3	3.89	0.981	2	3.06	0.971	2
30.0	0.20	3.93	0.986	2	3.89	0.981	2	3.06	0.971	2

APPENDIX C  
INSTRUCTIONS FOR USE OF  
COMPUTER PROGRAM

A. Required Input Data

The following table lists all the required inputs for a calculation of radome boresight error and/or antenna pattern properties. All data are read in from punched cards. The order of the input of the data depends upon the calculation and therefore can be varied.

TABLE XII

Variables	Description of Variable	Units
MC	Number of cases to be calculated	Integer Number
LL(I)	Number of look angles for which calculations are made for the I-th case on MC	Integer Number
PL(I)	The I-th look angle on LL	Decimal Degrees
NRE(I)	The number of equally spaced rays used for the I-th case on MC	Integer Number
POLIZ	Polarization: Either perpendicular or parallel	Alphabetic
TITLE	Description of Calculation	Alphanumeric
SOURCE	Specifies source type, taper, presence of obstacles, presence of radome, source taper, etc. See comment cards at beginning of program for complete description	Alphanumeric
FREQ	Frequency in megacycles	Decimal
NUM	One less than the number of points calculated in a partial pattern calculation	Integer Number
SPAN	One-half the angular range over which pattern points are calculated	Decimal Degrees
NOS	Number of geometry sections used to define the radome shape	Integer Number
N(I)	The number of layers in the I-th geometry section of NOS	Integer Number
SHAPE(I)	The shape of the I-th section on NOS	Alphabetic
DCE(I, IL)	The dielectric constant of the I-th layer of the IL-th geometry section	Decimal Number

TABLE XII (Cont.)

Variable	Description of Variable	Units
D(I, IL)	The thickness of the I-th layer of the IL-th geometry section	Decimal Inches
TD(I, IL)	The loss tangent of the I-th layer of the IL-th geometry section	Decimal Number
XOO, YOO	The coordinates of the center of an ogive radome section	Decimal Inches
ROO	The radius of an ogive section	Decimal Inches
XLIN, YLIN	Coordinates of a point on a conical section of a radome	Decimal Inches
PHLIN	Included angle of a conical section of a radome	Decimal Degrees
DFATSP	The distance from the coordinate axes to the source aperture plane	Decimal Inches
A	The length of the aperture plane	Decimal Inches
TAPER	Description of aperture amplitude taper	Alphanumeric
PHD	Phase allowance used in averaging the reconstructed aperture	Decimal Degrees
TRD	Transmission allowance used in averaging the reconstructed aperture	Decimal Number
NBLOK	The number of a geometry section which is an aperture block (metal). If none NBLOK = 0	Integer Number
XGB(I)	The x-coordinate of a boundary between two geometry sections, I and I+1	Decimal Inches
STAP(I)	The amplitude of a step used in a step + function amplitude taper. I on MC	Decimal Number

## B. Description Of A Typical Calculation

The SOURCE card plays a key role in determining the calculation procedure. SOURCE contains twelve alphanumeric words which control various phases of the calculation. Twelve comparison words are read into the program as data statements. By comparing the contents of the SOURCE card to the data statements the desired subroutines are called or the desired calculations are made. Each word of SOURCE contains 6 alphanumeric characters or blanks (which are designated by <sup>b</sup>),. Each word is explained below.

Source (1) indicates the calculation of the monopulse difference pattern by FMONOP. The sum pattern is calculated otherwise.

Source (2) is not used.

Source (3) indicates the calculation of the no-radome case by <sup>b</sup>NObbb.

Source (4) indicates the use of an aperture pedestal + function taper by the word STEP<sup>bb</sup>.

Source (5) indicates the absence of an aperture amplitude taper by FNOAAT.

Source (6) indicates the absence of an aperture phase taper by FNPST.

Source (7) causes the program to calculate sidelobe level and half-power beamwidth when the word OPTION occurs there.

Source (8) indicates the use of a circular aperture by CIRCLE.

Source (9) indicates the presence of an aperture block by <sup>b</sup>BLOCK.

Source (10) calls for a graph of the far-zone pattern by PLOT<sup>bb</sup>.

Source (11) indicates that special x-geometry boundaries are to be read in by the word SXGB<sup>bb</sup>.

Source (12) causes a write-out of ray-tracing and multilayer calculations by WRITER.

Similarly TITLE(1) indicates the calculation of boresight error by the word FNULL<sup>b</sup>. Otherwise a partial pattern calculation is carried out. All other alphanumeric input cards are similarly used, e.g., the words <sup>b</sup>OGIVE and <sup>b</sup>CONE<sup>b</sup> on the shape card cause the program to call either the ogive or cone subroutine respectively, to calculate the geometric constants associated with a radome section. One alphanumeric word enables the taper subroutine to utilize any one of a set of pre-programmed aperture tapers. The TAPER card specifies this word.

Thus for a typical calculation the number of different cases to be run and the various differences between cases are determined. Data which does not change from case to case is read in between the following two specific cards:

If (L.GT.1) Go to 937

Read .....

937 Continue

This prevents unnecessary duplication of computer reading time.

Two or more completely different sets of calculations, such as the boresight error curves for differing radomes, may be carried out on one run by utilizing the cards

DO 949 IY = 1,4

Complete program

949 Continue

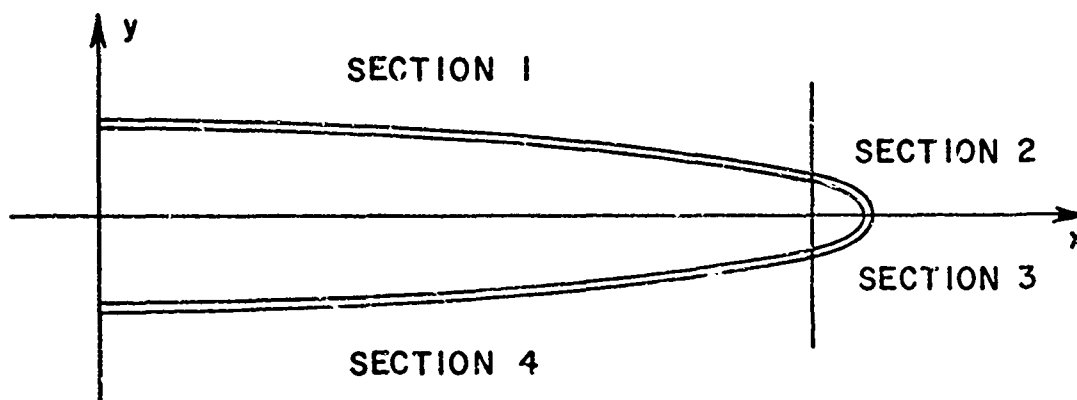
as shown. These cards are in the program permanently so that runs may be combined without re-compiling the program (which consumes about 1/2 minute). The number 4 is completely arbitrary. These cards cause an abnormal termination of the computer and consequent error message when less than 4 runs are made, however this is no problem because the calculations are finished when the termination occurs.

### C. Sample Data Lists

Two example calculations, one of boresight error and one of antenna pattern parameters, are discussed to illustrate the use of the program.

## 1. Boresight error

This example uses an ogive radome having a hemispheric nose cap. Since the calculation requires separate equations for the geometry of the ogive walls on the upper and lower sections, the cap is also divided into two sections to maintain symmetry in the geometrical description of the radome. This results in a four-section radome as shown in the sketch below.



Wall construction in all four sections is a constant A-sandwich. Five cases are to be calculated at four look angles. Referring to Table XIII case MC = 1 is the "no-radome" case which is calculated for reference. Since the pattern without radome is independent of look angle, PL = 0 is used. Cases MC = 2, 3 correspond to perpendicular, parallel polarization calculations for the same radome. Cases 4, 5 correspond to perpendicular, parallel calculations for a similar radome but with a different core dielectric constant. All data of Table XIII are explained on the right hand margin of the table. Reference to Table XII will define the variables.

## 2. Antenna pattern parameters

This example uses an ogive radome having a hemispheric nose cap. The aft portion of the radome is conical for fairing purposes. Thus there are 6 geometry sections, 3 on each side of the coordinate axes. Eight cases are calculated corresponding to four different aperture distributions with and without radome. The far-zone pattern is calculated and plotted for the angular range of  $\pm 45^\circ$  (span) about the beam axis. Sidelobe level and half-power beamwidth with and without radome are the

quantities being calculated as a function of source distribution. As can be seen from Table XIV the quantity of data read in after the initial run (MC = 1) is minimal. This is typical.

TABLE XIII

VARIABLE

5				
1	4	4	4	4
10.0				
100				
3.	.1			
1.				
501	501	501	501	501
FNULL CALCULATION				
9300.				
4				
3	3	3	3	
OGIVE	OGIVE	OGIVE	OGIVE	
FMONOPULSE	NO RADOME	FNOAATF	FNPST	
-2.00	2.000	3.000		
-2.00	69.000	80.000		
24.00	0.00	2.000		
24.00	0.00	2.000		
-2.00	69.000	80.000		
PERPENDICULAR				
0.				
8.9	2.8	8.9		
.040	.192	.040		
.0003	.0057	.0003		
8.9	2.8	8.9		
.040	.192	.040		
.0003	.0057	.0003		
8.9	2.8	8.9		
.040	.192	.040		
.0003	.0057	.0003		
4				
3	3	3	3	
OGIVE	OGIVE	OGIVE	OGIVE	
FMONOPULSE	NO RADOME	FNOAATF	FNPST	
-2.00	2.000	3.000		
-2.00	69.000	80.000		
24.00	0.00	2.000		
24.00	0.00	2.000		
-2.00	69.000	80.000		
PERPENDICULAR				
0.	8.	16.	24.	
8.9	2.8	8.9		
.040	.192	.040		
.0003	.0057	.0003		

2.000 SXGB -2.00

2.000 SXGB -2.00

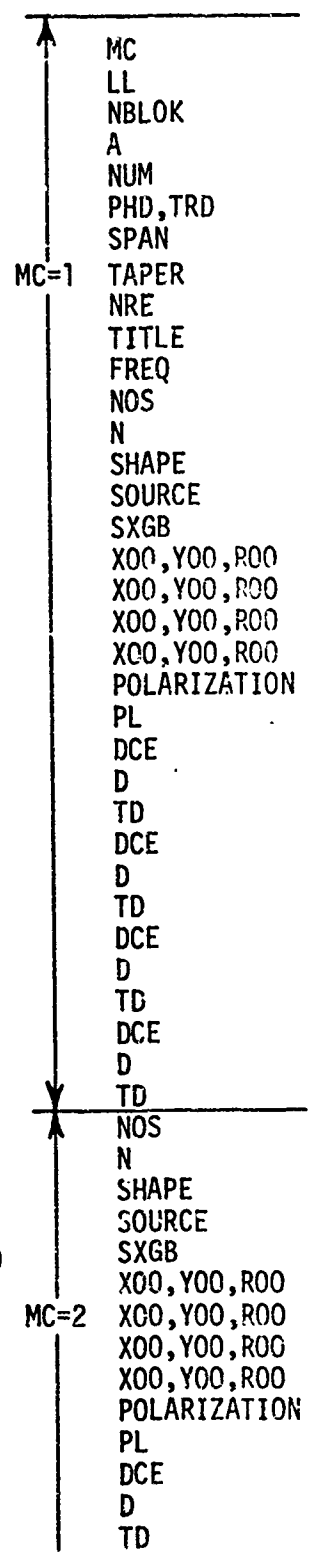
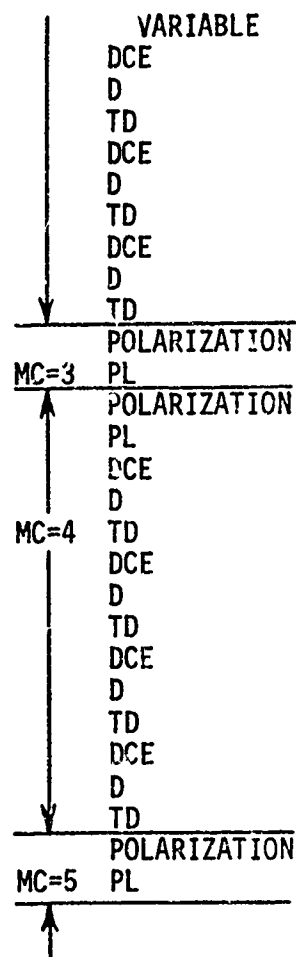


TABLE XIII (Cont.)

	8.9	2.8	8.9
	.040	.192	.040
	.0003	.0057	.0003
	8.9	2.8	8.9
	.040	.192	.040
	.0003	.0057	.0003
	8.9	2.8	8.9
	.040	.192	.040
	.0003	.0057	.0003
PARALLEL			
0.	8.	16.	24.
PENPENDICULAR			
0.	8.	16.	24.
	8.9	2.4	8.9
	.040	.192	.040
	.0003	.0053	.0003
	8.9	2.4	8.9
	.040	.192	.040
	.0003	.0053	.0003
	8.9	2.4	8.9
	.040	.192	.040
	.0003	.0053	.0003
	8.9	2.4	8.9
	.040	.192	.040
	.0003	.0053	.0003
PARALLEL			
0.	8.	16.	24.





D. Computer Programs

C ALL CALCULATIONS NOW ASSUME THE RADOME IS SYMMETRIC ABOUT THE AXIS  
 C AA,BB,CC,DD,EE,FF ARE THE DEFINING CONSTANTS FOR A GIVEN RADOME.  
 C AF N LENGTH OF NTH SUBAPERTURE.  
 C CF N PHASE CORRECTION DUE TO THE NTH SUBAPERTURE LOCATION AWAY  
 C FROM THE ORIGIN.  
 C P IS THE PATTERN ANGLE PHI. MEASURED IN THE X-Y PLANE  
 C PL I IS THE ITH LOOK ANGLE IN DEGREES.  
 C AF IS THE FAR FIELD AMPLITUDE.  
 C O IS THE OUTPUT PARAMETER FOR THE GRAPH SUBROUTINE.  
 C RPL I IS THE LOOK ANGLE IN RADIANS.  
 C RFPD IS THE INSERTION PHASE DELAY FOR A RAY.  
 C PH IS THE TOTAL PHASE TERM FOR A GIVEN SUBAPERTURE.  
 C TI IS THE ANGLE OF INCIDENCE FOR A RAY.  
 C AAT APERTURE AMPLITUDE TAPER.  
 C TITLE INDICATES WHETHER TO CALCULATE THE NULL OR A PARTIAL PATTERN.  
 C B IS THE ANGLE USED IN GRAPH TO PLOT THE PHI AXIS.  
 C MM INDICATES THE DIVISION BETWEEN THE TWO HALVES OF THE APERTURE.  
 C MM IS THE NUMBER OF THAT SUBAPERTURE IMMEDIATELY BELOW THE X-AXIS.  
 C YC IS THE Y-COORD OF THE CENTER OF A SUBAPERTURE AT LOOK ANGLE O.  
 C PHST IS THE PHASE TAPER.  
 C DCF IS THE REAL PART OF THE RELATIVE PERMITIVITY.  
 C DCE I,L IS THE DIELECTRIC CONSTANT FOR THE ITH LAYER OF THE ITH  
 C GEOMETRY SECTION.  
 C TD I,L IS THE LOSS TANGENT FOR ITH LAYER,LTH GEOMETRY SECTION.  
 C DI,L IS THE THICKNESS IN INCHES FOR THE ITH LAYER,LTH GEOMETRY  
 C TC IS THE AMPLITUDE TRANSMISSION COEFFICIENT FOR A RAY.  
 C TR IS THE TOTAL TRANSMISSION FACTOR FOR A SUBAPERTURE.  
 C POLIZ INDICATES PERP OR PAR POLARIZATION FOR MULTILAYER CALC .  
 C XGB IS THE X-COORDINATE OF A RADOME GEOMETRY DISCONTINUITY.  
 C YGB IS THE Y-COORDINATE OF A RADOME GEOMETRY DISCONTINUITY.  
 C NRE IS THE NUMBER OF EQUALLY SPACED RAYS USED  
 C NRE IS CHOSEN UNEVEN TO GET A RAY THROUGH THE ORIGIN.  
 C T IS THE ANGLE OF INCIDENCE FROM THE CENTER OF A SUBAPERTURE TO  
 C THE RADOME INNER WALL.  
 C LL INDICATES THE TOTAL NUMBER OF DIFFERENT LOOK ANGLES EXAMINED.  
 C X00,Y00,R00 INDICATE THE CENTER,RADIUS FOR AN OSGIVE SECTION IN  
 C THE X,Y PLANE.  
 C Y0 IS THE MAXIMUM MAGNITUDE OF Y-COORDINATE FOR A SUBAPERTURE AT  
 C LOOK ANGLE 0.0 DEGREES.  
 C MC IS THE TOTAL NUMBER OF CASES TO BE RUN  
 C A TOTAL SOURCE APERTURE LENGTH.  
 C NOS IS THE NUMBER OF RADOME SECTIONS HAVING DIFFERENT GEOMETRY.  
 C FREQ IS THE FREQUENCY IN MEGACYCLES.  
 C ANFA IS THE NUMBER OF EQUAL-LENGTH SUBAPERTURES.  
 C NUM IS ONE LESS THAN THE NUMBER OF FIELD POINTS TO BE CALCULATED  
 C IN A PARTIAL PATTERN TYPE CALCULATION.  
 C FJ IS THE COMPLEX NUMBER J  
 C SPAN IS THE ANGULAR RANGE OF CALCULATION ABOUT THE BEAM AXIS.

Fig. 57. Main program - Page 1.

```

C PSEM IS THE BORESIGHT ERROR IN MILLIRADIANS
C TS IS THE SLOPE OF THE TANGENT TO THE RADOME CURVE AT P X,Y .
C TL IS THE SLOPE OF THE RAY AT THE SAME POINT P X,Y
C SLL IS SIDLOBE LEVEL IN PER CENT.
C SLOB IS SIDLOBE LEVEL IN DB
C M1 IS THE NUMBER OF SUBAPERTURES
C ISCALE IS A SPREADING FACTOR FOR GRAPH WHEN FEW POINTS ARE USED.
C RPWR IS THE POWER AT BEAM MAXIMUM RELATIVE TO THE NO RADOME CASE.
C LIX IS THE PRESENT VALUE OF THE LOOK ANGLE INDEX I IN MAIN.
C THE TLIM VARIABLE PREVENTS COMPUTER ROUNDOFF ERROR.
C FNRP IS THE POWER NORMALIZING TERM.
C TAPER INDICATES (IN A ONE WORD HOLLERITH FIELD) THE SOURCE TAPER.
C DBST IS 1/2 THE LENGTH OF A SYMMETRICALLY PLACED APERTURE BLOCK.
C SOURCE(1) INDICATES THE CALCULATION OF A MONOPULSE DIFFERENCE
C PATTERN BY 'MONO' THE SUM PATTERN IS CALCULATED OTHERWISE.
C SOURCE(3) INDICATES CALCULATION OF THE NO RADOME CASE BY 'NO'
C SOURCE(4) INDICATES THE USE OF AN APERTURE PEDESTAL+FUNCTION TAPER
C BY THE WORD 'STEP'.
C SOURCE(5) INDICATES THE ABSENCE OF AN AMPLITUDE TAPER BY 'FNDAAT'.
C SOURCE(6) INDICATES THE ABSENCE OF AN PHASE TAPER BY 'FNPHST'.
C SOURCE 7 CALLS GRAPH,SLL,RPWR WHEN THE WORD OPTION OCCURS THERE.
C SOURCE(8) INDICATES THE USE OF A CIRCULAR APERTURE BY 'CIRCLE'.
C SOURCE(9) INDICATES THE PRESENCE OF AN APERTURE BLOCK BY 'BLOCK'.
C SOURCE(10) CALLS FOR A GRAPH OF THE FAR-FIELD BY 'PLOT'.
C SOURCE(11) INDICATES THAT SPECIFIC X-GEOMETRY BOUNDARIES ARE TO BE
C READ IN BY 'SXGR'. OTHERWISE PROGRAM CALCULATES THE XGR'S.
C SOURCE(12) CAUSES A WRITE-OUT OF RAY-TRACE AND MULTILAYER CALCULAT
C IONS IF THE WORD WRITER OCCURS THERE.
C THE DO 949 LOOP ALLOWS THE ENTIRE PROGRAM TO BE RECYCLED.
C RAF,RCF,RTF,RPH ARE TEMPORARY LOCATIONS FOR RECONSTRUCTED APERTURE
C COEFFICIENTS AF,CF,TR,PH.
C DFATST = DISTANCE FROM AXIS TO SOURCE PLANE.
C THE SIDLOBE LEVEL SUBROUTINE CALCULATES THE POWER LEVEL AT THE 1ST
C LOBE LOCATION OF THE NO RADOME CASE EVERY TIME IN ADDITION TO THE
C MAXIMUM SIDLOBE LEVEL. WHEN NO SIDLOBE IS DETECTED THIS IS TAKEN
C AS SIDLOBE LEVEL.
C DFATST = DISTANCE FROM AXIS TO SOURCE PLANE.

```

```

DOUBLE PRECISION AA,BB,CC,DD,EE,FF,XGB,YGB,PI,BRR,CCC,DISC,DYDX,X,
1 Y,TS,TL,CL,CL2,SL,SL2,C2L,S2L,TL,RPL,DISCU,XOO,YOO,ROO
COMMON T(501,12),SOURCE(12),PI,RADEG,DEGRAD,M1,NOS,IX,MC,A,YC(501)
1 ,YA(501),YA(501),DFATSP,XLIN,YLIN,PHLIN,
1 PHST(501),AAT(501),TAPER,NBLOK1,NBLOK2 ,YO(501),PCX
COMMON /TPR/ Y,STAP(25)
COMMON /RR1/ RPL(25),XGB(12),TL,SL,S2L,CL2,SL2,XOO,YOO,ROO,CL,
1 AA(12),BB(12),CC(12),DD(12),EE(12),FF(12)

```

Fig. 57. Main program - Page 2.

```

1, ANEA, AF(501), CF(501), MM(25), LT, PL(25), NRE(25),
INR, MPOS, LEX, P52
COMMON /JRM/ N(12), D(12,12), DCL(12,12), TC(12,12), FIPQ(501), TC(501)
1, FREQ, POL17(3)
DIMENSION LL(25), IR(501), TITLE(12), P(501)
11), AB(501), PH(501), AC(501), PI(12), AL(501), SHAPE(12), PHD6(501)
DIMENSION RAF(501), RCF(501), RPH(501), RTR(501)
1 FORMAT(10F2.6)
2 FORMAT(16I5)
3 FORMAT(2X,6HMM I 15)
4 FORMAT(F10.3,8H SECONDS)
5 FORMAT(F10.3,8H MINUTES)
9 FORMAT(6D13.8)
10 FORMAT(16I5)
11 FORMAT (8F10.6)
12 FORMAT(3D10.6)
13 FORMAT (15,F10.4,15)
14 FORMAT(11H LOOK ANGLE,F10.3)
15 FORMAT(3H MC,15/11H WAVELENGTH,F10.6/29H NO. OF APERTURE SURDIVISIONS,15/28H NO. OF LOOK ANGLES EXAMINED,15//)
16 FORMAT(22H LOOK ANGLE IN RADIAN,2F10.6)
17 FORMAT(F10.2)
18 FORMAT(8F7.6)
19 FORMAT(16I1)
23 FORMAT(6E12.4)
40 FORMAT(F12.2,F11.3,F11.4)
42 FORMAT(13F6.2)
45 FORMAT(F13.5,F9.5)
100 FORMAT(/(2F10.4))
140 FORMAT(12H SPAN ANGLE ,F10.4)
141 FORMAT(19H PEDESTAL HEIGHT ,F10.5)
150 FORMAT(12(A4,2X))
151 FORMAT(3(A4,2X),F4.1,6(A4,2X),I4,A4,2X)
152 FORMAT(4X,17A4)
COMPLEX FJ,F(501),E3
DATA STEP/4HSTEP/
DATA PARALL/4H PAR /
DATA WRITLR/4HWRIT/
DATA SXGB/4HSXGB/
DATA PLOT/4HPLOT/
DATA FNULL/4HFNULL /
DATA FMONOP/4HFMON /
DATA FNORAD/4H NO /
DATA OGIVE/4H OGI /
DATA CONE/4H CON /
DATA OPTIGN/4HOPTI /
PI=3.1415926535897932
DEGPAD=PI/180.

```

Fig. 57. Main program - Page 3.

```

RADEG=180./PI
FJ=(0.,1.)
DO 949 1Y=1,2
MG2=1
READ(5,2) MC
READ(5,11) PHD,TRD
PHD=PHD*DEGRAD
READ(5,2) (LL(I),I=1,MC)
DO 300 L=1,MC
MG1=0
MYMM=0
RPHR=1.
LT=LL(L)
MCX=L
IF(L.GT.1) GO TO 937
READ(5,2) NBLOK1,NBLOK2
READ(5,12) DFATSP
READ(5,1) A
FNRP=A
READ(5,2) NUM
NUM2=NUM+1
TNUM =NUM
TNUM2=TNUM/2.
READ(5,17) SPAN
RSPAN=SPAN*DEGRAD
READ(5,150) TAPER
READ(5,2) (NRE(I),I=1,MC)
READ(5,150) (TITLE(I),I=1,12)
READ(5,2) NOS
NNOS=1+NOS
READ(5,10) (N(I),I=1,NOS)
READ(5,150) (SHAPE(I),I=1,NOS)
DO 121 I=1,NOS
IX=I
IF(SHAPE(IX).EQ.OCGIVE) GO TO 155
IF(SHAPE(IX).EQ.CONE) GO TO 157
READ(5,9) AA(IX),PB(IX),CC(IX),DD(IX),EE(IX),FF(IX)
GO TO 121
155 READ(5,12) X00,Y00,R00
CALL GIVE
GO TO 121
157 READ(5,12) XLIN,YLIN,PHLIN
CALL CONIC
121 CONTINUE
READ(5,150) (POLIZ(I),I=1,3)
READ(5,1) (PL(I),I=1,LT)
IF(POLIZ(1).EQ.PARALL) GO TO 909
DO 120 IL=1,NOS

```

Fig. 57. Main program - Page 4.

```

NL=N(IL)
READ(5,11) (DC(I,IL),I=1,NL)
READ(5,11) (D(I,IL),I=1,NL)
120 READ(5,11) (TD(I,IL),I=1,NL)
909 CONTINUE
WRITE(6,19)
READ(5,11) FREQ
Y=1.180314E+4/FREQ
W=2.*PI/Y
937 CONTINUE
READ(5,150) (SOURCE(J),J=1,12)
IF(SOURCE(11).EQ.SXGB) PLAL(5,9) (XGB(I),I=1,NGB)
IF(SOURCE(4).EQ.STEP) READ(5,42) (STAP(I),I=1,NC)
IF(SOURCE(3).EQ.FNGRAD) NG1=1
IF(TITLE(1).EQ.FRUILL) GO TO 938
WRITE(6,151) (TITLE(I),I=1,3),SPAC, (TITLE(I),I=5,10),NUM2,TITLE(12)
GO TO 939
938 WRITE(6,152) TITLE
939 WRITE(6,150) (SOURCE(IJ),IJ=1,12)
WRITE(6,150) (SHAPE(I), I=1,NCS)
WRITE(6,150) POLIZ
WRITE(6,152) TAPER
IF(STAP(L).GT.0.) WRITE(6,141) STAP(L)
DO 110 I=1,LT
ANEA=NRE(L)-1
M1=ANEA
NR=NRE(L)
DO 50 K=1,M1
AF(K)=1./ANEA
T1=K
50 CF(K)=T1/ANEA-(ANEA+1.)/(2.*ANEA)
LLX=I
RPL(I)=DEGRAD*PL(I)
CL=DCOS(RPL(I))
MM(I)=ANEA/2.
SL=DSIN(RPL(I))
CL2=DCOS(RPL(I))*2
SL2=DSIN(RPL(I))*2
S2L=DSIN(2.*RPL(I))
TL=SL/CL
CALL SCLOK1
CALL NKRR1
941 TIME=PCLOCK1(1.)
TIMEM=TIME/60.
WRITE(6,1001) TIME
WRITE(6,5) TIMEM
1001 FORMAT(1X,17H TIME IN RAY TRACE,FIG.3,PH SECONDS)
IF(SOURCE(3).EQ.FNGRAD) GO TO 557

```

Fig. 57. Main program - Page 5.

```

CALL SCLOCK1
CALL IRJ&M
TIME=RCLOCK1(1.)
TIMEM=TIME/60.
WRITE(6,1002) TIME
1002 FORMAT(1X,18H TIME IN MULTILAYER,F10.3,8H SECONDS)
WRITE(6,5) TIMEM
557 CALL SCLOCK1
CALL ATAPER
TIME=RCLOCK1(1.)
TIMEM=TIME/60.
WRITE(6,1003) TIME
WRITE(6,5) TIMEM
1003 FORMAT(1X,19H TIME TO CALC.TAPERS,F10.3,8H SECONDS)
IF(SOURCE(3).NE.FNORAD) GO TO 609
DO 558 NA=1,M1
FIPD(NA)=0.0
TC(NA)=1.
558 CONTINUE
609 CONTINUE
DO 710 I1=1,M1
TR(I1)=TC(I1)*AAT(I1)
PH(I1)=FIPD(I1)*DEGRAD+PHST(I1)
710 CONTINUE
WRITE(6,410) PHD,TRD
410 FORMAT(2X,26H ALLOWED PHASE DIFFERENCE F10.6/2X,33H ALLOWED TRANS.C
10FFF. DIFFERENCE F10.6)
CALL SCLOCK1
J1=0
J2=0
405 J0=MM(1)
J=J0
IF(J2.EQ.0) GO TO 411
J5=J1
J0=J0+1
J=J+1
412 J0=J0-1
TR1=TR(J0)
PH1=PH(J0)
413 J=J-1
IF(J.EQ.1) GO TO 414
DTR=TR(J)-TR1
DPH=PH(J)-PH1
IF(ABS(DTR)-120) 415,415,414
415 IF(ABS(DPH)-90) 413,414,414
414 PH2=0.
TR2=0.
AF2=0.

```

Fig. 57. Main program - Page 6.

```
CF2=0.
DO 416 JP=J, JO
CF2=CF2+CF(JP)
AF2=AF2+AF(JP)
TR2=TR2+TR(JP)
416 PH2=PH2+PH(JP)
J1=J1+1
T3=JO-J+1
RAF(J1)=AF2
RCF(J1)=CF2/T3
RPH(J1)=PH2/T3
RTR(J1)=TR2/T3
JO=J
IF(J.NE.1) GO TO 412
GO TO 418
411 J2=1
404 JO=JO+1
TR1=TR(JO)
PH1=PH(JO)
401 J=J+1
IF(J.EQ.M1) GO TO 402
DTR=TR(J)-TR1
DPH=PH(J)-PH1
IF(ABS(DTR)-TPD) 407,407,402
407 IF(ABS(DPH)-PHD) 401,402,402
402 PH2=0.
TR2=0.
AF2=0.
CF2=0.
DO 403 JP=JO, J
CF2=CF2+CF(JP)
AF2=AF2+AF(JP)
TR2=TR2+TR(JP)
403 PH2=PH2+PH(JP)
J1=J1+1
T3=J-JO+1
RAF(J1)=AF2
RCF(J1)=CF2/T3
RPH(J1)=PH2/T3
RTR(J1)=TR2/T3
JO=J
IF(M1-J) 405,405,404
418 M1=J1
ML=M1-J5
MM(I)=ML
J4=J1+1
WRITE(6,421) J1,M1,J4,ML,J5
421 FORMAT(2X,'J1='I5/' M1 'I5/' J4 'I5/' ML 'I5/' J5 'I5//')
```

Fig. 57. Main program - Page 7.

```

C   RAF,RCI,RTI,RPI ARE TEMPORARY LOCATIONS FOR RECONSTRUCTED APERTURE
C   COEFFICIENTS AF,CF,TR,PH.
WRITE(6,406) J1
406 FORMAT(2X,55HNUMBER OF SUPAPERTURES USED IN RECONSTRUCTED APERTURE
1 15)
DO 419 J=1,ML
AF(J)=RAF(J4-J)
CF(J)=RCF(J4-. )
TR(J)=RTR(J4-J)
419 PH(J)=RPH(J4-J)
DO 420 J=1,J5
AF(J+ML)=RAF(J)
CF(J+ML)=PCF(J)
TR(J+ML)=RTR(J)
420 PH(J+ML)=RPH(J)
DO 417 J=1,M1
417 PHDG(J)=PH(J)*RADEG
WRITE(6,408)
408 FORMAT(2X,35HRECONSTRUCTED APERTURE COEFFICIENTS/4X,2HAF,8X,2HCF,(
1X,2HTR,8X,2HPH//)
WRITE(6,409) (AF(J),CF(J),TR(J),PHDG(J),J=1,M1)
409 FORMAT(3F10.6,F10.4)
TIME=SCLOCK(1.)
TIMEM=TIME/60.
WRITE(6,1009) TIME
WRITE(6,5) TIMEM
1009 FORMAT(1X,36HTIME TO CALC. RECONSTRUCTED APERTURE,F10.3,8H SECONDS
1)
IF(I.GT.1) GO TO 943
943 CONTINUE
IF(SOURCE(1).NE.FYONOP) GO TO 25
DO 27 NN=1,ML
AF(NN)=-AF(NN)
27 CONTINUE
25 WRITE(6,15) NC,Y,M1,LT
WRITE(6,3) MM(1)
IF(TITLE(1).EQ.FNULL) GO TO 60
GO TO 34
60 K=0
CALL SCLOK1
KR=0
P(1)= RSPAN
P(2)=-RSPAN
500 K=K+1
E(K)=(0.,0.)
DO 900 M=1,M1
S=W*A*SIN(P(K))*AF(M)*.5
IF(S.LT.-0.10.AND.S.GT.-0.10) GO TO 800

```

Fig. 57. Main program - Page 8.

```

      SS=SIN(S)/S
      GO TO 810
800  SS=1.
      810 Q=W*A*CF(M)*SIN(P(K))-PH(M)
          CQ=COS(Q)
          SQ=SIN(Q)
          F1= TR(M)*A*AF(M)*SS
          E2= E1*CQ
          E3= E1*SQ*FJ
      900 E(K)=E(K)+L2+E3
      890 AE(K)=CABS(L(K))
          IF(K.EQ.1.AND.KR.EQ.0) GO TO 500
          IF(KR.EQ.1)GO TO 502
          KR=KR+1
          IF(AE(1)-AE(2)) 501,502,503
      501 P(2)=(P(1)+P(2))/2.
          K=1
          GO TO 500
      503 P(1)=(P(1)+P(2))/2.
          K=0
          GO TO 500
      502 BNULL=(P(1)+P(2))/2.
          TIME=RCLOCK(1.)
          TIMEM=TIME/60.
          WRITE(6,1004) TIME
          WRITE(6,5) TIMEM
1004  FORMAT(1X,17HTIME TO CALC.NULL,F10.3,8H SECONDS)
          DO 59 NJ=1,ML
      59  AF(NJ)=ABS(AF(NJ))
      34  CALL SCLOCK
          NU3=1
          IF(SOURCE(7).EQ.OPTION) NU3=NUM2
          DO 92 K=1,NU3
          F(K)=(0.,0.)
          T1=K
          IF(NU3.EQ.1) GO TO 510
          P(1)= RSPAN-(T1-1.)*RSPAN/TNUM2
          GO TO 511
      510 P(1)=0.
      511 DO 90 M=1,ML
          S=W*A*SIN(P(1))*AF(M)*.5
          IF(S.LT.0.10.AND.S.GT.-0.10) GO TO 80
          SS=SIN(S)/S
          GO TO 81
      80  SS=1.
      81  Q=W*A*CF(M)*SIN(P(1))-PH(M)
          CQ=CCS(Q)
          SQ=SIN(Q)

```

Fig. 57. Main program - Page 9.

```

F1= TR(M)*A*AF(M)*SS
E2= L1*CO
E3= E1*SO*FJ
90 F(K)=F(K)+E2+E3
   B(K)=(P(1)+RPL(I))*RADEG
89 AE(K)=CABS(E(K))
   IF(NU3.EQ.1.AND.SOURCE(3).EQ.FNORAD) FNRP=AE(K)
   IF(NU3.EQ.1.AND.SOURCE(3).NE.FNORAD) RPWR=(AL(K)/FNRP)**2
   IF(K.EQ.(NU3/2).AND.SOURCE(3).EQ.FNORAD) FNRP=AE(K)
   IF(K.EQ.(NU3/2).AND.SOURCE(3).NE.FNORAD) RPWR=(AF(K)/FNRP)**2
92 CONTINUE
   WRITE(6,504) RPWR
504 FORMAT(/,2X,26HRELATIVE POWER AT PNULL ,F10.6)
   TIME=RCLOCK(1.)
   TIMEM=TIME/60.
   WRITE(6,1005) TIME
1005 FORMAT(1X,28HTIME TO CALC.PARTIAL PATTERN,F10.3,8H SECONDS)
   WRITE(6,5) TIMEM
33 CONTINUE
   IF(TITLE(1).EQ.FNULL) GO TO 101
   XMAX= 0.0
   BMAX=0.0
   DO 200 J=1,NUM2
   IF(AE(J).GT.XMAX) GO TO 205
   GO TO 200
205 XMAX=AE(J)
   BMAX=B(J)
200 CONTINUE
101 CONTINUE
   IF(SOURCE(1).NE.FMONOP) GO TO 611
   IF(TITLE(1).EQ.FNULL) GO TO 610
   DO 62 J=1,NUM2
   IF(AE(J).LT.AE(J-1).AND.AE(J).LE.AE(J+1).AND.ABS(R(J)-PL(I)).LT.2.
1) GO TO 63
   GO TO 62
63 XNULL=AE(J)
   BNULL=B(J)
62 CONTINUE
   BSEM=(BNULL-PL(I))*DEGRAD*1000.
   GO TO 601
610 CONTINUE
   BSEM=BNULL*1000.
   BNULL=BNULL*RADEG
601 WRITE(6,602) BNULL,BSEM
602 FORMAT(/7H BNULL ,F10.6,9H DEGREES./7H BSEM ,F10.6,14H MILLIRADIA
INS.)
611 IF(TITLE(1).EQ.FNULL) GO TO 111
   WRITE(6,19)

```

Fig. 57. Main program - Page 10.

```

IF(SOURCE(7).NE.OPTION) GO TO 112
IF(SOURCE(10).NE.PLOT) GO TO 113
CALL SCLOCK
ISCALE=60/NUM
CALL GRAPH(AE,XMAX,0.,NUM2,B,ISCALE)
TIME=RCLOCK(1.)
TIMEM=TIME/60.
WRITE(6,1006) TIME
WRITE(6,5) TIMEM
1006 FORMAT(1X,13HTIME IN GRAPH,F10.3,8H SECONDS)
113 CALL SCLOCK
CALL HPRW(AE, XMAX, NUM2, B)
TIME=RCLOCK(1.)
TIMFM=TIME/60.
WRITE(6,1007) TIME
WRITE(6,5) TIMEM
1007 FORMAT(1X,12HTIME IN HPBW,F10.3,8H SECONDS)
CALL SCLOCK
961 MMM=1+MMM
CALL SLL(AE,XMAX,NUM2,AB,BSLMAX,AL,B,$950,$964,M61)
GO TO 951
964 MMM=0
950 IF(SOURCE(3).EQ.FNORAD) GO TO 962
WRITE(6,1551)
1551 FORMAT(///'THE POWER LEVEL AT THE POSITION OF THE 1ST SIDE LOBE
1 WITH NO PADOME IS CALCULATED BELOW'//)
P(1)=BSLMAX
K=1
KR=11
P(2)=P(1)
GO TO 952
951 K=0
KR=0
P(1)= BSLMAX-DEGRAD
P(2)= BSLMAX+DEGRAD
1500 K=K+1
952 E(K)=(0.,0.)
DO 1900 M=1,M1
S=W*A*SIN(P(K))*AF(M)*.5
IF(S.LT.0.10.AND.S.GT.-0.10) GO TO 1800
SS=SIN(S)/S
GO TO 1810
1800 SS=1.
1810 O=W*A*CF(M)*SIN(P(K))-PH(M)
CQ=COS(O)
SQ=SIN(O)
E1= TR(M)*A*AF(M)*SS
E2= E1*CQ

```

Fig. 57. Main program - Page 11.

```

      F3= F1*SQ*IJ
1900 F(K)=F(F)+E2+E3
1890 AL(K)=CABS(F(K))
      IF(K.EQ.1.AND.KR.EQ.0) GO TO 1500
      IF(KR.EQ.1)GO TO 1502
      KR=KR+1
      IF(AE(1)-AF(2)) 1503,1502,1501
1501 P(2)=(P(1)+P(2))/2.
      K=1
      PD=P(2)*RADEG
      WRITE(6,13) KR ,PD,K
      GO TO 1500
1503 P(1)=(P(1)+P(2))/2.
      K=0
      PD=P(1)*RADEG
      WRITE(6,13) KR ,PD,K
      GO TO 1500
1502 PSL =(P(1)+P(2))/2.
      IF((P(1)-P(2)).LT..00001) AE(2)=AE(1)
      SLMAX =(AE(1)+AF(2))/(2*XMAX)*100.
      SLDB=20.*ALOG10(100./SLMAX)
      PSLD=PSL*RADEG
      WRITE(6,1550)PSLD,SLDB
1550 FORMAT(' LOCATION OF MAXIMUM SIDELobe = ',F10.4,/' SIDELobe LEVEL
1= ',F10.4,' DB'
      IF(MMMM.EQ.1) GO TO 961
 962 CONTINUE
      TIME=RCLOCK(1.)
      TIMEM=TIME/60.
      WRITE(6,1008) TIME
      WRITE(6,5) TIMEM
1008 FORMAT(1X,11HTIME IN SLL,F10.2,8H SECONDS)
      GO TO 112
 111 CONTINUE
      WRITE(6,19)
112 CONTINUE
      IF(SOURCE(1).NE.FMGNOP) GO TO 110
110 CONTINUE
 300 CONTINUE
 949 CONTINUE
      STOP
      END

```

Fig. 57. Main program - Page 12.

GIVE

DATE = 69199

```
SUBROUTINE GIVE
DOUBLE PRECISION AA, BB, CC, DD, EE, FF, X00, Y00, PI, DBB, CCC, DISC, YDY, Y,
1Y, TS, TI, CL, CL2, SL, SL2, C2L, S2L, TL, RPL, DISCU, X00, Y00, R00
1 ,XA, YA, DFATSP, XLIN, YLIN, PHLIN
COMMON T(501,12), SOURCE(12), PI, RADEG, DEG, RAD, MI, NOS, IX, MC, A, Y0(501)
1, XA(501), YA(501), DFATSP, XLIN, YLIN, PHLIN,
1 PHST(501), AAT(501), TAPER, NBLOK1, NBLOK2, Y0(501), MCX
COMMON /ARRI/ RPL(25), XGB(12), TL, SL, S2L, CL2, SL2, X00, Y00, R00, CL,
1 AA(12), BB(12), CC(12), DD(12), EE(12), FF(12)
1, ANEA, AF(501), CF(501), FM(25), LT, PL(25), NRL(25),
1NR, NROS, LLX, MG?
I=IX
AA(I)=1.
BB(I)=1.
CC(I)=0.
DD(I)=-2.*X00
EE(I)=-2.*Y00
FF(I)=X00*X00+Y00*Y00-R00*R00
RETURN
END
```

Fig. 58. Ogive geometry subprogram.

CONIC

DATE = 69109

```
SUBROUTINE CONIC
  DOUBLE PRECISION AA, BB, CC, DD, FF, XGP, YGP, PI, B50, CCC, DISC, DYDX, X,
  1Y, TS, TI, CL, CL2, SL, SL2, CL2, S2L, TL, RPL, DISCU, X00, Y00, R00
  1, XA, YA, DFATSP, XLIN, YLIN, PHLIN
  COMMON T(50), 12), SOURCE(12), PI, RADEG, DEGRAD, MI, NOS, IX, MC, A, YC(50)
  1, XA(50), YA(50), DFATSP, XLIN, YLIN, PHLIN,
  1 PHST(50), AAT(50), TAPER, NBLOK1, NBLOK2, Y0(50), MCX
  COMMON /RR1/ RPL(25), XGB(12), TL, SL, S2L, CL2, SL2, X00, Y00, R00, CL,
  1 AA(12), BB(12), CC(12), DD(12), LF(12), FF(12)
  1, ANEA, AF(50), CF(50), MM(25), LI, PL(25), NKF(25),
  INF, NNOS, LLY, MG2
  RPHLIN=PHLIN*DEGRAD
  I=IX
  AA(I)=0.
  BB(I)=0.
  CC(I)=0.
  DD(I)=-TAN(RPHLIN)
  FF(I)=1.
  FF(I)=-XLIN*DD(I)-YLIN
  RETURN
  END
```

Fig. 59. Cone geometry subprogram.

```

SUBROUTINE NRRI
  DOUBLE PRECISION AA, BB, CC, DD, EE, FF, XGB, YGB, PL, RPL, CCC, DISC, DYDX, Y,
  1 Y, IS, TI, CL, CL2, SL, SL2, CL2, S2L, TL, RPL-DISC, XGB, YGB, RCP
  1 ,XA, YA, DEFTSP, XLIN, YLIN, PHLIN
  COMMON T(501,12), SOURCE(12), PI, RADLG, DEGRAD, MI, NOS, IX, MC, A, YC(501)
  1 ,XA(501), YA(501), DEFTSP, XLIN, YLIN, PHLIN,
  1 PHST(501), AAT(501), TAPER, NBLOK1, NBLOK2 , YQ(501), MCX
  COMMON /RR1/ RPL(25), XGB(12), TL, SL, S2L, CL2, SL2, XGB, YGB, RCP, CL,
  1 AA(12), BB(12), CC(12), DD(12), EE(12), FF(12)
  1, ANFA, AF(501), CF(501), MM(25), LT, PL(25), NKE(25),
  1 NR, NNOS, LLX, MG2
  DIMENSION TI(501), LG(501), YGB(12), PLI(25)
  DATA WRITER/4HWRIT/
  DATA SXGB/4HSXGB/
  DATA FNORAD/4HNO /
  DATA RMIN/.0000001/
  1 FORMAT(9F10.6)
  2 FORMAT(16I5)
  4 FORMAT(1H1)
  5 FORMAT(2X,4H NOS 15,8X,3HMC 15,8X,3HLL 15)
  6 FORMAT(4X,1H X,6X,1H X,9X,1H Y,8X,2HTI,6X,4HGEOM)
  7 FORMAT(2X,36HX-COORDINATE GEOMETRY BOUNDARIES XGP //(F10.4))
  8 FORMAT(15,3F10.3,15)
  9 FORMAT(2X,2H F10.4//(2X,6HPL I F10.4))
  11 FORMAT(2X,7HRE I 15//)
  12 FORMAT(1H0)
  13 FORMAT(6X,12HLOOK ANGLE ,F10.2//)
  50 FORMAT(4X,2HAA,8X,2HBB,8X,2HCC,8X,2HDD,8X,2HEE,8X,2HFF//)
  51 FORMAT(6F10.4//)
  52 FORMAT(2X,7HYGB L F10.4//)
  IF(SOURCE(3).NE.FNORAD) MG2=MG2+1
  PLI(MG2)=PL(LLX)
  IF(MG2.GT.2.AND.ABS(PLI(MG2)-PLI(MG2-1)).LT..01) GO TO 48
  IF(LLX.GT.1) GO TO 181
  REAL*8 RMIN
  RMIN=1.D-10
  IF(SOURCE(3).EQ.FNORAD) GO TO 181
  WRITE(6,5) NOS,MC,LT
  WRITE(6,11) (NRF(I),I=1,MCX)
  WRITE(6,12)
  WRITE(6,50)
  WRITE(6,51)(AA(I),BB(I),CC(I),DD(I),EE(I),FF(I),I=1,.NS)
  WRITE(6,9)A,(PL(I),I=1,LI)
  NOSS=NOS/2+1
  IF(SOURCE(11).EQ.SXGB) GO TO 200
  XGB(1)= XGB
  XGB(2)=XGB+DSORT(RCP*RCP-YGB*YGB)
  XGB(3)= XGB

```

Fig. 60. Ray trace subprogram - Page 1.

```

200 CONTINUE
WRITE(6,7) (XGB(I),I=1,NNOS)
DO 180 L=1,NOSS
IF(BB(L).EQ.0.) GO TO 182
TLIM=DABS(FF(L))
IF(DABS(AA(L)).GT.TLIM) TLIM= AA(L)
IF(DABS(BB(L)).GT.TLIM) TLIM= BB(L)
IF(DABS(CC(L)).GT.TLIM) TLIM= CC(L)
IF(DABS(DD(L)).GT.TLIM) TLIM= DD(L)
IF(DABS(EE(L)).GT.TLIM) TLIM= EE(L)
TLIM=TLIM*.000001
DISCU=(ICC(L)*XGB(L)+EE(L))/(2.*BB(L))**2-(AA(L)*XGB(L)**2+DD(L)
1*XGB(L)+FF(L))/BB(L)
IF(DABS(DISCU).LT.TLIM) DISCU=0.
IF(L.EQ.NOSS) GO TO 68
67 YGB(L)=-((CC(L)*XGB(L)+EE(L))/(2.*BB(L))+DSQRT(DISCU)
GO TO 183
68 YGB(L)=-((CC(L)*XGB(L)+EE(L))/(2.*BB(L))-DSQRT(DISCU)
GO TO 183
182 YGB(L)=-((AA(L)*XGB(L)*XGB(L)+DD(L)*XGB(L)+FF(L))/(CC(L)*XGB(L)+EE(
1L))
183 IF(DABS(YGB(L)).LT.1.E-3) YGB(L)=0.
IF(L.EQ.NOSS) GO TO 180
N1=NNOS+1-L
YGB(N1)=-YGB(L)
180 CONTINUE
WRITE(6,52) (YGB(I),I=1,NNOS)
181 WRITE(6,4)
WRITE(6,13) PL(LLX)
WRITE(6,6)
DO 20 I=1,NR
T2=I
20 YO(I)=A/(2.*ANEA)*(2.*T2-2.-ANEA)
IF(SOURCE(3).EQ.FNORAD) GO TO 48
DO 210 I=1,NR
XA(I)= CL*DFATSP-YO(I)*SL
210 YA(I)= SL*DFATSP+YO(I)*CL
DO 190 M=1,NR
DO 170 L=1,NOS
LG(M)=L
IF(BB(L).EQ.0.) GO TO 30
XAC=XA(M)
YAC=YA(M)
AAA=AA(L)+BB(L)*TL*TL+CC(L)*TL
BBB= -2.*BB(L)*TL*TL*XAC+2.*BB(L)*TL*YAC-CC(L)*TL*XAC+CC(L)*YAC+D
1 (L)+EE(L)*TL
CCC= -2.*BB(L)*TL*YAC*XAC+BB(L)*TL*TL*XAC*XAC+BB(L)*YAC*YAC-EE(L)*
1 TL*XAC+EE(L)*YAC+FF(L)

```

Fig. 60. Ray trace subprogram - Page 2.

```

BBB=BBB/(2.*AAA)
CCC=CCC/AAA
DISC=BBB*BBB-CCC
IF(DISC.LT.0.) GO TO 170
X=-BBB+USQRT(DISC)
IF(X.GT.XGB(NOSS)) X=XGB(NOSS)-RMINN
GO TO 18
30 M=-(EF(L)*YO(M)/CL+FF(L))/(DD(L)+EE(L)*TL)
18 Y=X*TL+YO(M)/CL
IF(XGB(L).LE.X.AND.X.LE.XGB(L+1).AND.YGB(L).GE.Y.AND.Y.GE.YGB(L+1)
1)GO TO 15
IF(XGB(L).GE.X.AND.X.GE.XGB(L+1).AND.YGB(L).GE.Y.AND.Y.GE.YGB(L+1)
1)GO TO 15
170 CONTINUE
15 IF(DABS(2.*BB(L)*Y+CC(L)*X+EE(L)) .LT.RMIN) GO TO 17
DYDX=-(2.*AA(L)*X+CC(L)*Y+DD(L))/(2.*BB(L)*Y+CC(L)*X+EE(L))
TS=DYDX
IF(DABS(1.+TL*TS) .LT.RMIN) GO TO 22
IF(Y.GE.0.)GO TO 115
TI(M)=PI/2.-DATAN2((TS-TL),(1.+TS*TL))
GO TO 16
115 TI(M)=PI/2.-DATAN2((TL-TS),(1.+TS*TL))
16 TI(M)=DABS(RADEG*TI(M))
GO TO 21
17 TI(M)=PL(LLX)
GO TO 21
22 TI(M)=0.
21 IF(SOURCE(12).EQ.WRITER) WRITE(6,8) M,X,Y,TI(M),L
190 CONTINUE
DO 70 I=1,M1
DO 70 K=1,NOS
70 T(I,K)=-1.
DO 49 KG=1,M1
TI(KG)=(TI(KG)+TI(KG+1))/2.
IF(LG(KG).NE.LG(KG+1).AND.LG(KG).GT.(NOS/2)) GO TO 71
LG(KG)=(LG(KG)+LG(KG+1))/2
71 K=LG(KG)
I=KG
49 T(I,K)=TI(KG)
48 RETURN
END

```

Fig. 60. Ray trace subprogram - Page 3.

```

SUBROUTINE NKJRM
DOUBLE PRECISION AA, BB, CC, DD, EE, FF, XGB, YGB, PI, BBA, CCC, DISC, DYDX, X,
1Y, TS, TI, CL, CL2, SL, SL2, C2L, S2L, TL, RPL, DISCU, X00, Y00, R00
1 ,XA, YA, DFATSP, XLIN, YLIN, PHLIN, DOBST
DOUBLE PRECISION TR
COMMON T(501,12), SOURCE(12), PI, RADEG, DEGRAD, M1, NOS, IX, MC, A, YC(501)
1 ,XA(501), YA(501), DFATSP, XLIN, YLIN, PHLIN, DOBST,
1 PHST(501), AAT(501), TAPER, NBLOK1, NBLOK2 ,YO(501), MCX
COMMON /JRM/ N(12), D(12,12), DCE(12,12), TD(12,12), FIPD(501), TC(501)
1 ,FREQ, POLIZ
DIMENSION R(12), G(12), SR(12), NN(12), DDD(12)
1 FORMAT(F10.2,9X,F11.6,1X,F10.6,2(10)
2 FORMAT (5F15.6)
3 FORMAT (I15,4F15.9)
4 FORMAT (F15.7,4F10.6,F15.7)
7 FORMAT(1H1)
8 FORMAT(7X,1HT,10X,4HFIPD,9X,11HTRANS COEFF,9X,1HK,9X,1HL)
999 FORMAT(' WALL THICKNESS = 'F10.6/)
DATA PARALL/4H PAR /
DATA RMIN/.0000001/
DATA WRITER/4HWIT/
DATA FNORAD/4H NO /
IF(SOURCE(3).EQ.FNORAD) GO TO 557
DO 6 L=1,NOS
NN(L)=N(L)+1
NNL=NN(L)
6 DCE(NNL,L)=1.
WRITE(6,8)
DO 5 L=1,NOS
NL=N(L)
DDD(L)=0.
DO 5 I=1,NL
IF(L.EQ.1) WRITE(6,999) D(I,L)
5 DDD(L)=DDD(L)+D(I,L)
DO 60 K=1,M1
DO 60 L=1,NOS
IF(T(K,L).LT.0.) GO TO 60
IF(L.EQ.NBLOK1.OR.L.EQ.NBLOK2) GO TO 100
GO TO 101
100 FIPD(K)=0.
TC(K)=0.
GO TO 60
101 TH=T(K,L)*DEGRAD
DD=2.*COS(TH)*DDD(L)*PI
S=SIN(TH)*SIN(TH)
SR(1)=SQRT(DCE(1,L)-S)
IF(POLIZ .EQ.PARALL)GO TO 210
RR=(SR(1)-COS(TH))/(SR(1)+COS(TH))

```

Fig. 61. Multilayer transmission subprogram - Page 1.

```

GO TO 211
210 RR=(SR(1)-DCE(1,L)*COS(TH))/(SR(1)+DCE(1,L)*COS(TH))
211 CONTINUE
NL=N(L)
DO 10 I=1,NL
  II=I+1
  SR(II)=SQRT(DCE(II,L)-S)
  G(I)=2.*PI*D(I,L)*SR(I)
  IF(POLIZ .EQ.PARALL)GO TO 110
  R(I)=(SR(II)-SR(I))/(SR(II)+SR(I))
  GO TO 10
110 R(I)=(DCE(I,L)*SR(II)-DCE(II,L)*SR(I))/(DCE(I,L)*SR(II)+DCE(II,L)
  1*SR(I))
10 CONTINUE
AQ=1.-RR
DO 15 I=1,NL
15 AQ=AQ*(1.-R(I))
  AQ=1./AQ
  W=1.180314E+4/FREQ
  GG=G(I)/W
  CG=COS(GG)
  SG=SIN(GG)
  AD=PI*DCE(I,L)*TD(I,L)*D(I,L)/(W*SR(I))
  X1=CG*(1.-AD)
  Y1=-SG*(1.-AD)
  X2=-RR*CG*(1.+AD)
  Y2=-RR*SG*(1.+AD)
  X3=-RR*CG*(1.-AD)
  Y3=RR*SG*(1.-AD)
  X4=CG*(1.+AD)
  Y4=SG*(1.+AD)
 >NNL=NN(L)
  DO 35 I=2,>NNL
  IF(I->NNL) 25,20,50
20 U1=1.
  U2=-R(NL)
  U3=-R(NL)
  U4=1.
  V1=0.
  V2=0.
  V3=0.
  V4=0.
  GO TO 30
25 II=I-1
  AD=PI*DCE(I,L)*TD(I,L)*D(I,L)/(W*SR(I))
  GG=G(I)/W
  CG=COS(GG)
  SG=SIN(GG)

```

Fig. 61. Multilayer transmission subprogram - Page 2.

```

U1=CG*(1.-AD)
V1=-SG*(1.-AD)
U2=-R(II)*CG*(1.+AD)
V2=-R(II)*SG*(1.+AD)
U3=-R(II)*CG*(1.-AD)
V3=R(II)*SG*(1.-AD)
U4=CG*(1.+AD)
V4=SG*(1.+AD)
30 P1=X1*U1-Y1*V1+X2*U3-Y2*V3
Q1=Y1*U1+X1*V1+Y2*U3+X2*V3
P2=X1*U2-Y1*V2+X2*U4-Y2*V4
Q2=Y1*U2+X1*V2+X2*V4+Y2*U4
P3=X3*U1-Y3*V1+X4*U3-Y4*V3
Q3=Y3*U1+X3*V1+X4*V3+Y4*U3
P4=X3*U2-Y3*V2+X4*U4-Y4*V4
Q4=Y3*U2+X3*V2+X4*V4+Y4*U4
X1=P1
X2=P2
X3=P3
X4=P4
Y1=Q1
Y2=Q2
Y3=Q3
35 Y4=Q4
RCR=(-X3*X4-Y3*Y4)/(X4*X4+Y4*Y4)
RCI=(-Y3*X4+X3*Y4)/(X4*X4+Y4*Y4)
RC2=RCR*RCR+RCI*RCI
RC=SQRT(RC2)
TR=(X1+X2*RCR-Y2*RCI)*AQ
TI=(Y1+Y2*RCR+X2*RCI)*AQ
TC2=TR*TR+TI*TI
TC(K)=SQRT(TC2)
IF(TR.EQ.0..AND.TI.EQ.0.) TI=TI+RMIN
XX=DATAN2(TI,TR)
48 FIPD(K)=-RADEG*(XX+DD/W)
IF(FIPD(K).LT.0.) FIPD(K)=FIPD(K)+360.
IF(SOURCE(12).EQ.WRITER) WRITE(6,1) T(K,L),FIPD(K),TC(K),K,L
60 CONTINUE
50 CONTINUE
557 RETURN
END

```

Fig. 61. Multilayer transmission subprogram - Page 3

```

SUPROUTINE ATAPER
DOUBLE PRECISION AA, PB, CC, DD, EE, FF, XGB, YGB, PI, PBA, CCC, DISC, PYDX, P,
1Y, TS, TI, CL, CL2, SL, SL2, C2L, S2L, TL, RPL, DISCU, XGC, YGC, RGC
1 ,XA, YA, DFATSP, XLIN, YLIN, PHLIN
COMMON /TPR/ Y, STAP(25)
COMMON T(501,12), SOURCE(12), PI, RADEG, DEGRAD, M1, NOS, IX, NC, A, YC(501)
1 ,XA(501), YA(501), DFATSP, XLIN, YLIN, PHLIN,
1 PHST(501), AAT(501), TAPER, NBLOK1, NBLOK2 ,YO(501), MCX
11 FORMAT (6F10.6)
152 FORMAT(3X,35HUNIFORM APERTURE DISTRIBUTION USED.//)
153 FORMAT(2X,2F10.4)
154 FORMAT(6X,18HOBSTACLE HEIGHT F10.6//)
155 FORMAT(6X,27HOBSTACLE HEIGHT MODIFIED F10.6//)
DATA FLIN/4HFLIN/
DATA COS6/4HCOS6/
DATA CIRCLE/6HCIRCLE/
DATA COS1/6HCOS1 /
DATA RAD4/6HRAD4 /
DATA RAD5/6HRAD5 /
DATA PL1/6HPL1 /
DATA COS2/6HCOS2 /
DATA FNDAAT/6HFNDAAT/
DATA FNPBST/6HFNPBST/
DATA BLOCK/4H BLO /
OBST=0.
RAD=.5*A
RADSQ=RAD*PAD
RADI=1./RAD
PADISQ=RADI*RADI
IF(SOURCE(9).NE.BLOCK) GO TO 13
READ(5,11) OBST
WRITE(6,154) OBST
IF(SOURCE(8).NE.CIRCLE) GO TO 13
RADY=RAD/Y
OBSTSQ=OBST*OBST
READ(5,11) OBSTD
THET= Y/(2.*A)
RATIO=OBST*OBST/(RADY+OBSTD*SIN(THET))*2
AO= RATIO*PI*RADSQ
THET1=170.
THET1= THET1*DEGRAD
DO 15 N=1,10
THET2=THET1-(THET1-SIN(THET1)-PI*(1.-RATIO))/(1.-COS(THET1))
IF(ABS(THET2-THET1).LT.1.E-4) GO TO 17
THET1D= RADEG*THET1
WRITE(6,19) THET1D
19 FORMAT('THE1A = 'F12.6)
15 THET1=THET2

```

Fig. 62. Aperture taper subprogram - Page 1.

```

17 OBST =RAD* $\cos$ (THET1/2.)
   WRITE(6,155) OBST
   ASTRIP=(PI-THET1+  $\sin$ (THET1))*RADSQ
   WRITE(6,18) AO,ASTRIP
18 FORMAT('OBSTACLE AREA = 'F12.6,/'STRIP AREA      = 'F12.6)
13 DO 87 IL=1,M1
   YC(IL)=(Y0(IL)+Y0(IL+1))/2.
   YCT=YC(IL)
   ABSYCT=ABS(YCT)
   IF(SOURCE(5).EQ.FNOAAT) GO TO 83
   CAM=1.
   IF(SOURCE(8).EQ.CIRCLE) CAM=SQRT(RADSQ-YCT*YCT)
   IF(TAPER.EQ.COS1)GO TO 1
   IF(TAPER.EQ.COS2)GO TO 2
   IF(TAPER.EQ.PL1) GO TO 3
   IF(TAPER.EQ.RAD4)GO TO 4
   IF(TAPER.EQ.RAD5)GO TO 5
   IF(TAPER.EQ.COS6)GO TO 6
   IF(TAPER.EQ.FLIN)GO TO 7
1  AAT(IL)=SQRT(.25*A*A-YC(IL)*YC(IL))
   GO TO 84
2  AAT(IL)=DCOS(PI*YC(IL)/A)
   GO TO 84
3  IF(ABS(YC(IL)).LT.0.986603) AAT(IL)=1.*CAM
   IF(ABS(YC(IL)).GE.0.986603.AND.ABS(YC(IL)).LT.1.183924)AAT(IL)=(.9
1789-(ABS(YC(IL))-0.986603)*0.0421/0.197321)*CAM
   IF(ABS(YC(IL)).GE.1.183924.AND.ABS(YC(IL)).LT.1.381244)AAT(IL)=(.9
1368-(ABS(YC(IL))-1.183924)*0.0631/0.197321)*CAM
   IF(ABS(YC(IL)).GE.1.381244.AND.ABS(YC(IL)).LT.1.578565)AAT(IL)=(.8
1737-(ABS(YC(IL))-1.381244)*0.3369/0.197321)*CAM
   IF(ABS(YC(IL)).GE.1.578565.AND.ABS(YC(IL)).LT.1.775885)AAT(IL)=(.5
1368-(ABS(YC(IL))-1.578565)*0.3684/0.197321)*CAM
   IF(ABS(YC(IL)).GE.1.775885.AND.ABS(YC(IL)).LT.1.973206)AAT(IL)=(.1
1684-(ABS(YC(IL))-1.775885)*0.0316/0.197321)*CAM
   IF(ABS(YC(IL)).GE.1.973206.AND.ABS(YC(IL)).LT.2.170526)AAT(IL)=(.1
1368-(ABS(YC(IL))-1.973206)*0.0210/0.197321)*CAM
   IF(ABS(YC(IL)).GE.2.170526.AND.ABS(YC(IL)).LT.2.762488)AAT(IL)=(.1
1158-(ABS(YC(IL))-2.170526)*0.0316/0.591962)*CAM
   IF(ABS(YC(IL)).GE.2.762488)AAT(IL)=0.0842*CAM
   GO TO 84
4  AAT(IL)=(1.-YCT*YCT*RADISQ)*CAM
   GO TO 84
5  AAT(IL)=((1.-YCT*YCT*RADISQ)**2)*CAM
   GO TO 84
6  AAT(IL)=DCOS(PI*YC(IL)/A)**2+STAP(MCX)
   GO TO 84
7  AAT(IL)=1-ABS(YC(IL))/RAD
   GO TO 84

```

Fig. 62. Aperture taper subprogram - Page 2.

```
83 AAT(IL)=1.
84 IF(ABS YC1.LT.PHST) AAT(IL)=0.
   IF(SOURCE(6).EQ.FNPHST) GO TO 85
   PHST(IL)=W*SQRT(110.25+YC(IL)*YC(IL))
   GO TO 82
85 PHST(IL)=0.
82 CONTINUE
   IF(SOURCE(5).EQ.FNOAAT.AND.SOURCE(6).EQ.FNPHST) WRITL(6,152)
   WRITE(6,153) (AAT(IL),PHST(IL),IL=1,M1,10)
RETURN
END
```

Fig. 62. Aperture taper subprogram - Page 3.

GRAPH

DATE = 69199

```
SUBROUTINE GRAPH(X,XMAX,XMIN,NUMBER,R,ISCALE)
DIMENSION X(NUMBER),O(26),P(4),      S(1),B(NUMBER)
DATA G/'  +'/
DATA S(1),P(1),P(2),P(3),P(4)/' ', '*', ' *', ' *', ' *'/
IF(ISCALE.EQ.0) ISCALE=1
FACTOR=100./(XMAX-XMIN)
WRITE(6,31)
31 FORMAT(1H1//20X,'FAR ZONE POWER PATTERN (DB)')
DO 2 K=1,26
  2 O(K)=S(1)
  L=0
  DO 5 N=1,NUMBER
    63 L=L+1
    IF(MOD(L-1,ISCALE)) 50,50,51
    51 WRITE(6,53)
    53 FORMAT(1H )
    GO TO 55
    50 J=1
    K=1
    Y=(X(N)-XMIN)*FACTOR
    IF(Y.EQ.0.) Y=1E-10
    Y= 20.*ALOG10(Y)+60.
    10 IF(Y.LT.3.5) GO TO 20
    Y=Y-4.0
    J=J+1
    GO TO 10
    20 IF(Y.LT.0.5) GO TO 30
    Y=Y-1.0
    K=K+1
    GO TO 20
    30 O(J)=P(K)
    WRITE(6,32) R(N),O
    32 FORMAT(3X,F10.4,2X,26A4)
    O(J)=S(1)
    55 IF(MOD(L-1,10))40,40,64
    40 WRITE(6,42) (G,I=1,11)
    42 FORMAT(1H+,6X,11A10)
    64 IF(MOD(L-1,ISCALE)) 5,5,63
    5 CONTINUE
    RETURN
  END
```

Fig. 63. Graph subprogram.

SLI

DATE = 69119

```

SUPPLEMENT SLI(AE,XMAX,NUMBER,1,BSLMAX,SLB,R,P,M,1)
DIMENSION AE(NUMBER),A(NUMBER),SLB(NUMBER),P(NUMBER)
PI=3.1415926535897932
DEGRAD=PI/180.
RADEG=180./PI
11 FORMAT(4X,8F10.5)
DATA MM/0/
1 (MM.EQ.1) GO TO 12
MM=0
M=0
I=NUMBER-1
DO 1 N=2,I
IF(AE(N-1).LT.AE(N).AND.AE(N+1).LT.AE(N)) GO TO 2
GO TO 1
2 M=M+1
A(M)=(AE(N)/XMAX)*100.
SLB(M)=B(N)
WRITE(6,11) A(M),SLB(M)
1 CONTINUE
IF(MG1.EQ.1.AND.M.GE.3) GO TO 13
GO TO 14
13 MM=M/2
SLB1=SLB(M)
WRITE(6,25) MG1,MM,M
25 FORMAT(' MG1='15,' MM='15,' M='15//)
14 SLMAX=0.0
DO 3 N=1,M
IF(A(N).GT.SLMAX.AND.A(N).LT.75.) GO TO 8
GO TO 3
8 SLMAX=A(N)
PSLMAX=SLB(N)*DEGRAD
WRITE(6,11) BSLMAX
3 CONTINUE
IF(SLMAX.LT.0.0000001) GO TO 6
SLDB=20.*ALOG10(100./SLMAX)
GO TO 7
6 WRITE(6,9)
9 FORMAT(' NO SIDLOBE DETECTED'
BSL1=SLP1*DEGRAD
BSLMAX=BSL1
RETURN 2
7 WRITE(6,5) SLMAX,SLDB
5 FORMAT(10X,25H MAXIMUM SIDLOBE LEVEL ,F10.4,5X,8HPERCENT.,5X,1H
1,F10.4,6H DB )
MM=1
RETURN
12 MM=0
BSL1=SLB1*DEGRAD
BSLMAX=BSL1
10 RETURN 1
END

```

Fig. 64. Sidelobe level subprogram.

HPBW

DATE = 69199

```
SUBROUTINE HPBW(AE,XMAX,NUMBER,B)
DIMENSION AE(NUMBER),B(NUMBER)
DO 1 N=2,NUMBLR
IF(AE(N).GE.0.7071*XMAX.AND.AE(N-1).LT.0.7071*XMAX) GO TO 10
2 IF(AE(N).LT.0.7071*XMAX.AND.AE(N-1).GE.0.7071*XMAX) GO TO 20
GO TO 1
10 A1=AE(N)
A2=AE(N-1)
PA1=B(N)
PA2=B(N-1)
GO TO 2
20 A3=AE(N)
A4=AE(N-1)
PA3=B(N)
PA4=B(N-1)
1 CONTINUE
30 ANG1=PA2-(PA2-PA1)*(0.7071*XMAX-A2)/(A1-A2)
ANG2=PA3+(PA4-PA3)*(0.7071*XMAX-A3)/(A4-A3)
BW=ANG1-ANG2
40 WRITE(6,40) BW
FORMAT(///10X,25H HALF-POWER BEAMWIDTH ,F10.4,3X,8HDEGREE.//)
RETURN
END
```

Fig. 65. Half-power beamwidth subprogram.



## REFERENCES

1. Van Doeren, R.E., "Application of an Integral Equation Method to Scattering from Dielectric Rings," Report 2485-2, 19 April 1968, ElectroScience Laboratory, The Ohio State University Research Foundation; prepared under Contract N62269-67-C-0582 for the Department of the Navy, U.S. Naval Air Development Center, Washington, D.C.
2. Hahn, G.M., and Pinney, E.J., "Three Dimensional Error Prediction," Proceedings of the OSU-WADC Radome Symposium, The Ohio State University, (August 1956).
3. Kilcoyne, N.R., "An Approximate Calculation of Radome Bore-sight Error," Presented at the Ninth Electromagnetic Windows Symposium, sponsored by the U.S. Air Force Avionics Laboratory, and The Georgia Institute of Technology, Atlanta, Georgia, (14 June 1968).
4. Richmond, J.H., "Efficient Recursive Solutions for Plane and Cylindrical Multilayers," Report 1968-1, 10 August 1965, ElectroScience Laboratory, The Ohio State University Research Foundation; prepared under Contract NOW 5-0329-d for Bureau of Naval Weapons, Washington, D.C. (AD 624 191).
5. Styron, J.B., and Hoots, L.C., "Antenna Distributions in High Performance Aircraft Radomes," presented at the Fifteenth Annual Symposium on USAF Antenna Research and Development, University of Illinois, (October 1965).
6. Collier, J.R., "Effects of Antenna Aperture Blocking," Report 1180-9, 30 September 1962, ElectroScience Laboratory, The Ohio State University Research Foundation, prepared under Contract AF 33(616)-7614 for Aeronautical Systems Division, AFSC, U.S. Air Force, Wright-Patterson Air Force Base, Ohio.
7. Breeden, K.H., et al., "Millimeter Radome Design Techniques," Report Number G.I.T. 68-38, February 1968, Engineering Experiment Station, Georgia Institute of Technology.
8. Corning Glass Works Materials Specification, Section 2, Sheet 1a, Material No. 9606, (March 9, 1961).

9. Personal communication from W. Beamer, U.S. Naval Air Development Center, Johnsville, Warminster, Pennsylvania, (22 September 1966).
10. Personal communication from W. Beamer, U.S. Naval Air Development Center, Johnsville, Warminster, Pennsylvania, (19 June 1969).
11. "Electrical Test Report for the U.S. Naval Air Development Center High Temperature Radomes." Brunswick Report BR-794-124-003, 9 August 1966, Brunswick Corporation Defense Products Division, Marion, Virginia.
12. Personal communication from W. Beamer, U.S. Naval Air Development Center, Johnsville, Warminster, Pennsylvania, (20 January 1969).

UNCLASSIFIED

Security Classification

DOCUMENT CONTROL DATA - R&D		
<i>(Security classification of title, body of abstract and indexing annotation must be entered when the overall report is classified)</i>		
1. ORIGINATING ACTIVITY (Corporate author) ElectroScience Laboratory Department of Electrical Engineering, The Ohio State University, Columbus, Ohio		2a. REPORT SECURITY CLASSIFICATION Unclassified
		2b. GROUP
3. REPORT TITLE A Two-Dimensional Ray-Tracing Method For The Calculation of Radome Boresight Error And Antenna Pattern Distortion		
4. DESCRIPTIVE NOTES (Type of report and inclusive dates) Technical Report		
5. AUTHOR(S) (Last name, first name, initial) Kilcoyne, N.R.		
6. REPORT DATE 2 October 1969	7a. TOTAL NO. OF PAGES 114	7b. NO. OF REFS 12
8a. CONTRACT OR GRANT NO. Contract N00019-69-C-0325	9a. ORIGINATOR'S REPORT NUMBER(S) ElectroScience Laboratory 2767-2	
b. PROJECT NO.		
c. TASK		
d.	9b. OTHER REPORT NO(S) (Any other numbers that may be assigned this report)	
10. AVAILABILITY/LIMITATION NOTICES		
11. SUPPLEMENTARY NOTES		
12. SPONSORING MILITARY ACTIVITY Department of the Navy Naval Air Systems Command Washington, D.C. 20360		
13. ABSTRACT <p>A two-dimensional ray tracing analysis for the calculation of radome boresight error and antenna pattern distortion is presented here. Emphasis has been placed on the development of a method having considerable flexibility, so as to enable application of the method to a wide range of antenna-radome problems, and on relative ease of calculations, so as to minimize calculation time. Several example problems are calculated to demonstrate the usefulness of the approach. Comparisons between calculations and measurements have been included whenever measured data were available. Instructions for use of this completely computerized method are included along with several tables describing variables and the complete computer program with necessary subroutines. Programs are written in Fortran IV language suitable for use on the OSU version of the IBM system 360/75 (some minor changes may be required for use on other 360/75 installations).</p>		

DD FORM 1473  
1 JAN 64

UNCLASSIFIED

Security Classification

**UNCLASSIFIED**  
Security Classification

14. KEY WORDS	LINK A		LINK B		LINK C	
	ROLE	WT	ROLE	WT	ROLE	WT
Two-dimensional Ray-tracing Boresight error Pattern distortion Source taper Aperture blocking Hyper-environment Design Analysis Computer program						

**INSTRUCTIONS**

1. **ORIGINATING ACTIVITY:** Enter the name and address of the contractor, subcontractor, grantee, Department of Defense activity or other organization (*corporate author*) issuing the report.
- 2a. **REPORT SECURITY CLASSIFICATION:** Enter the overall security classification of the report. Indicate whether "Restricted Data" is included. Marking is to be in accordance with appropriate security regulations.
- 2b. **GROUP:** Automatic downgrading is specified in DoD Directive 5200.10 and Armed Forces Industrial Manual. Enter the group number. Also, when applicable, show that optional markings have been used for Group 3 and Group 4 as authorized.
3. **REPORT TITLE:** Enter the complete report title in all capital letters. Titles in all cases should be unclassified. If a meaningful title cannot be selected without classification, show title classification in all capitals in parentheses immediately following the title.
4. **DESCRIPTIVE NOTES:** If appropriate, enter the type of report, e.g., interim, progress, summary, annual, or final. Give the inclusive dates when a specific reporting period is covered.
5. **AUTHOR(S):** Enter the name(s) of author(s) as shown on or in the report. Enter last name, first name, middle initial. If military, show rank and branch of service. The name of the principal author is an absolute minimum requirement.
6. **REPORT DATE:** Enter the date of the report as day, month, year, or month, year. If more than one date appears on the report, use date of publication.
- 7a. **TOTAL NUMBER OF PAGES:** The total page count should follow normal pagination procedures, i.e., enter the number of pages containing information.
- 7b. **NUMBER OF REFERENCES:** Enter the total number of references cited in the report.
- 8a. **CONTRACT OR GRANT NUMBER:** If appropriate, enter the applicable number of the contract or grant under which the report was written.
- 8b, 8c, & 8d. **PROJECT NUMBER:** Enter the appropriate military department identification, such as project number, subproject number, system numbers, task number, etc.
- 9a. **ORIGINATOR'S REPORT NUMBER(S):** Enter the official report number by which the document will be identified and controlled by the originating activity. This number must be unique to this report.
- 9b. **OTHER REPORT NUMBER(S):** If the report has been assigned any other report numbers (*either by the originator or by the sponsor*), also enter this number(s).

10. **AVAILABILITY/LIMITATION NOTICES:** Enter any limitations on further dissemination of the report, other than those imposed by security classification, using standard statements such as:

- (1) "Qualified requesters may obtain copies of this report from DDC."
- (2) "Foreign announcement and dissemination of this report by DDC is not authorized."
- (3) "U. S. Government agencies may obtain copies of this report directly from DDC. Other qualified DDC users shall request through \_\_\_\_\_."
- (4) "U. S. military agencies may obtain copies of this report directly from DDC. Other qualified users shall request through \_\_\_\_\_."
- (5) "All distribution of this report is controlled. Qualified DDC users shall request through \_\_\_\_\_."

If the report has been furnished to the Office of Technical Services, Department of Commerce, for sale to the public, indicate this fact and enter the price, if known.

11. **SUPPLEMENTARY NOTES:** Use for additional explanatory notes.
12. **SPONSORING MILITARY ACTIVITY:** Enter the name of the departmental project office or laboratory sponsoring (*paying for*) the research and development. Include address.
13. **ABSTRACT:** Enter an abstract giving a brief and factual summary of the document indicative of the report, even though it may also appear elsewhere in the body of the technical report. If additional space is required, a continuation sheet shall be attached.

It is highly desirable that the abstract of classified reports be unclassified. Each paragraph of the abstract shall end with an indication of the military security classification of the information in the paragraph, represented as (TS), (S), (C), or (U).

There is no limitation on the length of the abstract. However, the suggested length is from 150 to 225 words.

14. **KEY WORDS:** Key words are technically meaningful terms or short phrases that characterize a report and may be used as index entries for cataloging the report. Key words must be selected so that no security classification is required. Identifiers, such as equipment model designation, trade name, military project code name, geographic location, may be used as key words but will be followed by an indication of technical context. The assignment of links, rules, and weights is optional.